Electronic Supplementary Material (ESI) for Inorganic Chemistry Frontiers.

Supporting Information

Long-cavity $[Pd_2L_4]^{4+}$ cages and designer 1,8-naphthalimide sulfonate guests: rich variation in affinity and differentiated binding stoichiometry

Dan Preston,[,a,b] Komal M. Patil,[a] Alex T. O'Neil,[c] Roan A. S. Vasdev,[d] Jonathan A. Kitchen,*[,c] and Paul E. Kruger[a]*

[a]*MacDiarmid Institute for Advanced Materials and Nanotechnology, School of Physical and Chemical Sciences, University of Canterbury, Christchurch 8041, New Zealand.*
[b]*Research School of Chemistry, the Australian National University, Canberra, ACT 2600, Australia.*
[c]*Chemistry, School of Natural and Computational Sciences, Massey University, Auckland, New Zealand.*
[d]*Department of Chemistry, University of Otago, PO Box 56, Dunedin 9054, New Zealand.*

***Daniel.Preston@anu.edu.au**
***J.Kitchen@massey.ac.nz**

Contents

1. Experimental

1.1. General

Unless otherwise stated, all reagents were purchased from commercial sources and used without further purification, except for 1,3-bis(4-iodophenyl)-adamantane,[1] [pyridinium]**para-H**[2] and [pyridinium]**meta-H**,[2] which were synthesised according to literature procedures. Solvents were laboratory reagent grade. Petroleum ether (PE) refers to the fraction of petrol boiling in the range 40 – 60 °C, isopropyl alcohol (IPA), methanol (MeOH), dichloromethane (DCM), ethylenediaminetetraacetate (EDTA), tetrahydrofuran (THF), dimethyl sulfoxide (DMSO), dimethylformamide (DMF). ^{1}H and ^{13}C NMR spectra were recorded on either a 400 MHz Varian 400-MR, a Varian 500 MHz AR, a JEOL 400 MHz, or a JEOL 600 MHz spectrometer. Chemical shifts are reported in parts per million and referenced to residual solvent peaks ($CDCl_3$: ^{1}H δ 7.26 ppm, ^{13}C δ 77.16 ppm; [D_6]DMSO: ^{1}H δ 2.50 ppm; ^{13}C δ 39.52 ppm). Coupling constants (*J*) are reported in Hertz (Hz). Standard abbreviations indicating multiplicity were used as follows: m = multiplet, q = quartet, quin = quintet, t = triplet, dt = double triplet, d = doublet, dd = double doublet, s = singlet, br = broad. Electrospray mass spectra (HR ESI-MS) were collected on a Bruker micrOTOF-Q spectrometer.

1.2. L

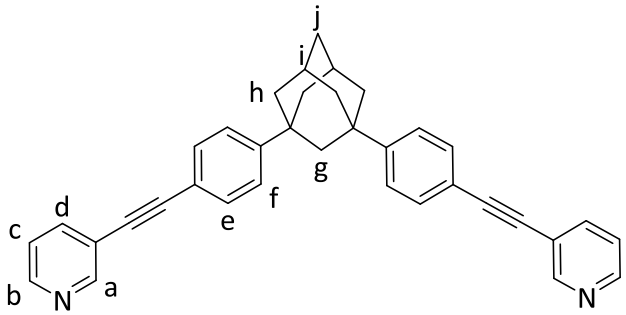

A mixture of 2-ethynylpyridine (72 mg, 0.69 mmol), 1,3-bis(4-iodophenyl)-adamantane[1] (150 mg, 0.28 mmol) in THF (2 mL) and diisopropylamine (3 mL) were degassed with nitrogen in a tube. To the tube was added CuI (5 mg, 0.03 mmol) and $[Pd(PPh_3)_2Cl_2]$ (10 mg, 0.014 mmol), before capping and heating at 80 °C under a nitrogen atmosphere overnight. The reaction mixture was added to DCM (50 mL) and 0.1 M aqueous EDTA/NH_4OH solution (100 mL) and stirred for 30 minutes. The organic layer was washed with water (100 mL), and the solvent was removed under vacuum. Column chromatography on silica (PE to 1:20 acetone/PE to 1:8 acetone/PE to 1:10 acetone/DCM) gave the product as a colourless solid (80 mg, 0.16 mmol, 59%). ^{1}H NMR (600 MHz, $CDCl_3$, 298 K) δ: 8.78 (2H, broad, H_a), 8.56 (2H, broad, H_b), 7.83 (2H, d, J = 7.9 Hz, H_d), 7.52 (4H, d, J = 8.5 Hz, H_e), 7.40 (4H, d, J = Hz, H_f), 7.31 (2H, broad, H_c), 2.35 (2H, broad, H_i), 2.03 (2H, broad, H_g), 1.97 – 1.97 (2H, m, H_h), 1.81 (2H, broad, H_j). ^{13}C NMR (150 MHz, [D_6]DMSO, 298 K) δ: 151.7, 151.6, 149.0, 138.6, 131.4, 125.5, 123.7, 119.6, 119.0, 92.5, 85.7, 47.6, 41.3, 37.2, 35.1, 28.9. HR ESI-MS (DCM/MeOH) m/z = 491.2501 $[MH]^+$ (calc. for $C_{36}H_{31}N_2$, 491.2482). IR ν (cm^{-1}) 3036, 2901, 2846, 2217, 1580, 1407, 1015, 811.

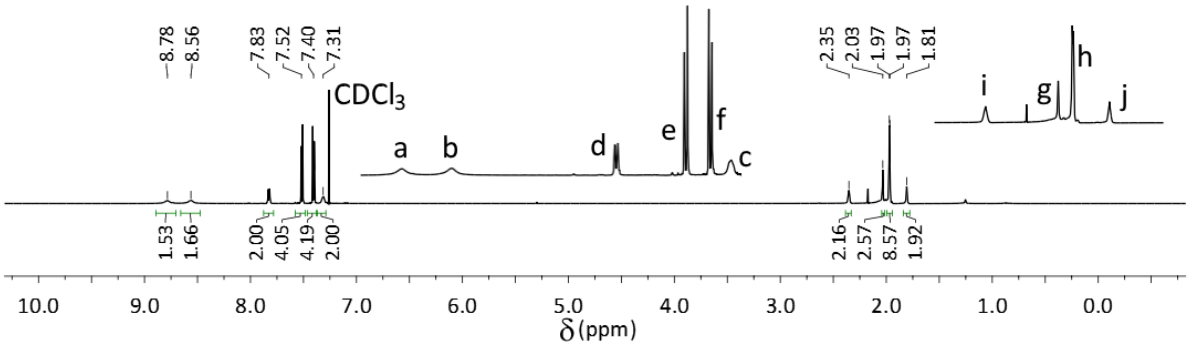

Figure 1.1 ^{1}H NMR spectrum (600 MHz, $CDCl_3$, 298 K) of **L**.

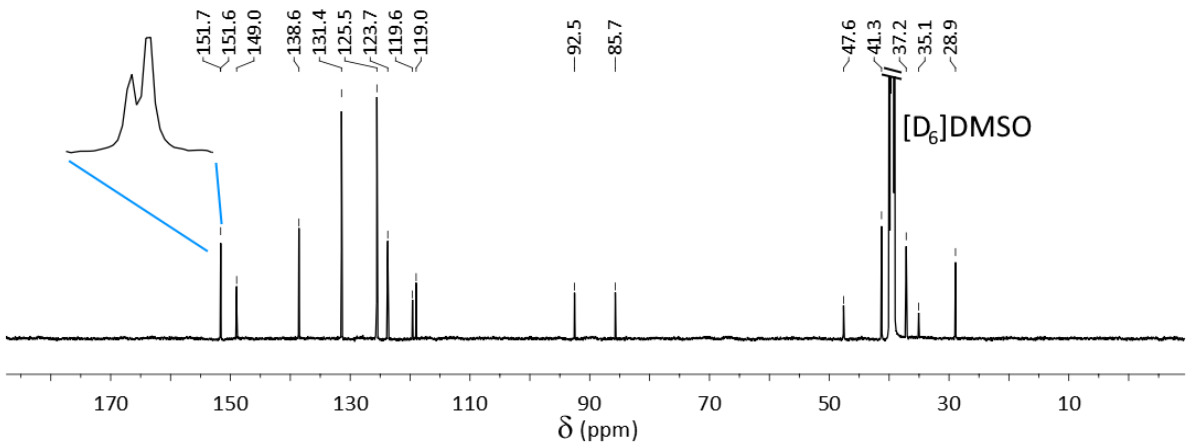

Figure 1.2 ^{13}C NMR spectrum (150 MHz, [D_6]DMSO, 298 K) of **L**.

CCDC#: 1993277. Hot recrystallization of a DMSO solution of **L** gave colourless plate crystals of **L**. X-ray data were collected at 100 K on an Agilent Technologies Supernova system using Mo Kα radiation with exposures over 1.0°, and data were treated using CrysAlisPro[3] software. The structure was solved using SHELXT within OLEX2 and weighted full-matrix refinement on F^2 was carried out using SHELXL-97[4] running within the OLEX2[5] package. All non-hydrogen atoms were refined anisotropically. Hydrogen atoms attached to carbons were placed in calculated positions and refined using a riding model. The structure was solved in the monoclinic space group *P*-1 and refined to an R_1 value of 3.1%. The asymmetric unit contained one ligand.

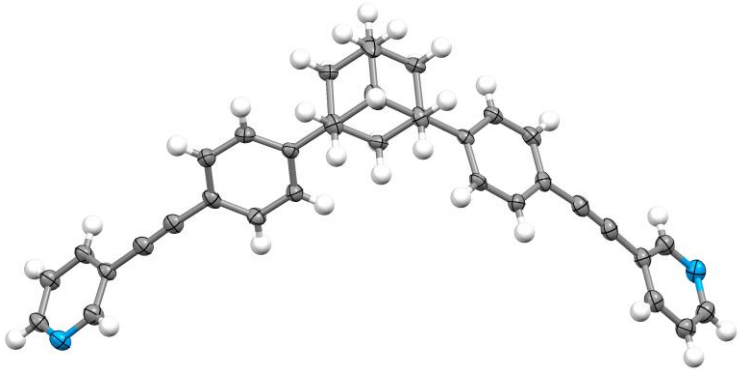

Figure 1.3 Mercury ellipsoid plot of the asymmetric unit of **L**. Ellipsoids shown at 50% probability level. Colour scheme: carbon grey, hydrogen white, nitrogen blue.

Crystals were prone to decomposition during the collection process: trade-offs were required between frame lengths, data quality and completeness.

Empirical formula	$C_{36}H_{30}N_2$	μ/mm^{-1}	0.551
Formula weight	490.62	F(000)	520.0
Temperature/K	120.00(10)	Crystal size/mm^3	0.304 × 0.195 × 0.025
Crystal system	Monoclinic	Radiation	CuKα (λ = 1.54184)
Space group	$P2_1$	2Θ range for data collection/°	10.216 to 105.25
a/Å	6.8979(2)	Index ranges	-6 ≤ h ≤ 7, -7 ≤ k ≤ 7, -26 ≤ l ≤ 26
b/Å	7.2952(2)	Reflections collected	6638
c/Å	26.1502(9)	Independent reflections	2736 [R_{int} = 0.0288, R_{sigma} = 0.0347]
α/°	90	Data/restraints/parameters	2736/1/343
β/°	96.625(3)	Goodness-of-fit on F^2	1.034
γ/°	90	Final R indexes [I>=2σ (I)]	R_1 = 0.0318, wR_2 = 0.0754
Volume/Å^3	1307.13(7)	Final R indexes [all data]	R_1 = 0.0359, wR_2 = 0.0780
Z	2	Largest diff. peak/hole / e Å^{-3}	0.12/-0.14
ρ_{calc}g/cm^3	1.247	Flack parameter	-0.4(5)

1.3. $C(BF_4)_4$

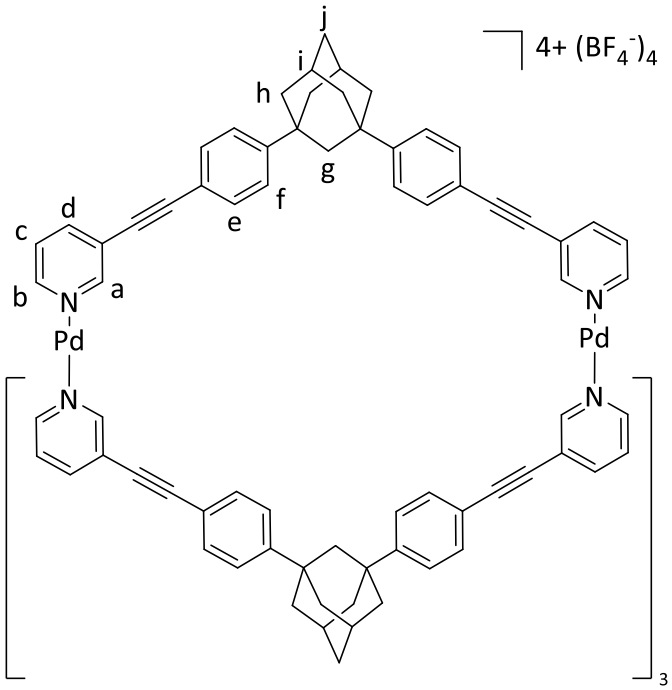

A mixture of **L** (7.7 mg, 16 µmol) and $[Pd(CH_3CN)_4](BF_4)_2$ (3.5 mg, 7.9 µmol) in $[D_6]$DMSO (600 µL) was sonicated until a solution formed. After addition of acetonitrile (2000 µL), vapour diffusion of diethyl ether into the solution gave a tan powder (7.0 mg, 2.7 µmol, 71%). ^{1}H NMR (600 MHz, $[D_6]$DMSO, 298 K) *integration given per ligand* δ: 9.47 (2H, s, H_a), 9.23 (2H, d, J = 5.8 Hz, H_b), 8.23 (2H, d, J = 7.9 Hz, H_d), 7.78 (2H, t, J = 7.5 Hz, H_c), 7.58 (8H, apparent singlet, $H_{e,f}$), 2.21 (2H, br, H_i), 2.12 (2H, br, H_g), 1.92 (4H, d, J = 9.5 Hz, H_h), 1.83 – 1.74 (6H, m, $H_{h',j}$). ^{13}C NMR (150 MHz, $[D_6]$DMSO, 298 K) δ: 153.1, 152.9, 150.8, 143.3, 132.1, 127.8, 126.3, 123.0, 118.7, 95.7, 83.9, 46.4, 42.1, 37.7, 31.3, 29.3, 23.0. HR ESI-MS (DMF) *m/z* = 543.6986 $[\mathbf{C}]^{4+}$ (calc. for $C_{144}H_{120}N_8Pd_4$, 543.6934), 575.1728 $[\mathbf{C} + BF_4 + K]^{4+}$ (calc. for $C_{144}H_{120}BF_4KN_8Pd_4$, 575.1853), 739.9298 $[\mathbf{C} + COOH]^{3+}$ (calc. for $C_{145}H_{121}N_8O_2Pd_4$, 739.9241), 753.9320 $[\mathbf{C} + BF_4]^{3+}$ (calc. for $C_{144}H_{120}BF_4N_8Pd_4$, 753.9261), 795.8693 $[\mathbf{C} + 2BF_4 + K]^{3+}$ (calc. for $C_{144}H_{120}B_2F_8KN_8Pd_4$, 795.9152). IR ν (cm^{-1}) 2904, 2848, 2232, 2221, 1598, 1572, 1511, 1420, 1057, 814.

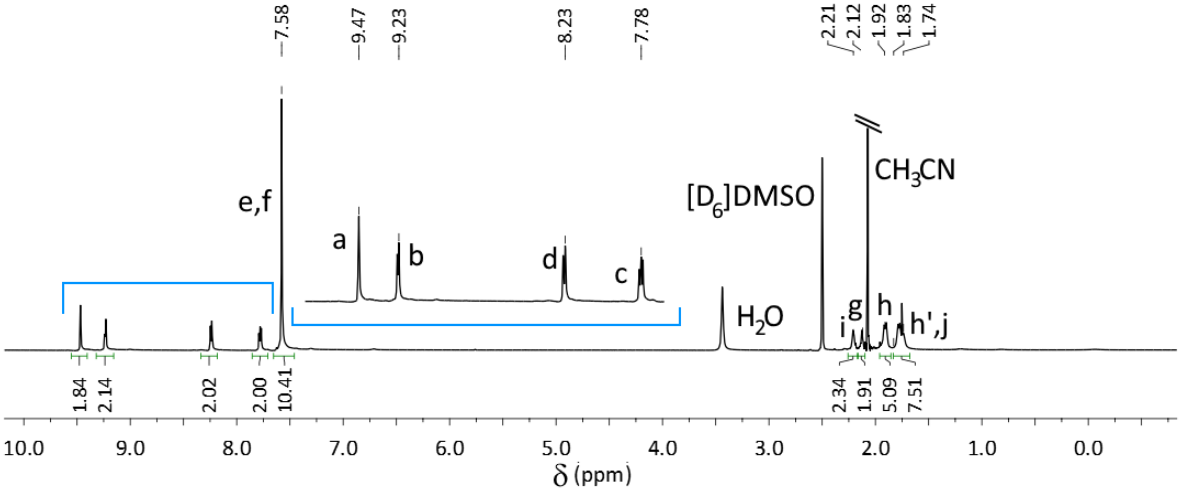

Figure 1.4 ^{1}H NMR spectrum (600 MHz, $[D_6]$DMSO, 298 K) of $\mathbf{C}(BF_4)_4$.

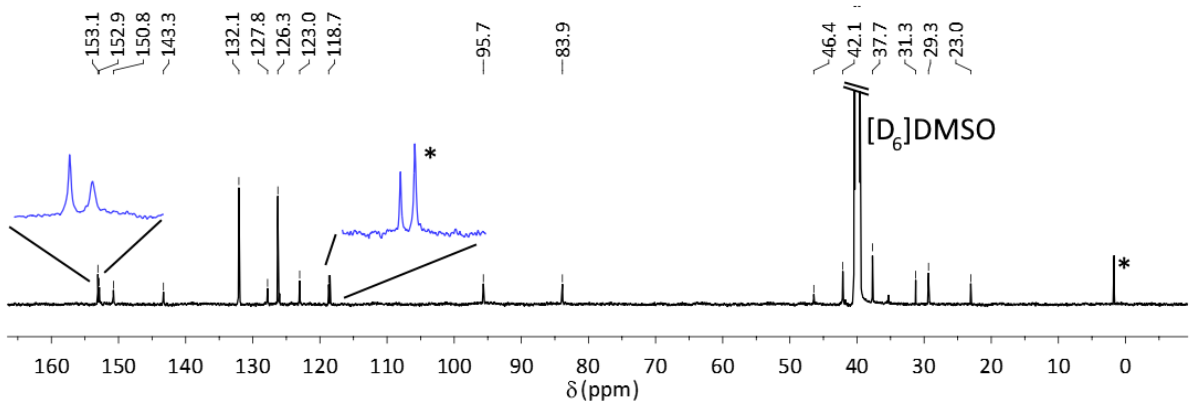

Figure 1.5 ^{13}C NMR spectrum (150 MHz, [D_6]DMSO, 298 K) of **C**$(BF_4)_4$. *denotes acetonitrile.

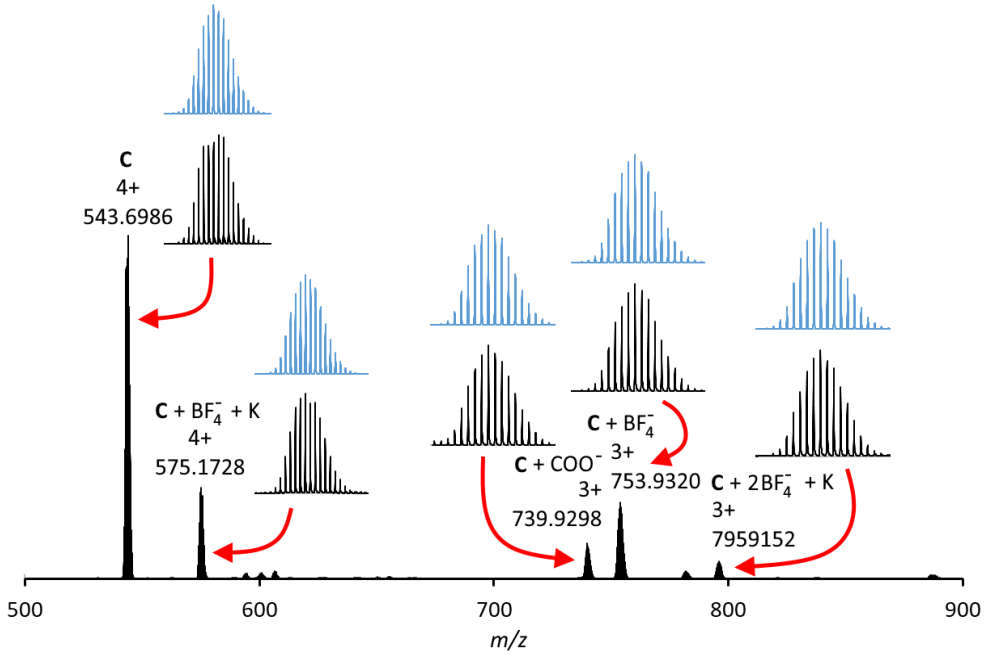

Figure 1.6 Partial mass spectrum (DMF) of **C**$(BF_4)_4$, observed peaks shown in black and calculated distributions above in blue.

CCDC#: 1993278. Vapour diffusion of diethyl ether into a DMF solution of **C**$(BF_4)_4$ gave colourless block crystals of **C**$(BF_4)_4$·2DMF. X-ray data were collected at 100 K on an Agilent Technologies Supernova system using Mo Kα radiation with exposures over 1.0°, and data were treated using CrysAlisPro[3] software. The structure was solved using SHELXT within OLEX2 and weighted full-matrix refinement on F^2 was carried out using SHELXL-97[4] running within the OLEX2[5] package. All non-hydrogen atoms were refined anisotropically. Hydrogen atoms attached to carbons were placed in calculated positions and refined using a riding model. The structure was solved in the monoclinic space group $P2_1/c$ and refined to an R_1 value of 10.02%. The asymmetric unit contained one half of the cage (i.e. two ligands, one Pd^{II} ion), one BF_4^- counterion, and one DMF solvent molecule.

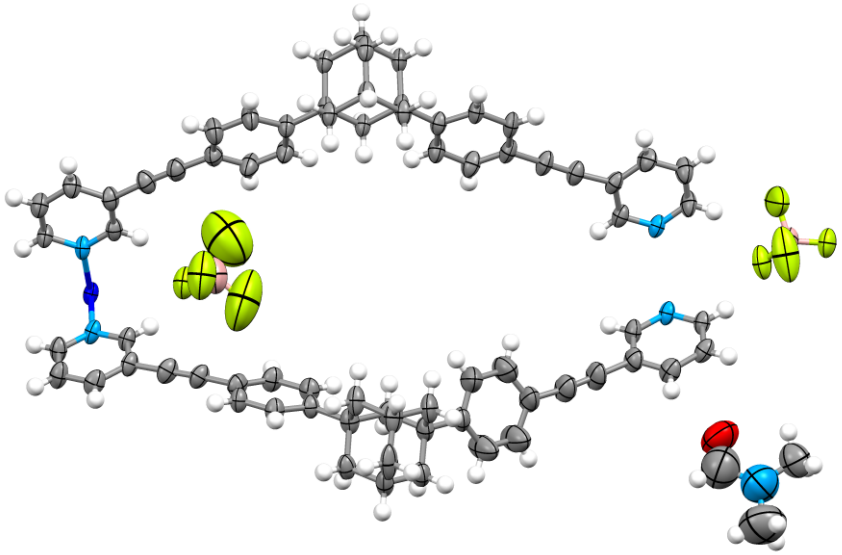

Figure 1.7 Mercury ellipsoid plot of the asymmetric unit of **C**$(BF_4)_4$·2DMF. Ellipsoids shown at 50% probability level. Colour scheme: carbon grey, hydrogen white, boron salmon, fluorine yellow, nitrogen blue, oxygen red, palladium dark blue.

The two BF_4^- counterions and the DMF solvent molecule were disordered. This disorder was resolved using the SADI, DFIX and ISOR commands. There was diffuse electron density within the lattice that could not be appropriately modelled, the SOLVENT MASK routine from within OLEX2 was employed to resolve this problem. There were two equivalent voids (each 1038 Å^3, 240 electrons) which we assign in each case to six DMF solvent molecules.

Empirical formula	$C_{158}H_{134}B_4F_{16}N_{10}O_4Pd_2$	μ/mm^{-1}	2.295
Formula weight	2796.78	F(000)	2880.0
Temperature/K	120.01(10)	Crystal size/mm^3	0.28 × 0.209 × 0.119
Crystal system	Monoclinic	Radiation	CuKα (λ = 1.54184)
Space group	$P2_1/c$	2Θ range for data collection/°	6.938 to 146.652
a/Å	16.7045(7)	Index ranges	-20 ≤ h ≤ 20, -32 ≤ k ≤ 23, -24 ≤ l ≤ 17
b/Å	26.5471(5)	Reflections collected	38641
c/Å	19.7547(6)	Independent reflections	16007 [R_{int} = 0.0258, R_{sigma} = 0.0297]
α/°	90	Data/restraints/parameters	16007/91/831
β/°	107.715(4)	Goodness-of-fit on F^2	1.486
γ/°	90	Final R indexes [I>=2σ (I)]	R_1 = 0.1002, wR_2 = 0.3176
Volume/Å^3	8344.9(5)	Final R indexes [all data]	R_1 = 0.1074, wR_2 = 0.3320
Z	2	Largest diff. peak/hole / e Å^{-3}	3.65/-1.24
ρ_{calc}g/cm^3	1.113		

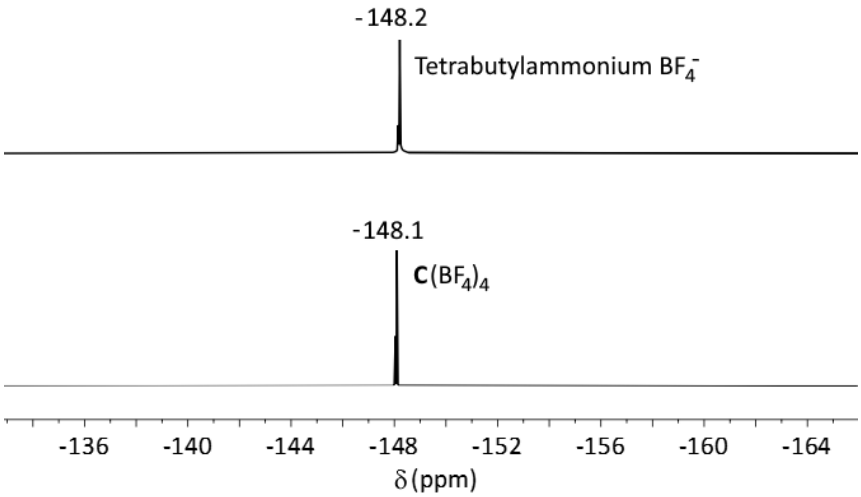

Figure 1.8 Partial stacked ^{19}F NMR spectra (379 MHz, [D_6]DMSO, 298 K) for tetrabutylammonium tetrafluoroborate and for **C**$(BF_4)_4$.

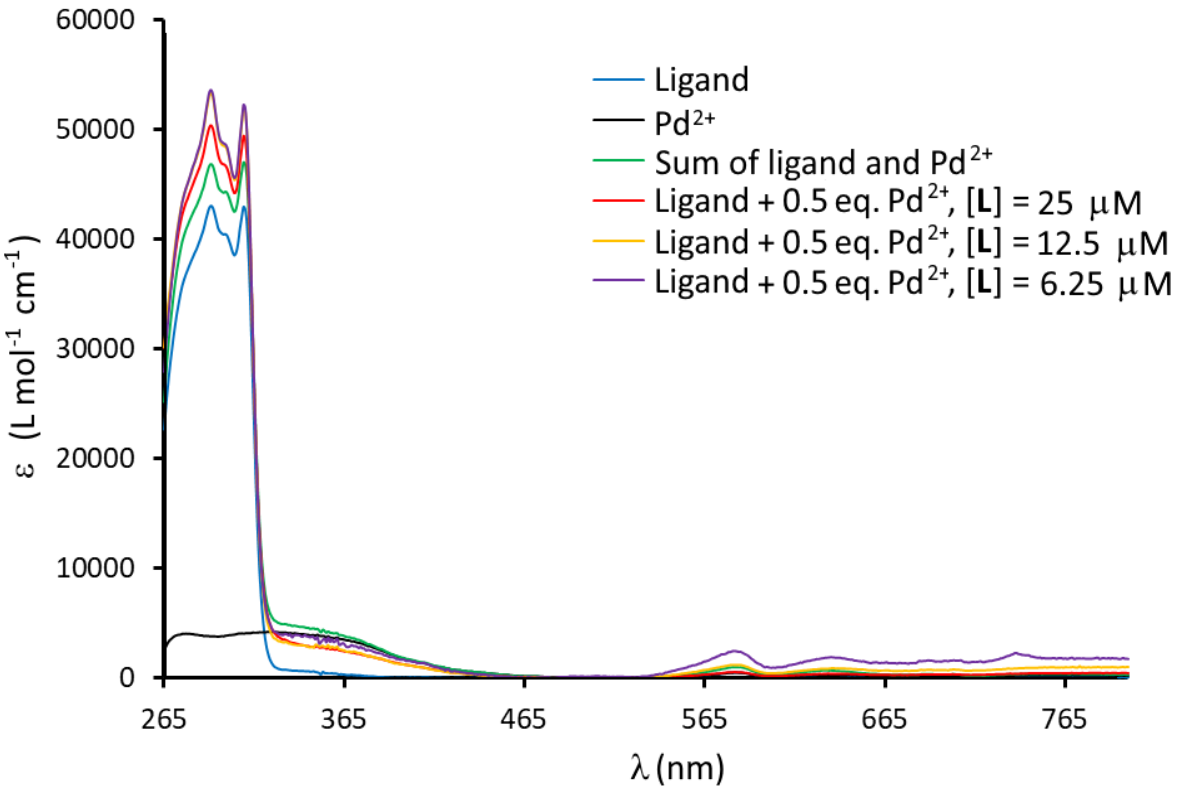

Figure 1.9 UV-Vis spectra (DMSO) for **L** and Pd^{II} and combinations at different concentrations thereof. There is little difference between the spectrum of 4:2 **L**/Pd^{II} and the summation of their two individual spectra, making it difficult to ascertain whether the cage is fully intact at low concentrations in DMSO.

1.4. $C(NO_3)_4$

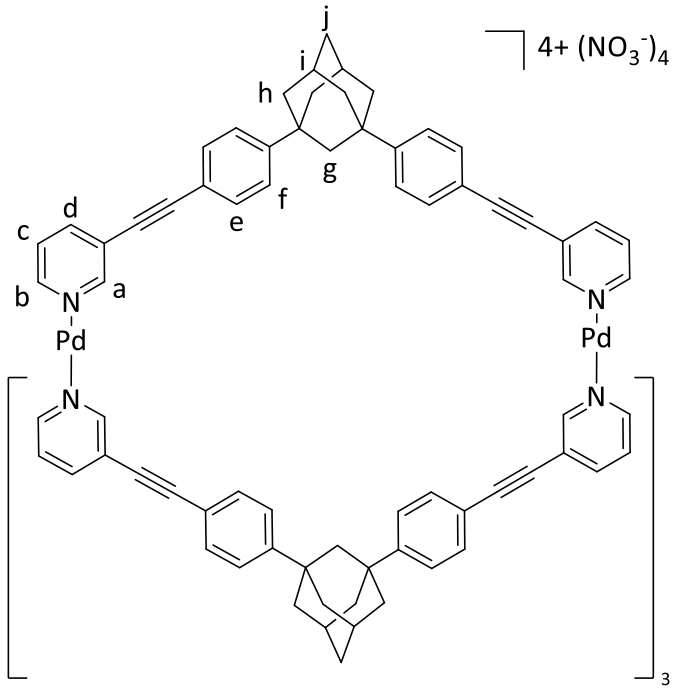

A mixture of **1** (7.7 mg, 16 µmol) and $Pd(NO_3)_2{\cdot}2H_2O$ (2.1 mg, 7.8 µmol) in [D_6]DMSO (600 µL) was sonicated until a solution formed. After addition of DMF (2000 µL), vapour diffusion of diethyl ether into the solution gave small orange block crystals (10.0 mg, 3.21 µmol, 82%). ^{1}H NMR (600 MHz, [D_6]DMSO, 298 K) *integration given per ligand* δ: 9.46 (2H, s, H_a), 9.22 (2H, d, J = 5.5 Hz, H_b), 8.20 (2H, d, J = 8.1 Hz, H_d), 7.75 (2H, d, J = 7.6 Hz, H_c), 7.52 (8H, apparent singlet, $H_{e,f}$), 2.13 (2H, broad, H_i), 2.07 (2H, broad, H_g), 1.84 (4H, d, J = 9.9 Hz, H_h), 1.71 – 1.66 (6H, m, $H_{h',j}$). ^{13}C NMR (150 MHz, [D_6]DMSO, 298 K) δ: 153.0, 152.9, 150.9, 143.3, 132.1, 127.8, 126.2, 123.0, 118.5, 95.7, 83.9, 46.4, 42.1, 37.7, 35.3, 31.3, 29.3. HR ESI-MS (DMSO/CH_3CN) *m/z* = 543.7016 [**C**]$^{4+}$ (calc. for $C_{144}H_{120}N_8Pd_4$, 543.6934), 745.5950 [**C** + NO_3]$^{3+}$ (calc. for $C_{144}H_{120}N_9O_3Pd_4$, 745.8575). IR ν (cm^{-1}) 2900, 2847, 2222, 2150, 2019, 1599, 1572, 1507, 1421, 1052, 814.

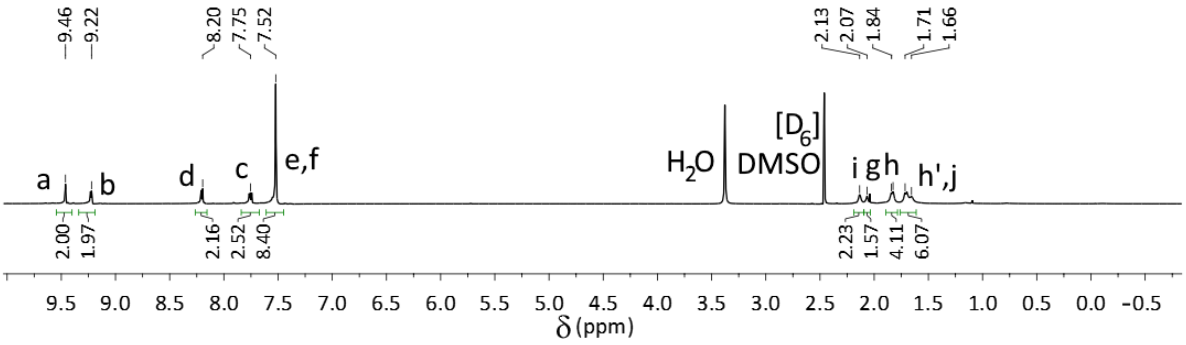

Figure 1.10 ^{1}H NMR spectrum (600 MHz, [D_6]DMSO, 298 K) of **C**$(NO_3)_4$.

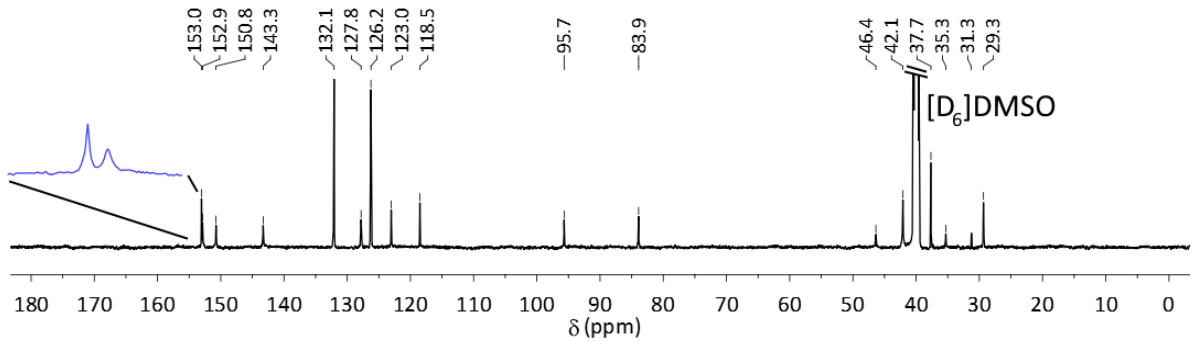

Figure 1.11 ^{13}C NMR spectrum (150 MHz, $[D_6]$DMSO, 298 K) of $\mathbf{C}(NO_3)_4$.

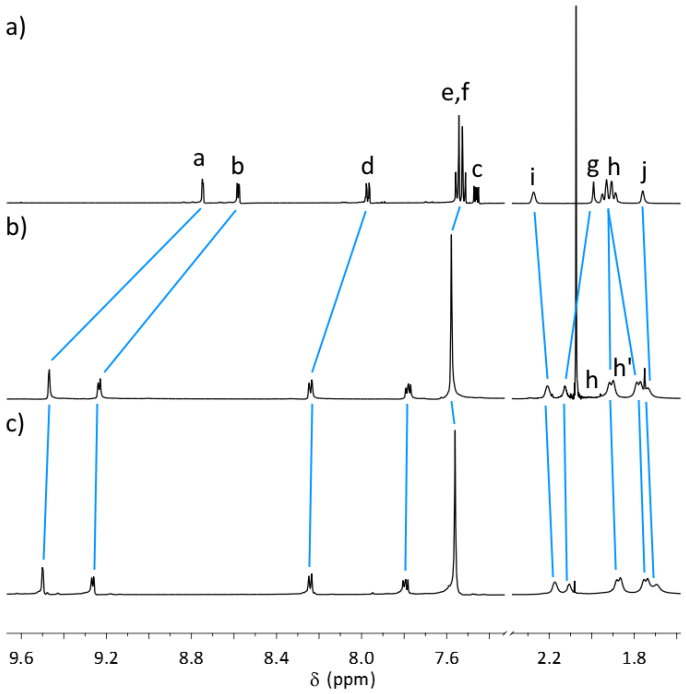

Figure 1.12 Partial stacked ^{1}H NMR spectra (600 MHz, $[D_6]$DMSO, 298 K) of a) **L**, b) $\mathbf{C}(BF_4)_4$ and c) $\mathbf{C}(NO_3)_4$.

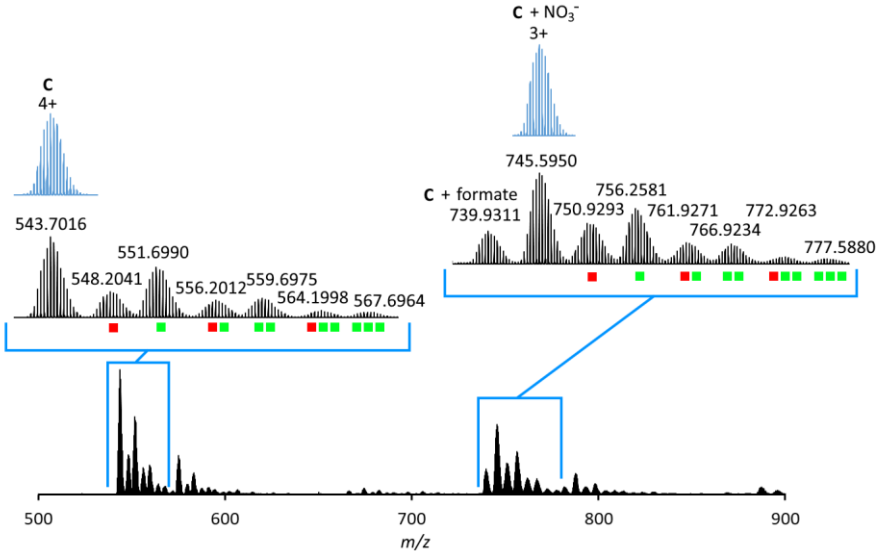

Figure 1.13 Partial mass spectrum (DMSO/CH_3CN) of $\mathbf{C}(NO_3)_4$. Red and green squares represent the species generated from addition of water (red) or methanol (green) to the parent peak (i.e., for 3+, $[\mathbf{C} + NO_3]^{3+}$, so the peak at *m/z* = 766.9234 is generated from $[\mathbf{C} + NO_3 + 2CH_3OH]^{3+}$).

CCDC#: 1993279. Vapour diffusion of diethyl ether into a [D_6]DMSO/DMF solution of **C**$(NO_3)_4$ gave colourless block crystals of **C**$(NO_3)_2 \cdot 2H_2O$. X-ray data were collected at 100 K on an Agilent Technologies Supernova system using Mo Kα radiation with exposures over 1.0°, and data were treated using CrysAlisPro[3] software. The structure was solved using SHELXT within OLEX2 and weighted full-matrix refinement on F^2 was carried out using SHELXL-97[4] running within the OLEX2[5] package. All non-hydrogen atoms were refined anisotropically. Hydrogen atoms attached to carbons were placed in calculated positions and refined using a riding model. The structure was solved in the monoclinic space group $P2_1/c$ and refined to an R_1 value of 5.2%. The asymmetric unit contained one half of the cage (i.e. two ligands, one Pd^{II} ion), one NO_3^- counterion, and one water solvent molecule.

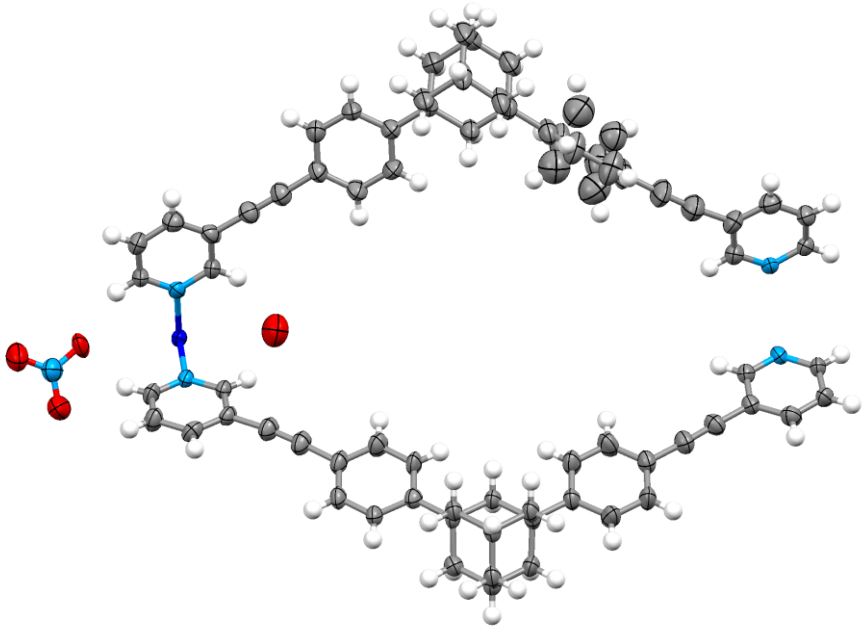

Figure 1.14 Mercury ellipsoid plot of the asymmetric unit of **C**$(NO_3)_2 \cdot 2H_2O$. Ellipsoids shown at 50% probability level. Colour scheme: carbon grey, hydrogen white, nitrogen blue, oxygen red, palladium dark blue.

One of the phenyl rings was disordered and modelled with the PART command. There was diffuse electron density within the lattice that could not be appropriately modelled, the SOLVENT MASK routine from within OLEX2 was employed to resolve this problem. There were two equivalent voids (3700 Å^3, 170 electrons) which we assign to two NO_3^- counterions per cage and various disordered solvent molecules.

Empirical formula	$C_{144}H_{120}N_{10}O_8Pd_2$	μ/mm^{-1}	0.261
Formula weight	2331.29	F(000)	2420
Temperature/K	120.00(10)	Crystal size/mm^3	0.13 × 0.122 × 0.051
Crystal system	Monoclinic	Radiation	MoKα (λ = 0.71073)
Space group	$P2_1/c$	2Θ range for data collection/°	6.756 to 45.972
a/Å	16.7945(8)	Index ranges	-18 ≤ h ≤ 18, -28 ≤ k ≤ 29, -20 ≤ l ≤ 21
b/Å	26.5512(8)	Reflections collected	59333
c/Å	19.6002(10)	Independent reflections	11370 [R_{int} = 0.0749, R_{sigma} = 0.0574]
α/°	90	Data/restraints/parameters	11370/30/775
β/°	106.767(5)	Goodness-of-fit on F^2	0.989
γ/°	90	Final R indexes [I>=2σ (I)]	R_1 = 0.0521, wR_2 = 0.1338
Volume/Å^3	8368.4(7)	Final R indexes [all data]	R_1 = 0.0756, wR_2 = 0.1474
Z	2	Largest diff. peak/hole / e Å^{-3}	1.10/-0.37
ρ_{calc}g/cm^3	0.925		

1.5. Precursors to guests

1.5.1. [Pyridinium]Para-NO_2

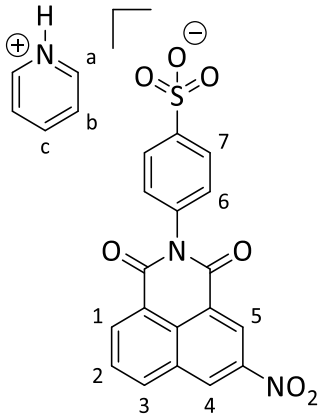

A solution of 3-nitro-1,8-naphthalic anhydride (1.05 g, 4.33 mmol) and 4-aminobenzenesulfonic acid (0.76 g, 4.4 mmol) in pyridine (15 mL) was heated at reflux for 8 hours. The solution turned yellow-orange and a pale white solid precipitated. This solution was filtered while hot, and the solid was washed with diethyl ether (50 mL) before being air dried (1.83 g, 3.71 mmol, 85%). ^{1}H NMR (600 MHz, [D_6]DMSO, 298 K) δ: 9.53 (1H, d, J = 2.2 Hz, H_4), 8.95 (1H, d, J = 2.3 Hz, H_5), 8.93 (2H, d, J = 5.0 Hz, H_a), 8.83 (1H, d, J = 8.3 Hz, H_3), 8.70 (1H, d, J = 6.7 Hz, H_1), 8.56 (1H, t, J = 7.8 Hz, H_c), 8.09 (1H, t, J = 7.4 Hz, H_2), 8.04 (2H, t, J = 7.5 Hz, H_b), 7.76 (2H, d, J = 8.5 Hz, H_7), 7.37 (2H, d, J = 8.4 Hz, H_6). ^{13}C NMR (150 MHz, [D_6]DMSO, 298 K) δ: 163.1, 162.6, 148.4, 145.9, 145.7, 142.9, 136.5, 135.7, 134.0, 131.0, 130.0, 129.9, 129.3, 128.4, 127.1, 126.3, 124.7, 123.2, 122.9. HR ESI-MS (DMSO/DCM/MeOH, negative mode) m/z = 397.0185 $[M]^-$ (calc. for $C_{18}H_9N_2O_7S$, 397.0136). IR ν (cm^{-1}) 3082, 1709, 1670, 1658, 1589, 1487, 1421, 1342, 1230, 1152. UV-vis (MeOH) λ_{max} (nm) (ε (L mol^{-1} cm^{-1})) 217 (109945), 256 (68258), 329 (31710).

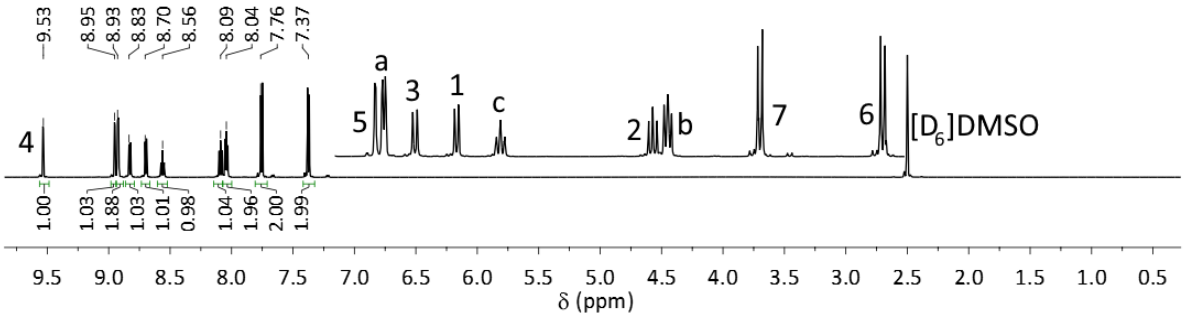

Figure 1.15 ^{1}H NMR spectrum (600 MHz, [D_6]DMSO, 298 K) for [pyridinium]**Para-NO_2**.

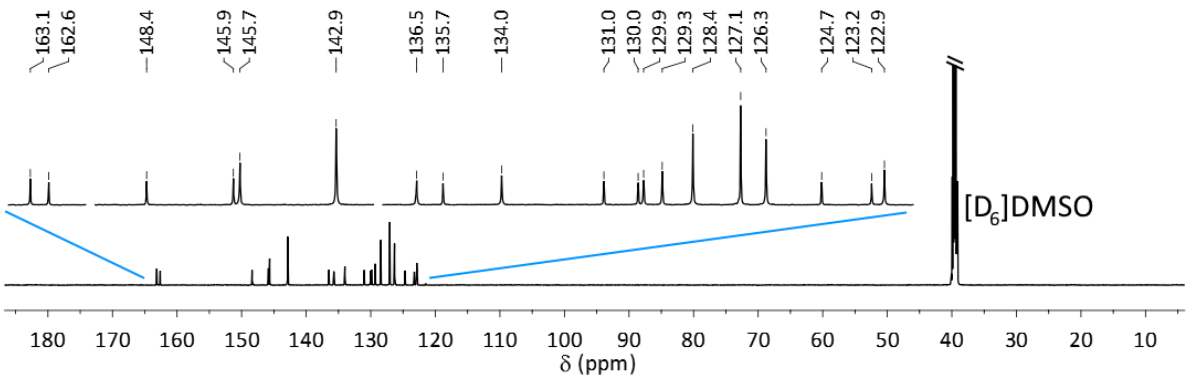

Figure 1.16 ^{13}C NMR spectrum (150 MHz, [D_6]DMSO, 298 K) for [pyridinium]**Para-NO_2**.

1.5.2. [Pyridinium]Meta-NO_2

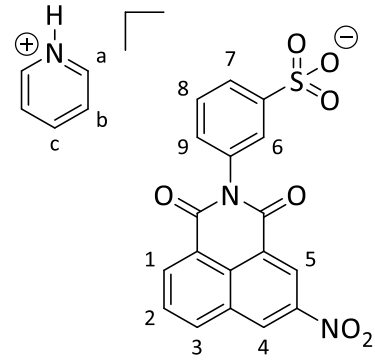

A solution of 3-nitro-1,8-naphthalic anhydride (1.00 g, 4.11 mmol) and 3-aminobenzenesulfonic acid (0.73 g, 4.2 mmol) in pyridine (15 mL) was heated at reflux for 8 hours. The solution turned yellow orange and a pale solid precipitated. This solution was filtered while hot, and the solid was washed with diethyl ether (50 mL), before being air dried overnight (1.85 g, 3.75 mmol, 94%). 9.53 (1H, d, *J* = 2.3 Hz, H_4), 8.95 (1H, d, *J* = 2.2 Hz, H_5), 8.92 (2H, br, H_a), 8.82 (1H, d, *J* = 8.3 Hz, H_3), 8.70 (1H, d, *J* = 8.3 Hz, H_1), 8.54 (1H, t, *J* = 7.8 Hz, H_c), 8.09 (1H, t, *J* = 8.1 Hz, H_2), 8.03 (2H, t, *J* = 7.3 Hz, H_b), 7.69 (1H, d, *J* = 7.7 Hz, H_7), 7.66 (1H, s, H_6), 7.50 (1H, t, *J* = 7.8 Hz, H_8), 7.35 (1H, d, *J* = 8.6 Hz, H_9). ^{13}C NMR (150 MHz, [D_6]DMSO, 298 K) *δ*: 163.2, 162.6, 149.3, 145.9, 145.4, 143.0, 136.4, 135.1, 133.9, 131.0, 130.1, 129.8, 129.3, 129.1, 128.4, 127.0, 126.3, 125.8, 124.9, 123.4, 122.7. HR ESI-MS (DMSO/DCM/MeOH, negative mode) *m/z* = 397.0053 $[M]^-$ (calc. for $C_{18}H_9N_2O_7S$, 397.0136). IR *v* (cm^{-1}) 3090, 1715, 1672, 1593, 1593, 1419, 1338, 1244, 1219, 1156, 1034. UV-vis (Methanol) λ_{max}(nm) (ε (L mol^{-1} cm^{-1})) 214 (121880), 261 nm (73000), 328 (33130).

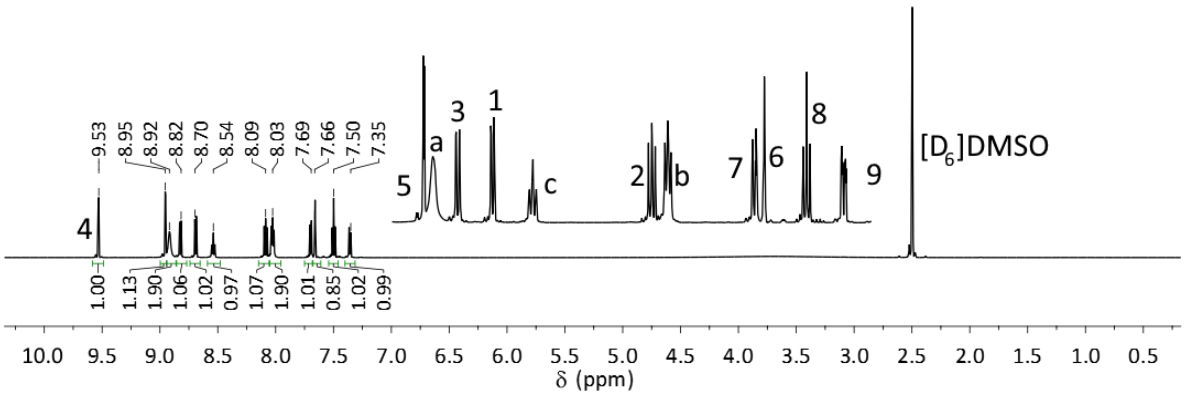

Figure 1.17 ^{1}H NMR spectrum (600 MHz, [D_6]DMSO, 298 K) for [pyridinium]**Meta-NO_2**.

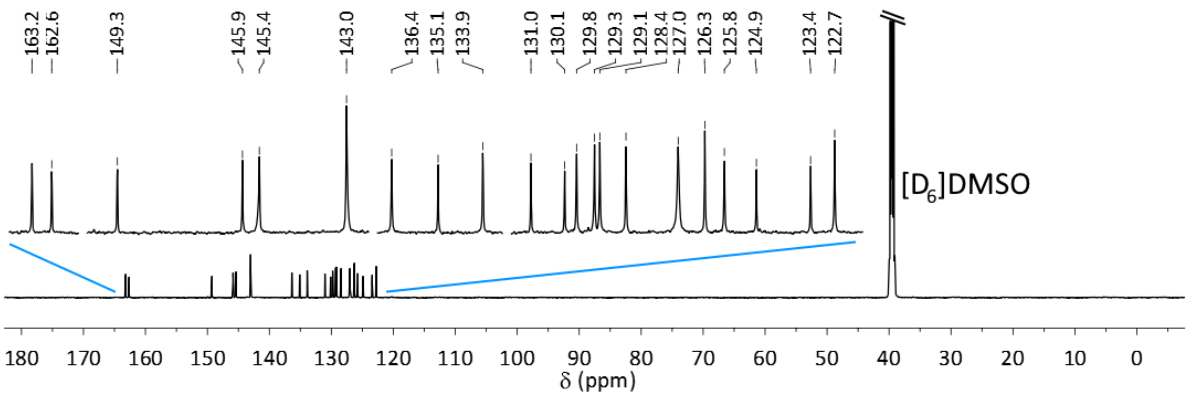

Figure 1.18 ^{13}C NMR spectrum (150 MHz, [D_6]DMSO, 298 K) for [pyridinium]**Meta-NO_2**.

1.6. Guests

1.6.1. Para-H

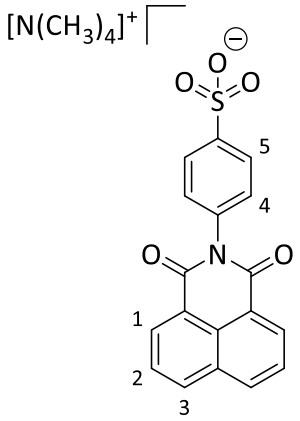

To a solution of [pyridinium](**Para-H**)[2] (50 mg, 0.12 mmol) and $[N(CH_3)_4]OH{\cdot}5H_2O$ (22 mg, 0.12 mmol) in DMSO (3 mL) was added DCM (5 mL) and then diethyl ether (22 mL). The precipitate was collected via centrifugation (4000 RPM, 15 minutes), and then resuspended with sonication in DCM (10 mL). The precipitate was collected via centrifugation (4000 RPM, 15 minutes) and dried to give the product as a colourless powder (44 mg, 0.10 mmol, 90%). ^{1}H NMR (600 MHz, [D_6]DMSO, 298 K) δ: 8.49 – 8.47 (4H, m, $H_{1,3}$), 7.87 (2H, t, J = 7.9 Hz, H_2), 7.69 (2H, d, J = 8.4 Hz, H_7), 7.31 (2H, d, J = 8.3 Hz, H_6), 3.05 (12H, s, $[N(CH_3)_4]^+$). ^{13}C NMR (150 MHz, [D_6]DMSO, 298 K) δ: 163.8, 148.2, 136.1, 134.6, 131.5, 130.8, 128.5, 127.9, 127.3, 126.2, 122.7, 54.4. HR ESI-MS (DMSO/DCM/MeOH, negative mode) *m/z* = 352.0622 $[M]^-$ (calc. for $C_{18}H_{10}NO_5S$, 352.0285). IR *v* (cm^{-1}) 3094, 1711, 1673, 1654, 1489, 1215, 1197, 1012, 948. UV-vis (DMSO) λ_{max}(nm) (ε (L mol^{-1} cm^{-1})) 336 (21500).

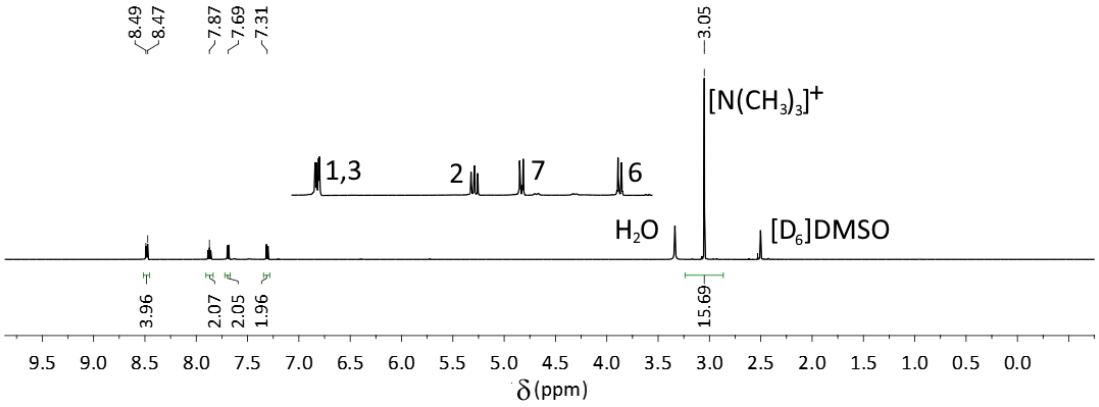

Figure 1.19 ^{1}H NMR spectrum (600 MHz, [D_6]DMSO, 298 K) of **Para-H**.

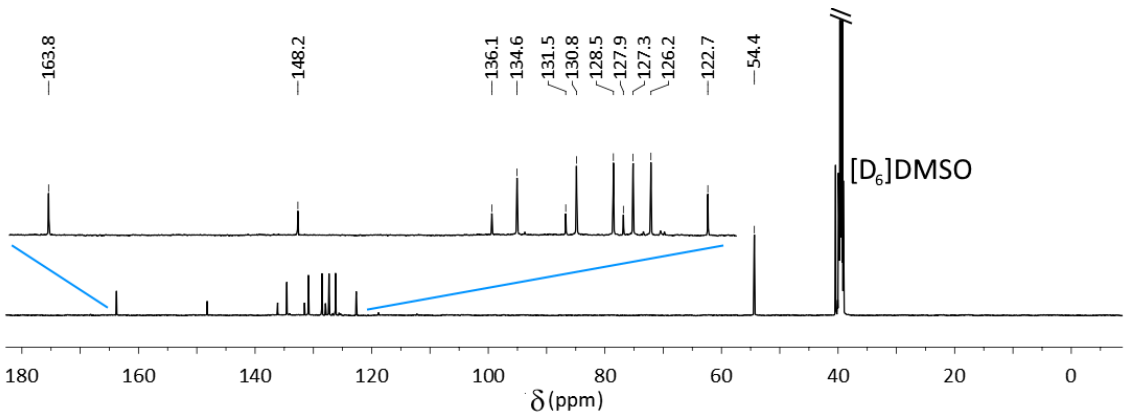

Figure 1.20 ^{13}C NMR spectrum (150 MHz, [D_6]DMSO, 298 K) of **Para-H**.

1.6.2. Meta-H

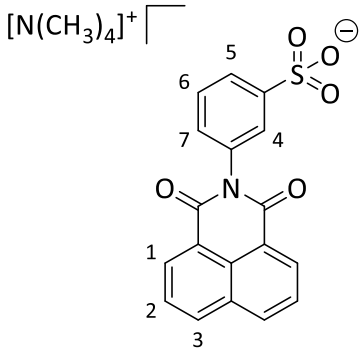

To a solution of [pyridinium](**Meta-H**)[2] (50 mg, 0.12 mmol) and $[N(CH_3)_4]OH{\cdot}5H_2O$ (22 mg, 0.12 mmol) in DMSO (3 mL) was added DCM (5 mL) and then diethyl ether (22 mL). The precipitate was collected via centrifugation (4000 RPM, 15 minutes), and then resuspended with sonication in DCM (10 mL). The precipitate was collected via centrifugation (4000 RPM, 15 minutes) and dried to give the product as a colourless powder (45 mg, 0.11 mmol, 92%). ^{1}H NMR (600 MHz, [D_6]DMSO, 298 K) δ: 8.48 – 8.47 (4H, m, $H_{1,3}$), 7.87 (2H, t, J = 7.9 Hz, H_2), 7.64 (1H, d, J = 6.4 Hz, H_5), 7.55 (1H, s, H_4), 7.44 (1H, t, J = 7.8 Hz, H_6), 7.30 (1H, d, J = 7.8 Hz, H_7), 3.05 (12H, s, $[N(CH_3)_4]^+$). ^{13}C NMR (150 MHz, [D_6]DMSO, 298 K) δ: 163.8, 149.2, 135.5, 134.5, 131.5, 130.8, 129.3, 128.4, 128.0, 127.3, 126.3, 125.5, 122.8, 54.3. HR ESI-MS (DMSO/DCM/MeOH, negative mode) *m/z* = 352.0527 $[M]^-$ (calc. for $C_{18}H_{10}NO_5S$, 352.0285). IR ν (cm^{-1}) 3076, 1713, 1673, 1490, 1339, 1214, 1197, 1011, 949. UV-vis (DMSO) λ_{max}(nm) (ε (L mol^{-1} cm^{-1})) 338 (23600).

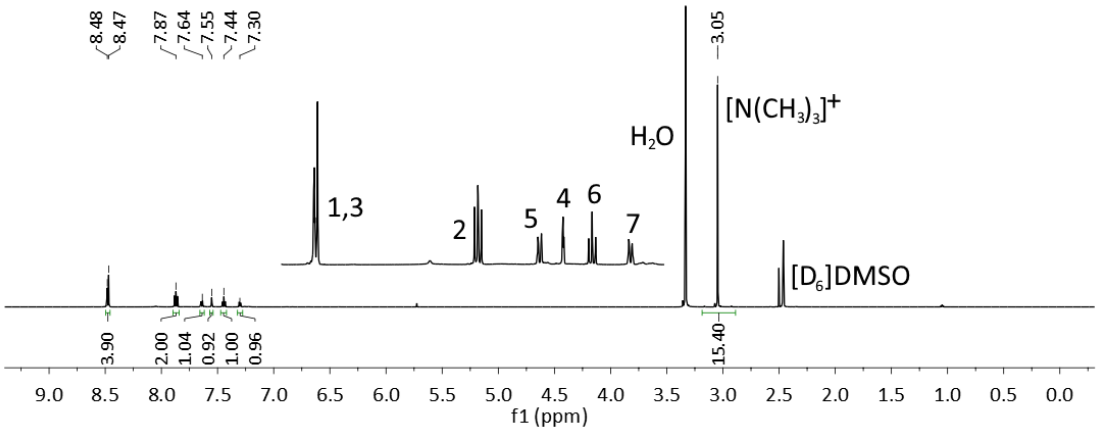

Figure 1.21 ^{1}H NMR spectrum (600 MHz, [D_6]DMSO, 298 K) of **Meta-H**.

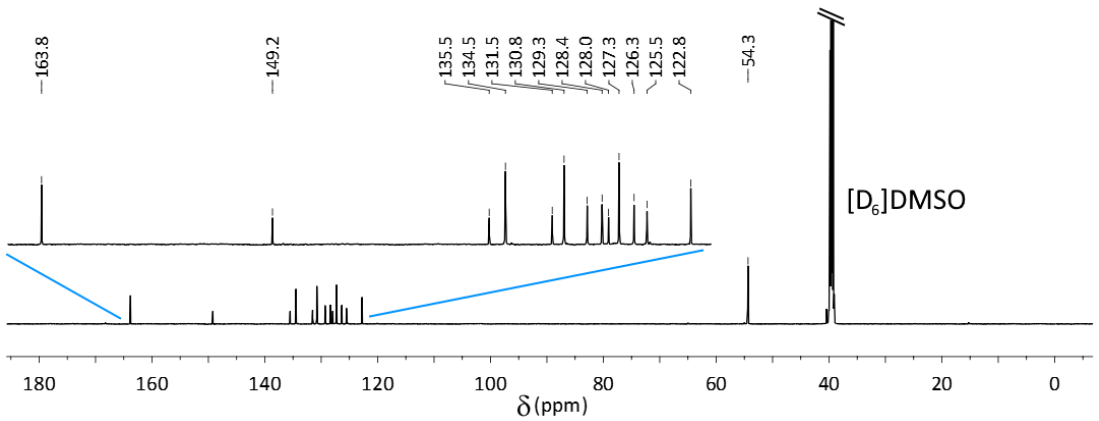

Figure 1.22 ^{13}C NMR spectrum (150 MHz, [D_6]DMSO, 298 K) of **Meta-H**.

1.6.3. Para-NH_2

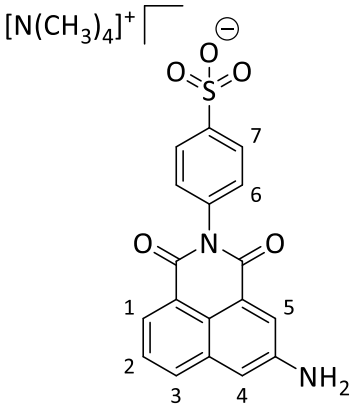

Pyridinium(**para-NO_2**) (190 mg, 0.41 mmol) and 10% Pd/C (20 mg) were stirred under a hydrogen atmosphere in methanol (20 mL) for 24 hours. The suspension was filtered to give a bright yellow solution that on removal of solvent under vacuum gave an orange solid. The solid was dissolved in DMSO (2 mL), and $[N(CH_3)_4]OH{\cdot}5H_2O$ (57 mg, 0.31 mmol) in DMSO (1 mL) was added. To this solution was added DCM (5 mL) and then diethyl ether (22 mL). The precipitate was collected via centrifugation (4000 RPM, 15 minutes), and then resuspended with sonication in DCM (10 mL). The precipitate was collected via centrifugation (4000 RPM, 15 minutes) and dried to give the product as a brown solid (154 mg, 0.350 mmol, 85%). ^{1}H NMR (600 MHz, [D_6]DMSO, 298 K) δ: 8.09 – 8.08 (2H, m, $H_{1,3}$), 7.99 (1H, d, J = 2.6 Hz, H_4), 7.70 (2H, d, J = 8.3 Hz, H_7), 7.64 (1H, t, J = 8.1 Hz, H_2), 7.32 (1H, d, J = 2.6 Hz, H_5), 7.31 (2H, d, J = 8.7 Hz, H_4), 6.03 (2H, br, NH_2), 3.07 (16H, s, $[N(CH_3)_4]^+$. ^{13}C NMR (150 MHz, [D_6]DMSO, 298 K) δ: 164.1, 163.9, 148.2, 147.9, 136.3, 133.8, 131.7, 128.5, 127.0, 126.2, 125.5, 123.1, 122.3, 121.8, 121.1, 118.0, 54.0. HR ESI-MS (DMSO/DCM/MeOH, negative mode) m/z = 367.0399 $[M]^-$ (calc. for $C_{18}H_{11}N_2O_5S$, 367.0394). IR ν (cm^{-1}) 3408, 1661, 1622, 1211, 1182, 1120, 1032, 1012, 950. UV-vis (DMSO) λ_{max}(nm) (ε (L mol^{-1} cm^{-1})) 283 (15600), 345 (9381), 447 (4380).

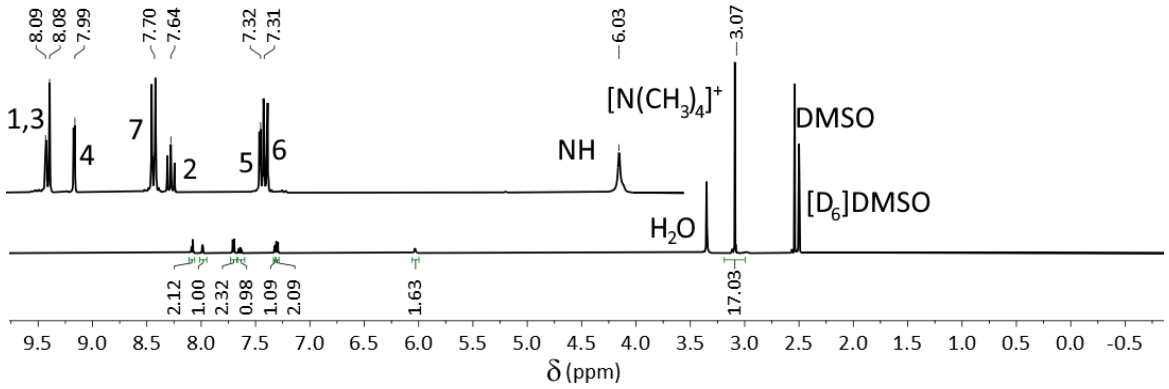

Figure 1.23 ^{1}H NMR spectrum (600 MHz, [D_6]DMSO, 298 K) of **Para-NH_2**.

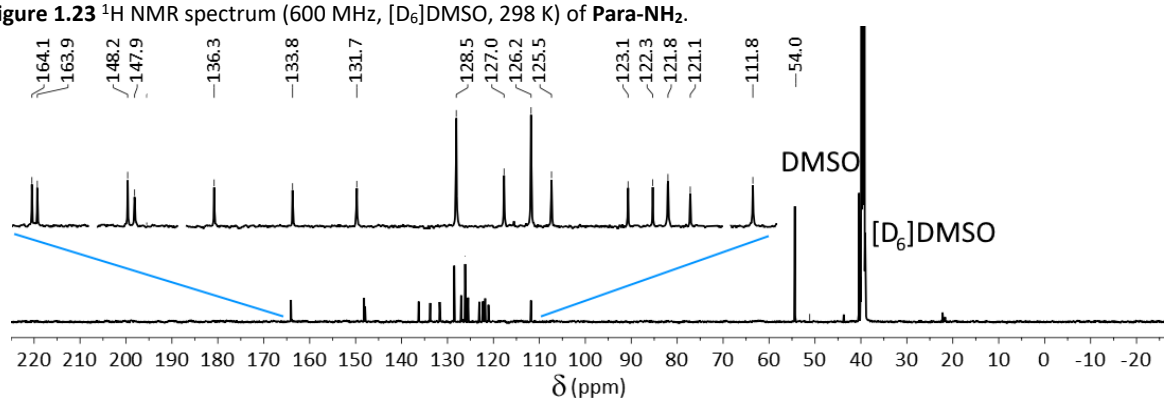

Figure 1.24 ^{13}C NMR spectrum (150 MHz, [D_6]DMSO, 298 K) of **Para-NH_2**.

1.6.4. Meta-NH_2

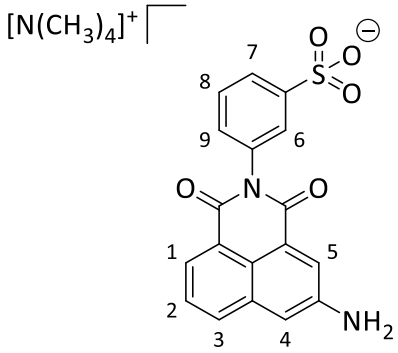

Pyridinium(**meta-NO_2**) (99 mg, 0.21 mmol) and 10% Pd/C (20 mg) were stirred under a hydrogen atmosphere in methanol (20 mL) for 24 hours. The suspension was filtered to give a bright yellow solution that on removal of solvent under vacuum gave a red/orange solid. The solid was dissolved in DMSO (2 mL), and $[N(CH_3)_4]OH{\cdot}5H_2O$ (22 mg, 0.12 mmol) in DMSO (1 mL) was added. To this solution was added DCM (5 mL) and then diethyl ether (22 mL). The precipitate was collected via centrifugation (4000 RPM, 15 minutes), and then resuspended with sonication in DCM (10 mL). The precipitate was collected via centrifugation (4000 RPM, 15 minutes) and dried to give the product as a brown solid (60 mg, 0.14 mmol, 64%). ^{1}H NMR (600 MHz, [D_6]DMSO, 298 K) δ: 8.08 – 8.07 (2H, m, $H_{1,3}$), 7.99 (1H, d, J = 1.1 Hz, H_4), 7.67 – 7.63 (2H, m, $H_{2,7}$), 7.53 (1H, t, J = 1.2 Hz, H_6), 7.46 (1H, t, J = 3.8 Hz, H_8), 7.32 (1H, d, J = 1.3 Hz, J = H_5), 7.30 (1H, d, J = 3.8 Hz, H_9), 6.04 (2H, br, NH_2), 3.09 (12H, s, $[N(CH_3)_4]^+$). ^{13}C NMR (150 MHz, [D_6]DMSO, 298 K) δ: 164.1, 163.9, 149.2, 147.9, 135.6, 133.8, 131.6, 129.3, 128.3, 127.0, 126.3, 125.4, 125.4, 123.1, 122.3, 121.7, 121.1, 111.8, 54.4. HR ESI-MS (DMSO/DCM/MeOH, negative mode) m/z = 367.0396 $[M]^-$ (calc. for $C_{18}H_{11}N_2O_5S$, 367.0394). IR ν (cm^{-1}) 3448, 3367, 3228, 3068, 2924, 2853, 2770, 1696, 1655, 1619, 1578, 1220, 1170, 1030, 616. UV-vis (DMSO) λ_{max}(nm) (ε (L mol^{-1} cm^{-1})) 277 (16200), 347 (8890), 445 (3810).

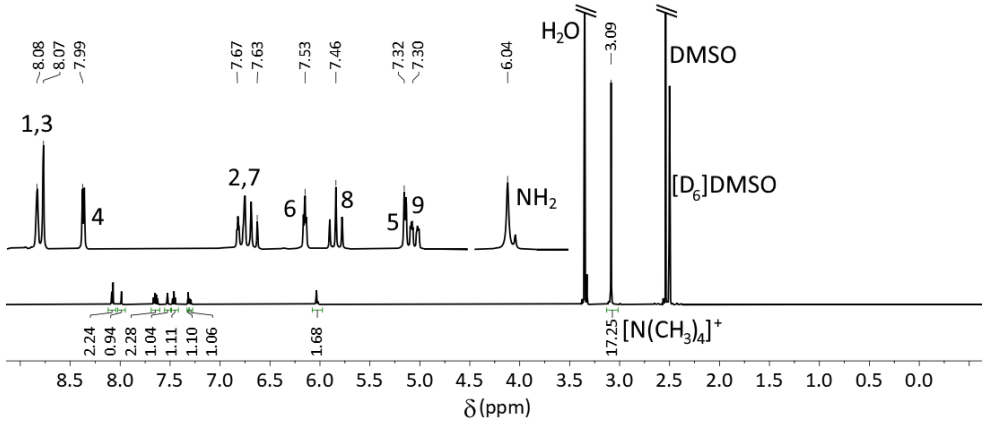

Figure 1.25 ^{1}H NMR spectrum (600 MHz, [D_6]DMSO, 298 K) of **Meta-NH_2**.

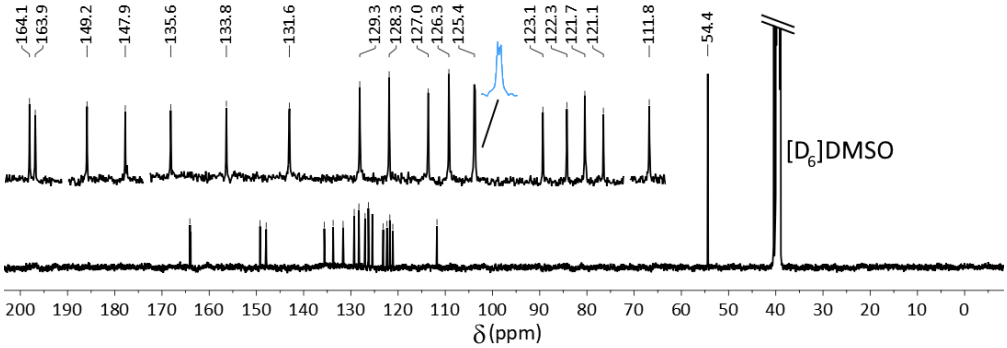

Figure 1.26 ^{13}C NMR spectrum (150 MHz, [D_6]DMSO, 298 K) of **Meta-NH_2**.

1.6.5. Para-NO_2

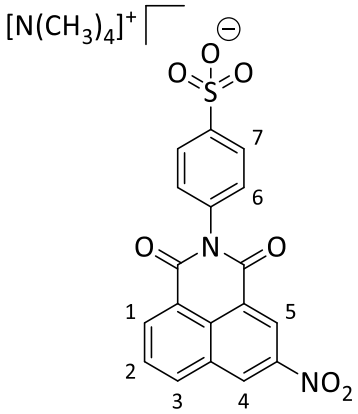

To a solution of [pyridinium](**Para-NO_2**) (50 mg, 0.11 mmol) and $[N(CH_3)_4]OH{\cdot}5H_2O$ (21 mg, 0.12 mmol) in DMSO (3 mL) was added DCM (5 mL) and then diethyl ether (22 mL). The precipitate was collected via centrifugation (4000 RPM, 15 minutes), and then resuspended with sonication in DCM (10 mL). The precipitate was collected via centrifugation (4000 RPM, 15 minutes) and dried to give the product as a violet powder (46 mg, 0.10 mmol, 94%). ^{1}H NMR (600 MHz, [D_6]DMSO, 298 K) δ: 9.55 (1H, d, J = 2.2 Hz, H_4), 8.97 (1H, d, J = 2.2 Hz, H_5), 8.83 (1H, d, J = 8.2 Hz, H_3), 8.70 (1H, d, J = 6.7 Hz, H_1), 8.10 (1H, t, J = 7.7 Hz, H_2), 7.73 (2H, d, J = 8.3 Hz, H_7), 7.36 (2H, d, J = 8.3 Hz, H_6), 3.09 (12H, s, $[N(CH_3)_4]^+$). ^{13}C NMR (150 MHz, [D_6]DMSO, 298 K) δ: 163.2, 162.6, 148.5, 145.9, 136.5, 135.6, 134.0, 131.0, 130.1, 129.9, 129.3, 128.4, 126.3, 124.7, 123.3, 122.9, 54.4. HR ESI-MS (DMSO/DCM/MeOH, negative mode) m/z = 397.0225 $[M]^-$ (calc. for $C_{18}H_9N_2O_7S$, 397.0136). IR ν (cm^{-1}) 3095, 1713, 1675, 1535, 1490, 1215, 1197, 1177, 1030, 1011, 796. UV-vis (DMSO) λ_{max}(nm) (ε (L mol^{-1} cm^{-1})) 283 (15600), 345 (9381), 447 (4380).

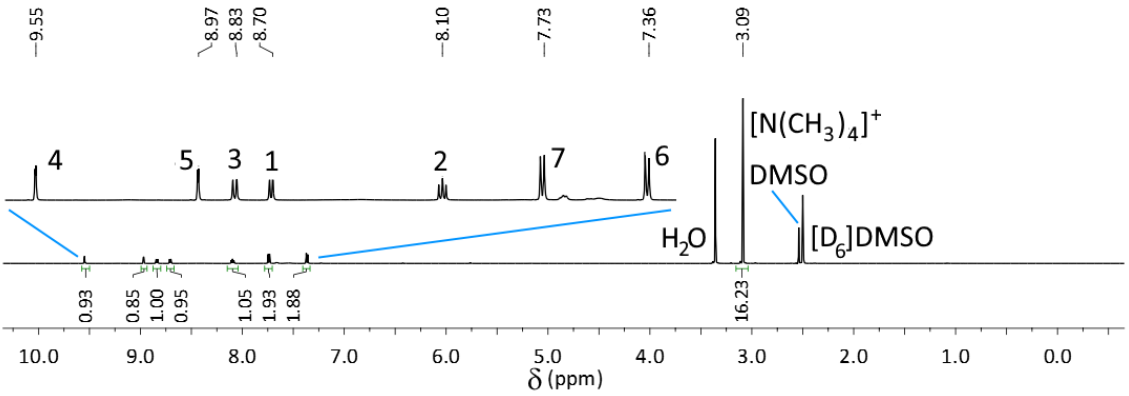

Figure 1.27 ^{1}H NMR spectrum (600 MHz, [D_6]DMSO, 298 K) of **Para-NO_2**.

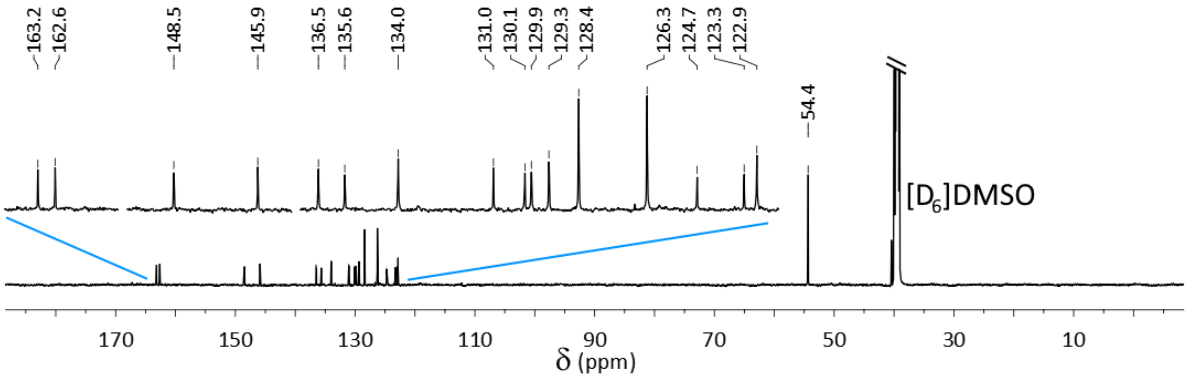

Figure 1.28 ^{13}C NMR spectrum (150 MHz, [D_6]DMSO, 298 K) of **Para-NO_2**.

1.6.6. Meta-NO_2

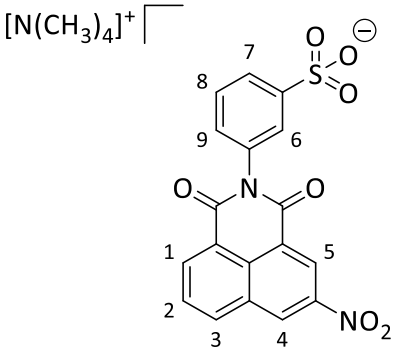

To a solution of [pyridinium](**Meta-NO_2**) (50 mg, 0.11 mmol) and $[N(CH_3)_4]OH{\cdot}5H_2O$ (21 mg, 0.12 mmol) in DMSO (3 mL) was added DCM (5 mL) and then diethyl ether (22 mL). The precipitate was collected via centrifugation (4000 RPM, 15 minutes), and then resuspended with sonication in DCM (10 mL). The precipitate was collected via centrifugation (4000 RPM, 15 minutes) and dried to give the product as a violet powder (47 mg, 0.11 mmol, 96%). ^{1}H NMR (600 MHz, [D_6]DMSO, 298 K) δ: 9.54 (1H, d, J = 2.2 Hz, H_5), 8.96 (1H, d, J = 2.3 Hz, H_4), 8.82 (1H, d, J = 8.0 Hz, H_3), 8.69 (1H, d, J = 6.7 Hz, H_1), 8.09 (1H, t, J = 7.8 Hz, H_2), 7.69 (1H, d, J = 7.8 Hz, H_9), 7.66 (1H, s, H_7), 7.50 (1H, t, J = 7.7 Hz, H_8), 7.35 (1H, d, J = 7.9 Hz, H_9), 3.09 (12H, s, $[N(CH_3)_4]^+$). ^{13}C NMR (150 MHz, [D_6]DMSO, 298 K) δ: 163.2, 162.7, 149.3, 145.9, 136.4, 135.1, 133.9, 131.0, 130.1, 129.8, 129.3, 129.1, 128.4, 126.3, 125.7, 124.9, 123.4, 122.7, 54.3. HR ESI-MS (DMSO/DCM/MeOH, negative mode) m/z = 397.0092 $[M]^-$ (calc. for $C_{18}H_9N_2O_7S$, 397.0136). IR ν (cm^{-1}) 3076, 1713, 1674, 1591, 1535, 1339, 1245, 1215, 1197, 1030, 795. UV-vis (DMSO) λ_{max}(nm) (ε (L mol^{-1} cm^{-1})) 283 (28200), 336 (*shoulder*, 11200).

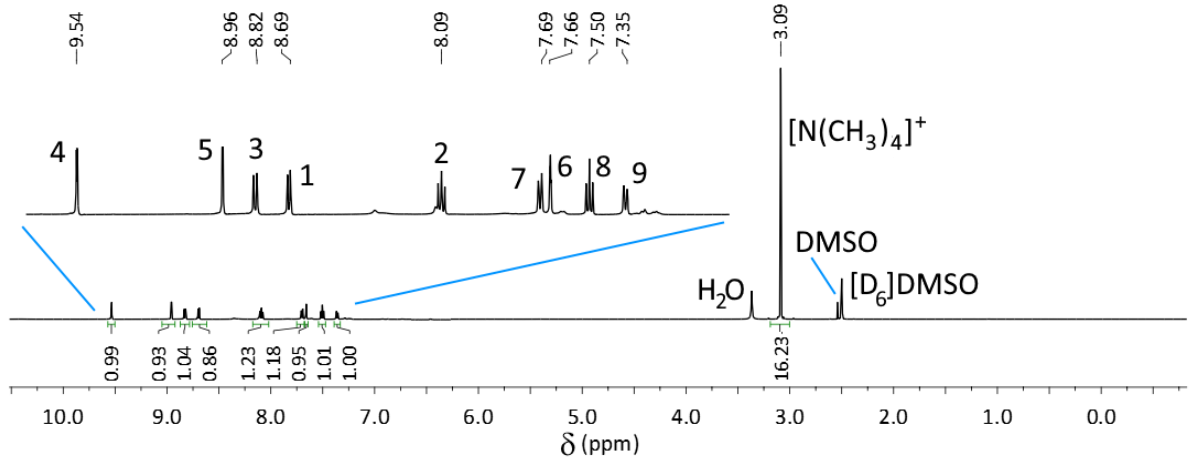

Figure 1.29 ^{1}H NMR spectrum (600 MHz, [D_6]DMSO, 298 K) of **Meta-NO_2**.

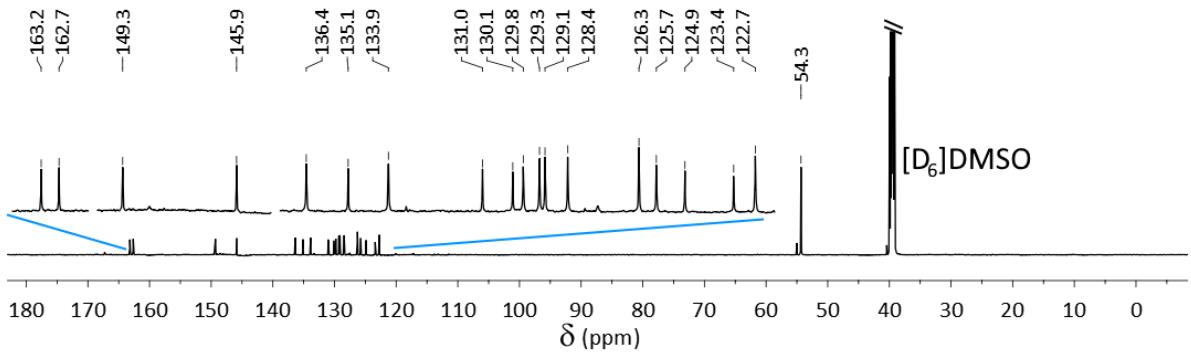

Figure 1.30 ^{13}H NMR spectrum (150 MHz, [D_6]DMSO, 298 K) of **Meta-NO_2**.

1.6.7. Para-SO_3

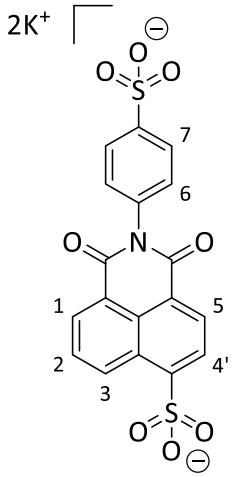

Potassium 4-sulfonate-1,8-naphthalic anhydride (0.50 g, 1.6 mmol) and 4-aminobenzenesulfonic acid (0.27 g, 1.6 mmol) were heated at 100 °C in pyridine (10 mL) and H_2O (5 mL) for 48 hours. On cooling to room temperature a precipitate formed which was filtered to give an off-white solid (0.37 g, 0.85 mmol, 54%). ^{1}H NMR (600 MHz, [D_6]DMSO, 298 K) δ: 9.29 (1H, d, J = 9.8 Hz, H_3), 8.50 (1H, d, J = 8.3 Hz, H_1), 8.48 (1H, d, J = 7.5 Hz, H_5), 8.24 (1H, d, J = 7.6 Hz, $H_{4'}$), 7.91 (1H, dd, J = 8.9 Hz, 8.6 Hz, H_2), 7.74 (2H, d, J = 8.4 Hz, H_7), 7.36 (2H, d, J = 8.4 Hz, H_6). ^{13}C NMR (150 MHz, [D_6]DMSO, 298 K) δ: 163.9, 163.5, 149.9, 148.1, 136.1, 134.3, 130.5, 130.2, 128.6, 128.6, 127.7, 126.9, 126.2, 125.0, 123.3, 122.6. HR ESI-MS (DMSO/DCM/MeOH, negative mode) m/z = $[M]^{2-}$ 215.4837 (calc. for $C_{18}H_9NO_8S_2$, 215.4879) 469.9394 $[MK]^-$ (calc. for $C_{18}H_9NO_8S_2$, 469.9401). IR ν (cm^{-1}) 3435, 3069, 2922, 2852, 1707, 1666, 1585, 1362, 1211, 1180, 1121, 1102, 1032, 748. UV-vis (DMSO) λ_{max}(nm) (ε (L mol^{-1} cm^{-1})) 343 (16900).

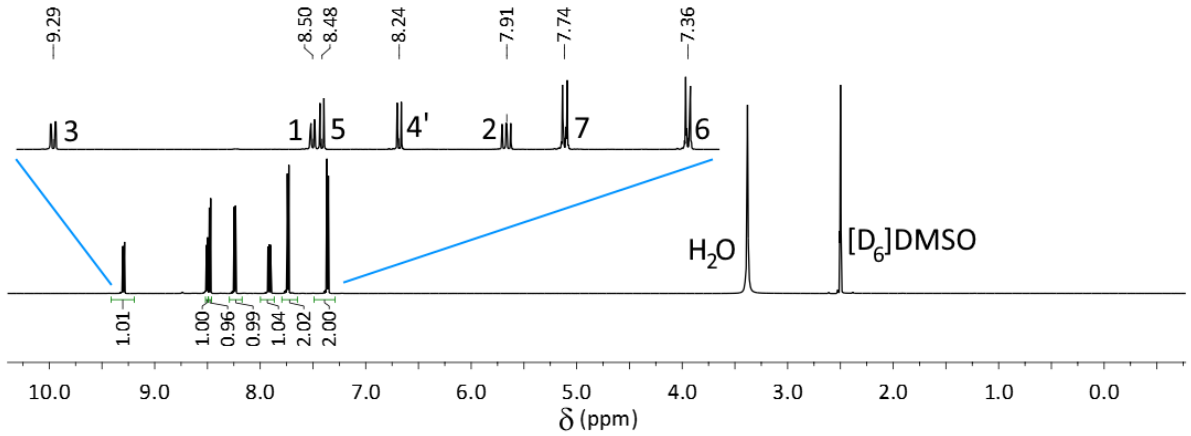

Figure 1.31 ^{1}H NMR spectrum (600 MHz, [D_6]DMSO, 298 K) of **Para-SO_3**.

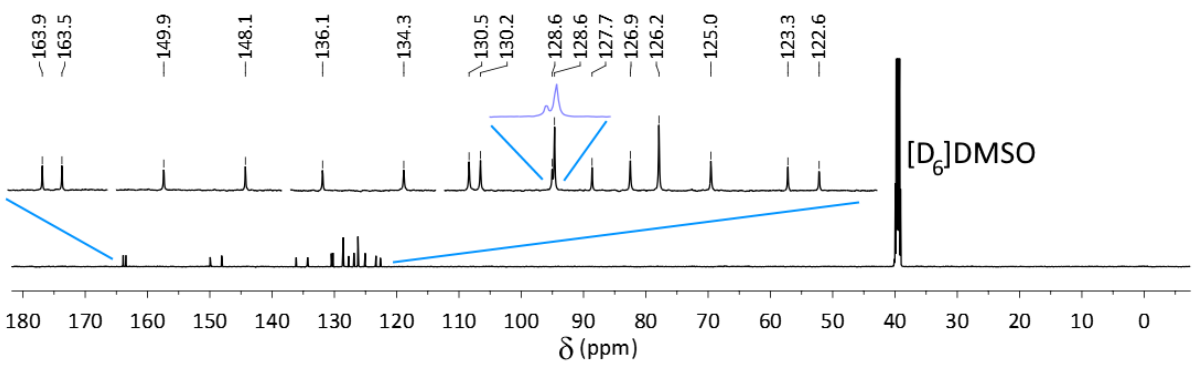

Figure 1.32 ^{13}C NMR spectrum (150 MHz, [D_6]DMSO, 298 K) of **Para-SO_3**.

1.6.8. Meta-SO_3

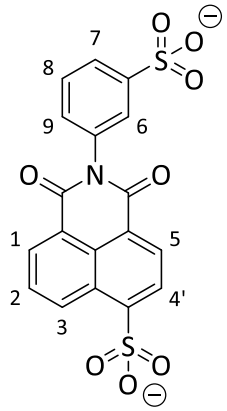

Potassium 4-sulfonate-1,8-naphthalic anhydride (0.50 g, 1.6 mmol) and 3-aminobenzenesulfonic acid (0.27 g, 1.6 mmol) were heated at 100 °C in pyridine (10 mL) and H_2O (5 mL) for 48 hours. On cooling to -20 °C a precipitate formed which was filtered to give an off-white solid (0.31 g, 0.71 mmol, 45%). ^{1}H NMR (600 MHz, [D_6]DMSO, 298 K) δ: 9.28 (1H, d, J = 7.6 Hz, H_3), 8.49 (1H, d, J = 7.2 Hz, H_1), 8.47 (1H, d, J = 7.6 Hz, H_5), 7.90 (1H, d, J = 7.5 Hz, $H_{4'}$), 7.90 (1H, dd, J = 8.1 Hz, 7.2 Hz, H_2), 7.68 (1H, d, J = 7.8 Hz, H_7), 7.61 (1H, s, H_6), 7.48 (1H, t, J = 7.8 Hz, H_8), 7.35 (1H, d, J = 8.0 Hz, H_9). ^{13}C NMR (150 MHz, [D_6]DMSO, 298 K) δ: 163.9, 163.5, 149.9, 149.1, 135.5, 134.2, 130.4, 130.1, 129.3, 128.6, 128.3, 127.7, 126.8, 126.4, 125.5, 125.0, 123.4, 122.7. HR ESI-MS (DMSO/DCM/MeOH, negative mode) m/z = $[M]^{2-}$ 215.4908 (calc. for $C_{18}H_9NO_8S_2$, 215.4879) 469.9423 $[MK]^-$ (calc. for $C_{18}H_9NO_8S_2$, 469.9401). IR ν (cm^{-1}) 3422, 3062, 1706, 1666, 1584, 1209, 1179, 1032, 748. UV-vis (DMSO) λ_{max}(nm) (ε (L mol^{-1} cm^{-1})) 344 (20700).

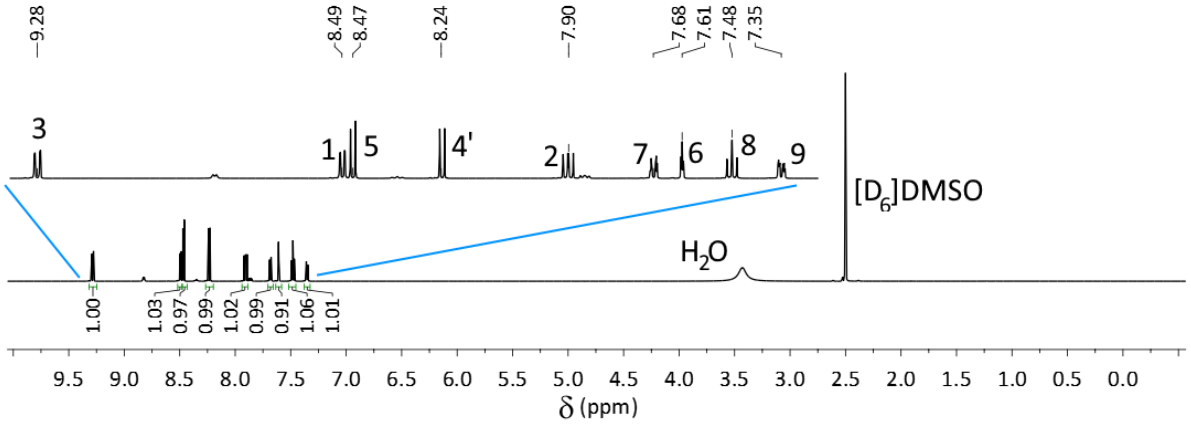

Figure 1.33 ^{1}H NMR spectrum (600 MHz, [D_6]DMSO, 298 K) of **Meta-SO_3**.

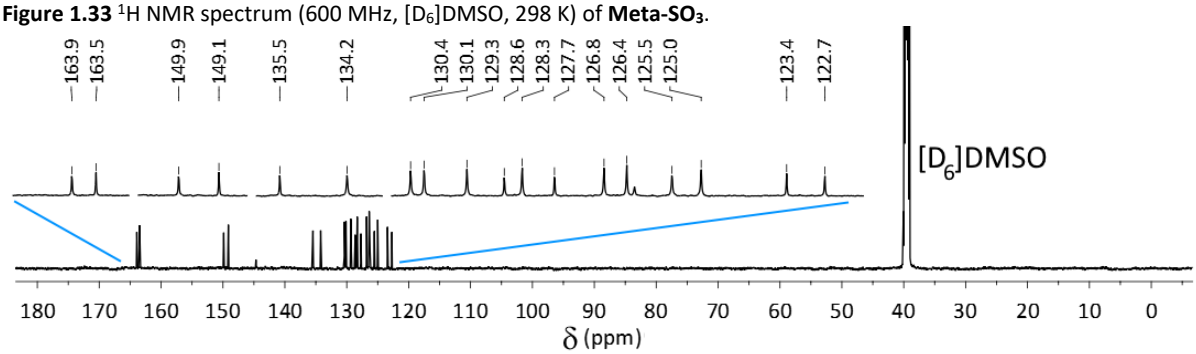

Figure 1.34 ^{13}C NMR spectrum (150 MHz, [D_6]DMSO, 298 K) of **Meta-SO_3**.

1.6.9. Comparison via ^{1}H NMR spectroscopy of naphthalimide sulfonate guests

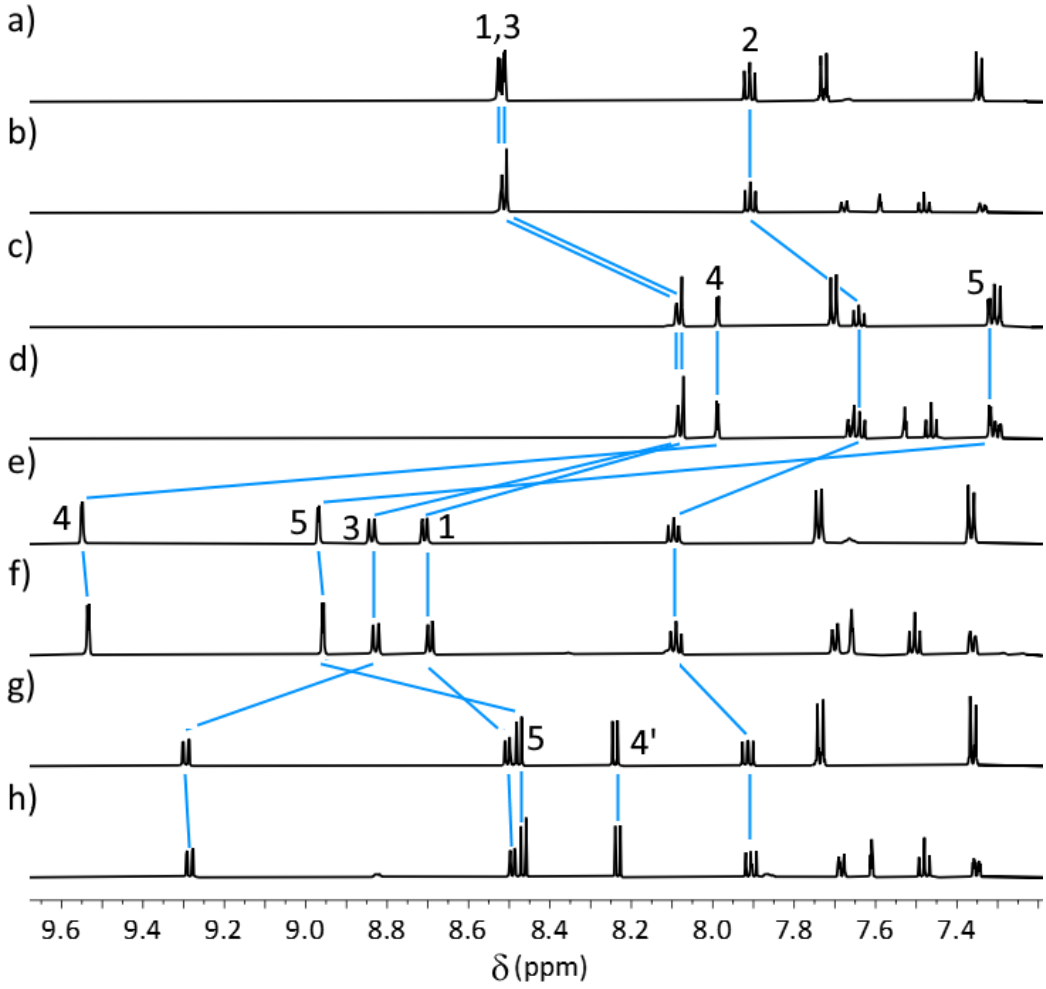

Figure 1.35 Partial stacked ^{1}H NMR spectra (600 MHz, [D_6]DMSO, 298 K) of a) **para-H**, b) **meta-H**, c) **para-NH$_2$**, d) **meta-NH$_2$**, e) **para-NO$_2$**, f) **meta-NO$_2$**, g) **para-SO$_3$**, and h) **meta-SO$_3$**.

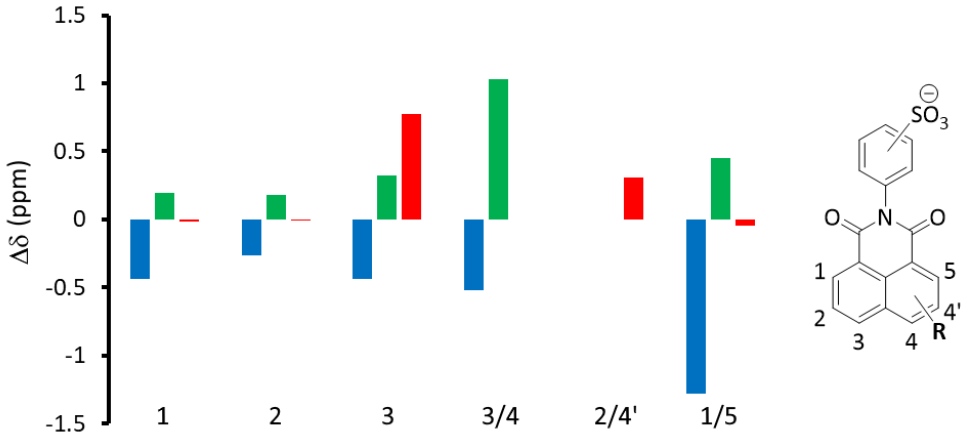

Figure 1.36 ^{1}H NMR spectroscopic data (600 MHz, [D_6]DMSO, 298 K) comparing the chemical shifts for –NH_2 (■), -NO_2 (■) and –SO_3 (■) naphthalimide sulfonate guests, relative to the unsubstituted (-H) guests. Direct comparison of resonances 1,2 and 3, in substituted guests position four compared with 3 of -H substituted guest, position 4’ compared with 2 of -H substituted guest, position 5 compared with 1 of -H substituted guest.

2. Host-guest chemistry

2.1. Crystallography

2.1.1. [(Para-NO_2)$_2$⊂C](BF_4)$_2$

CCDC#: 1993280. Vapour diffusion of diethyl ether into a DMF solution of **C(BF_4)$_4$** and **Para-NO_2** gave colourless block crystals of (**Para-NO_2**)$_2$⊂**C1**(BF_4)$_2$. X-ray data were collected at 100 K on an Agilent Technologies Supernova system using Mo Kα radiation with exposures over 1.0°, and data were treated using CrysAlisPro[3] software. The structure was solved using SHELXT within OLEX2 and weighted full-matrix refinement on F^2 was carried out using SHELXL-97[4] running within the OLEX2[5] package. All non-hydrogen atoms were refined anisotropically. Hydrogen atoms attached to carbons were placed in calculated positions and refined using a riding model. The structure was solved in the monoclinic space group $P2_1/c$ and refined to an R_1 value of 13.0%. The asymmetric unit contained one half of the cage (i.e. two ligands, one Pd^{II} ion), one BF_4^- counterion, and one **Para-NO_2** molecule.

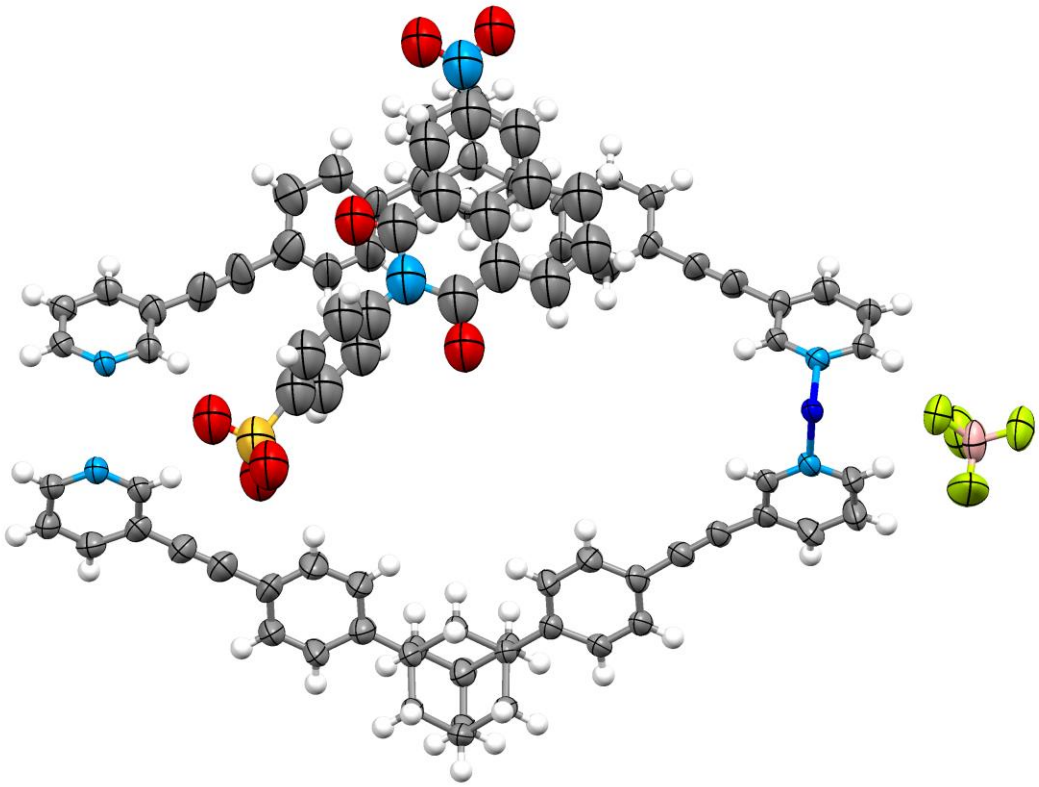

Figure 2.1 Mercury ellipsoid plot of the asymmetric unit of (**Para-NO_2**)$_2$⊂**C**(BF_4)$_2$. Ellipsoids shown at 50% probability level. Colour scheme: carbon grey, hydrogen white, boron salmon, fluorine yellow, nitrogen blue, oxygen red, palladium dark blue, sulphur orange.

Disorder in the guest **Para-NO_2** molecule was modelled with the DFIX, SADI, FLAT and SIMU commands. There was diffuse electron density within the lattice that could not be appropriately modelled, the SOLVENT MASK routine from within OLEX2 was employed to resolve this problem. There were two equivalent voids (each one 524 Å^3, 112 electrons) which we assign to, in each case, 2 x DMF and 2 x water solvent molecules.

Empirical formula	$C_{180}H_{138}B_2F_8N_{12}O_{14}Pd_2S_2$	μ/mm^{-1}	2.475
Formula weight	3143.56	F(000)	3240.0
Temperature/K	120.01(10)	Crystal size/mm^3	0.241 × 0.154 × 0.086
Crystal system	Monoclinic	Radiation	CuKα (λ = 1.54184)
Space group	$P2_1/c$	2Θ range for data collection/°	6.834 to 123.534
a/Å	17.4601(3)	Index ranges	-19 ≤ h ≤ 19, -29 ≤ k ≤ 29, -22 ≤ l ≤ 22
b/Å	25.8700(3)	Reflections collected	51249
c/Å	19.8200(3)	Independent reflections	13280 [R_{int} = 0.0284, R_{sigma} = 0.0267]
α/°	90	Data/restraints/parameters	13280/804/991
β/°	105.025(2)	Goodness-of-fit on F^2	1.670
γ/°	90	Final R indexes [I>=2σ (I)]	R_1 = 0.1301, wR_2 = 0.3579
Volume/Å^3	8646.5(2)	Final R indexes [all data]	R_1 = 0.1480, wR_2 = 0.3829
Z	2	Largest diff. peak/hole / e Å^{-3}	2.69/-1.57
ρ_{calc}g/cm^3	1.207		

2.1.2. [Meta-SO_3⊂C]Meta-SO_3·5DMF

CCDC#: 1993281. A 4:2:2 **L**/$Pd(SbF_6)_2$/**Meta-SO_3** solution was generated in the DMF ($Pd(SbF_6)_2$ was generated from the 1:2 combination of $[Pd(CH_3CN)_2Cl_2]$ and $AgSbF_6$ in DMF followed by centrifugation). Vapour diffusion of diethyl ether into this solution gave colourless needle crystals of [**Meta-SO_3⊂C**]**Meta-SO_3**·5DMF. X-ray data were collected at 100 K on an Agilent Technologies Supernova system using Mo Kα radiation with exposures over 1.0°, and data were treated using CrysAlisPro[3] software. The structure was solved using SHELXT within OLEX2 and weighted full-matrix refinement on F^2 was carried out using SHELXL-97[4] running within the OLEX2[5] package. All non-hydrogen atoms were refined anisotropically. Hydrogen atoms attached to carbons were placed in calculated positions and refined using a riding model. The structure was solved in the monoclinic space group *P*-1 and refined to an R_1 value of 15.9%. The asymmetric unit contained one cage (i.e. four ligands, two Pd^{II} ions), two **Meta-SO_3** molecules and five DMF solvent molecules.

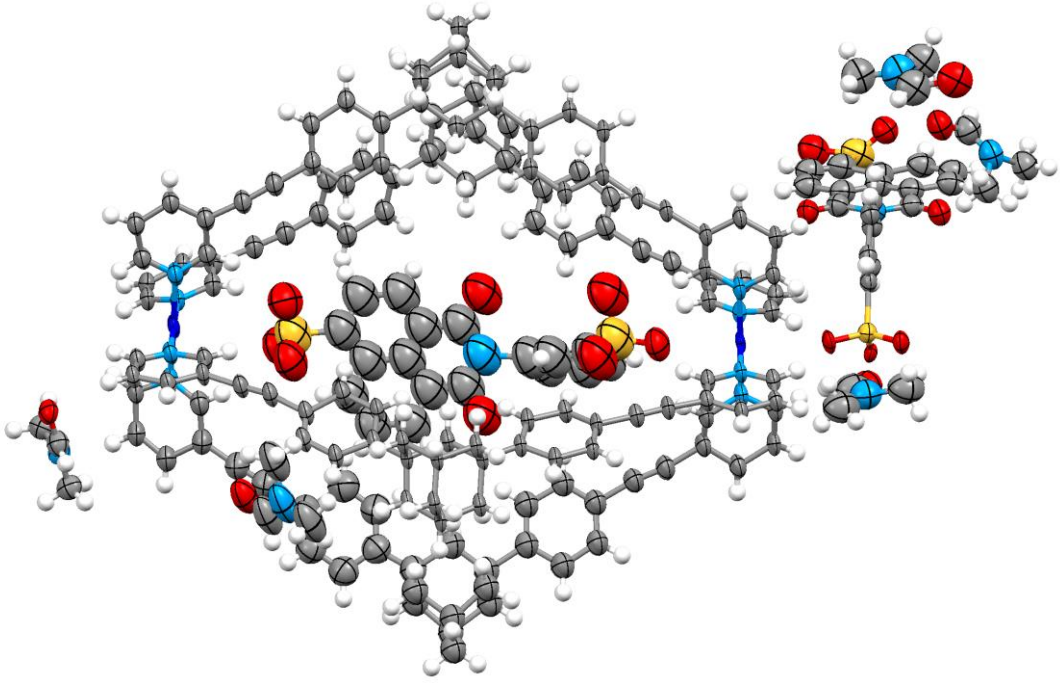

Figure 2.2 Mercury ellipsoid plot of the asymmetric unit of [**Meta-SO_3⊂C**]**Meta-SO_3**·5DMF. Ellipsoids shown at 50% probability level. Colour scheme: carbon grey, hydrogen white, boron salmon, fluorine yellow, nitrogen blue, oxygen red, palladium dark blue, sulphur orange.

The crystal selected was the best of multiple screenings. The diffraction was poor. The structure required extensive modelling, of the cage architecture, the two **Meta-SO_3** guests, and the DMF solvent molecules. This was carried out using the DFIX, ISOR, SIMU, SADI and FLAT commands. There was diffuse electron density within the lattice that could not be appropriately modelled, the SOLVENT MASK routine from within OLEX2 was employed to resolve this problem. There were two voids (1955 $Å^3$, 446 electrons, and 1001 $Å^3$, 201 electrons) which we assign to assorted solvent molecules.

Empirical formula	$C_{195}H_{171}N_{15}O_{21}Pd_2S_4$	μ/mm^{-1}	2.263
Formula weight	3401.50	F(000)	3540.0
Temperature/K	119.99(14)	Crystal size/mm^3	0.483 × 0.085 × 0.024
Crystal system	Triclinic	Radiation	CuKα (λ = 1.54184)
Space group	P-1	2Θ range for data collection/°	6.786 to 70.85
a/Å	17.7223(9)	Index ranges	-13 ≤ h ≤ 11, -18 ≤ k ≤ 18, -20 ≤ l ≤ 20
b/Å	25.0866(16)	Reflections collected	23428
c/Å	27.1532(15)	Independent reflections	8949 [R_{int} = 0.0864, R_{sigma} = 0.1069]
α/°	115.589(6)	Data/restraints/parameters	8949/5901/2144
β/°	98.126(5)	Goodness-of-fit on F^2	1.884
γ/°	101.174(5)	Final R indexes [I>=2σ (I)]	R_1 = 0.1590, wR_2 = 0.4091
Volume/$Å^3$	10330.3(11)	Final R indexes [all data]	R_1 = 0.2031, wR_2 = 0.4497
Z	2	Largest diff. peak/hole / e $Å^{-3}$	2.29/-1.25

2.2. Mass spectrometry

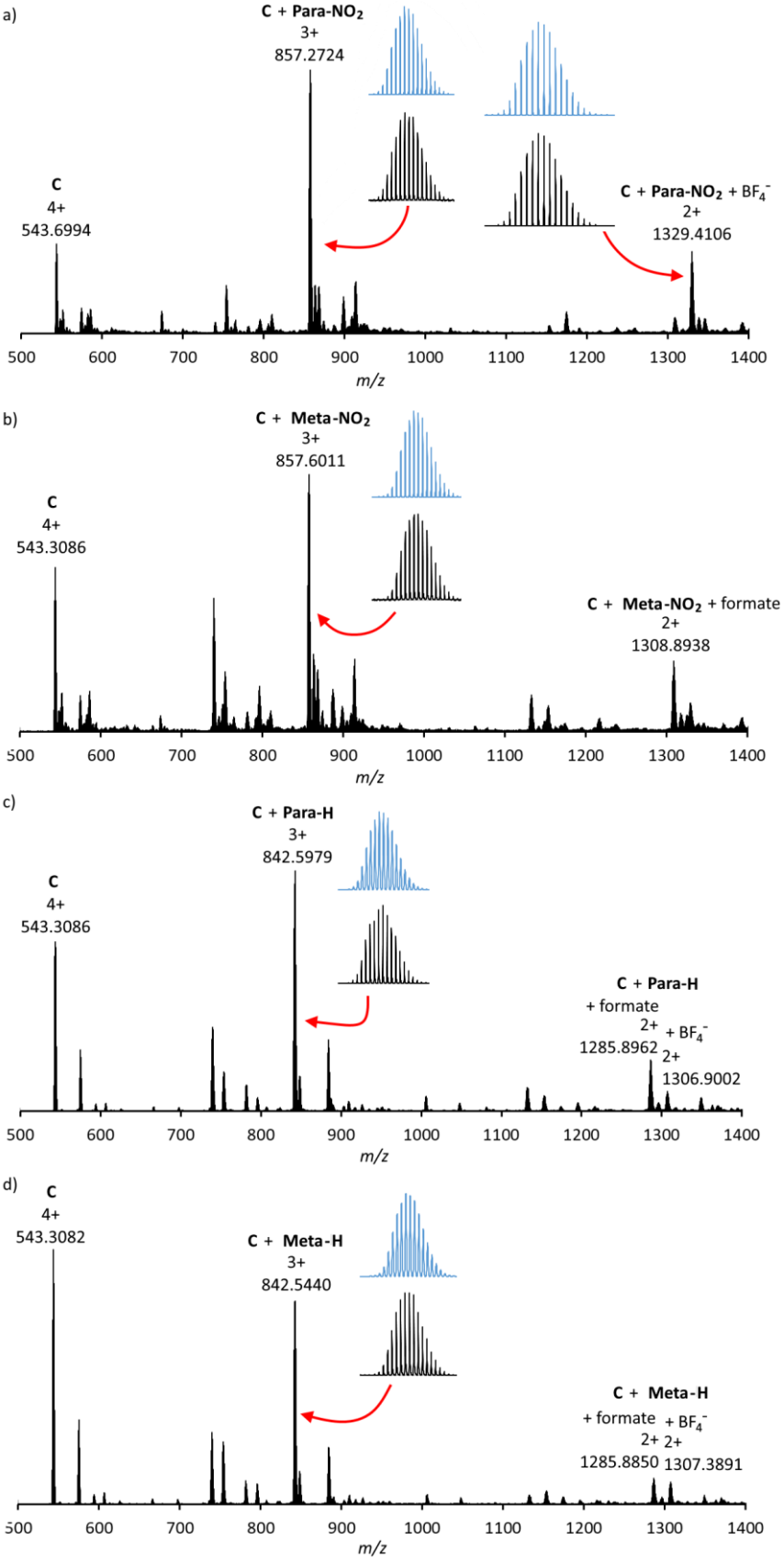

Figure 2.3 Partial mass spectra (DMSO/DMF) of 1:1 mixtures of **C**$(BF_4)_4$ and a) **Para-NO$_2$**, b) **Meta-NO$_2$**, c) **Para-H**, and d) **Meta-H**, observed peaks in black band calculated distributions above in blue.

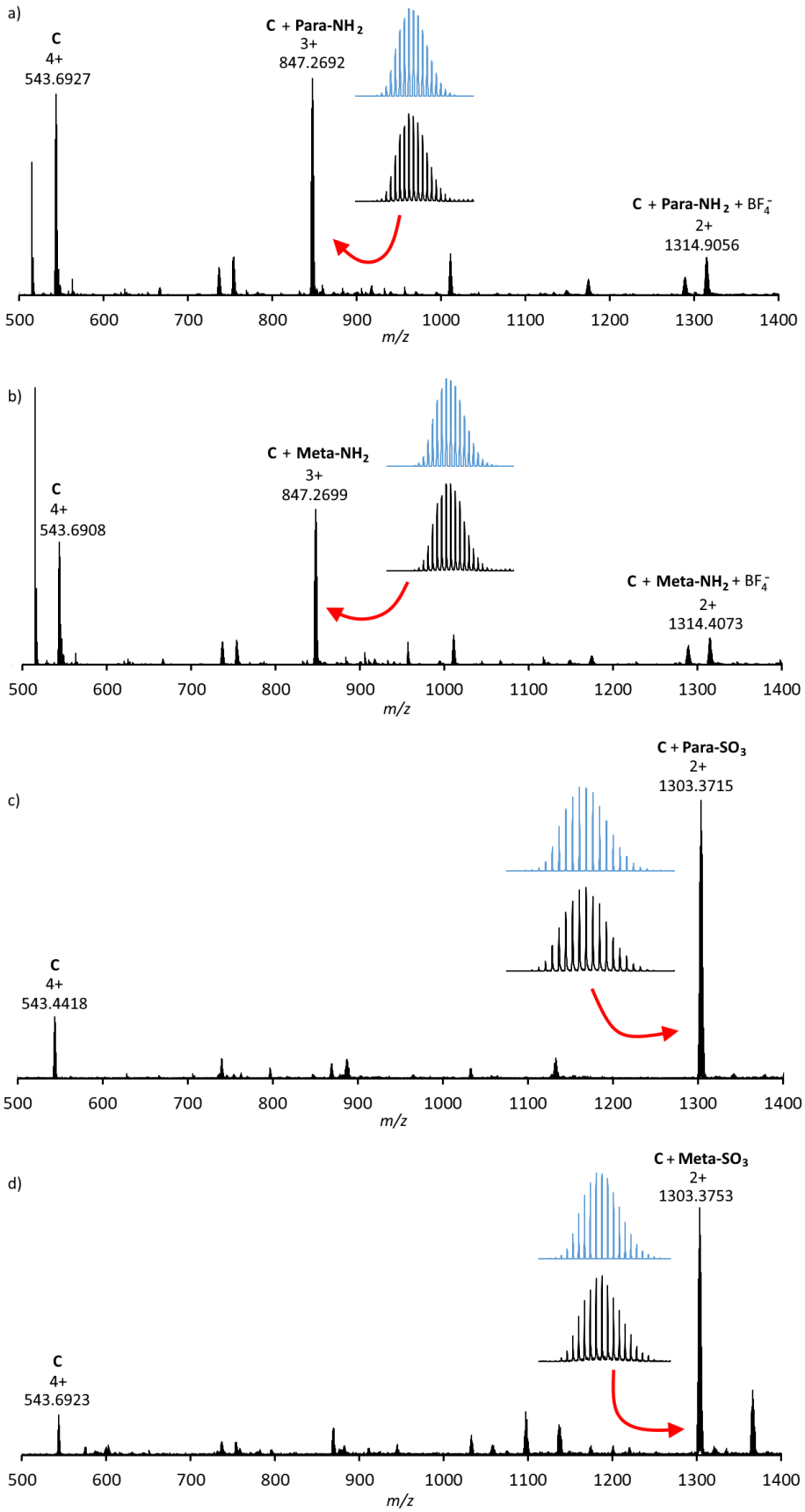

Figure 2.4 Partial mass spectra (DMSO/DMF) of 1:1 mixtures of **C**$(BF_4)_4$ and a) **Para-NH$_2$**, b) **Meta-NH$_2$**, c) **Para-SO$_3$**, and d) **Meta-SO$_3$**, observed peaks in black band calculated distributions above in blue.

2.3. NMR data

2.3.1. General titration information

Solutions of **C**$(BF_4)_4$ at 1.25 mM in [D_6]DMSO were treated with aliquots of equal volume of **C**$(BF_4)_4$ (2.5 mM) and the guest, both in [D_6]DMSO, such that the overall concentration of $\mathbf{C}^{4+}$ remained constant and the concentration of the guest increased with each aliquot. Calculated equivalencies were compared to those observed via integration in the ^{1}H NMR spectra, with good agreement. Titration end points were decided by either observance of free ligand or other untidiness (cage decomposition) in the ^{1}H NMR spectra, or by visual observation of precipitation in the NMR tube, whichever came first.

2.3.2. Model compounds

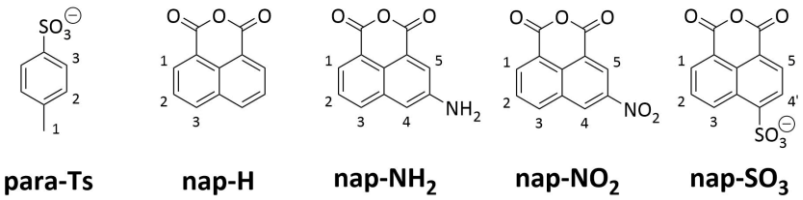

Figure 2.5 Chemical structures and labelling of model complexes used in this study

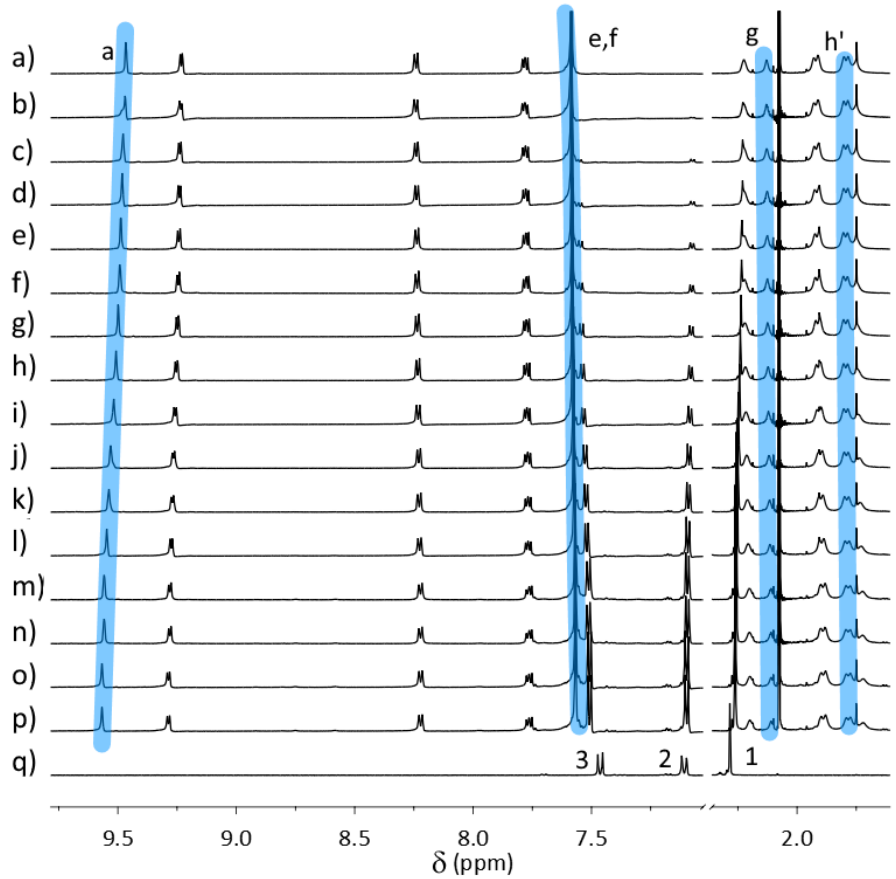

Figure 2.6 Partial stacked ^{1}H NMR spectra (600 MHz, [D_6]DMSO, 298 K, [**C**] = 1.25 mM) of a) **C**$(BF_4)_4$, b) **C**$(BF_4)_4$ + 0.15 eq. **Para-Ts**, c) **C**$(BF_4)_4$ + 0.45 eq. **Para-Ts**, d) **C**$(BF_4)_4$ + 0.70 eq. **Para-Ts**, e) **C**$(BF_4)_4$ + 1.00 eq. **Para-Ts**, f) **C**$(BF_4)_4$ + 1.25 eq. **Para-Ts**, g) **C**$(BF_4)_4$ + 1.67 eq. **Para-Ts**, h) **C**$(BF_4)_4$ + 2.00 eq. **Para-Ts**, i) **C**$(BF_4)_4$ + 2.25 eq. **Para-Ts**, j) **C**$(BF_4)_4$ + 2.80 eq. **Para-Ts**, k) **C**$(BF_4)_4$ + 3.75 eq. **Para-Ts**, l) **C**$(BF_4)_4$ + 4.50 eq. **Para-Ts**, m) **C**$(BF_4)_4$ + 5.50 eq. **Para-Ts**, n) **C**$(BF_4)_4$ + 7.50 eq. **Para-Ts**, o) **C**$(BF_4)_4$ + 9.00 eq. **Para-Ts**, p) **C**$(BF_4)_4$ + 11.00 eq. **Para-Ts**, and q) **Para-Ts**.

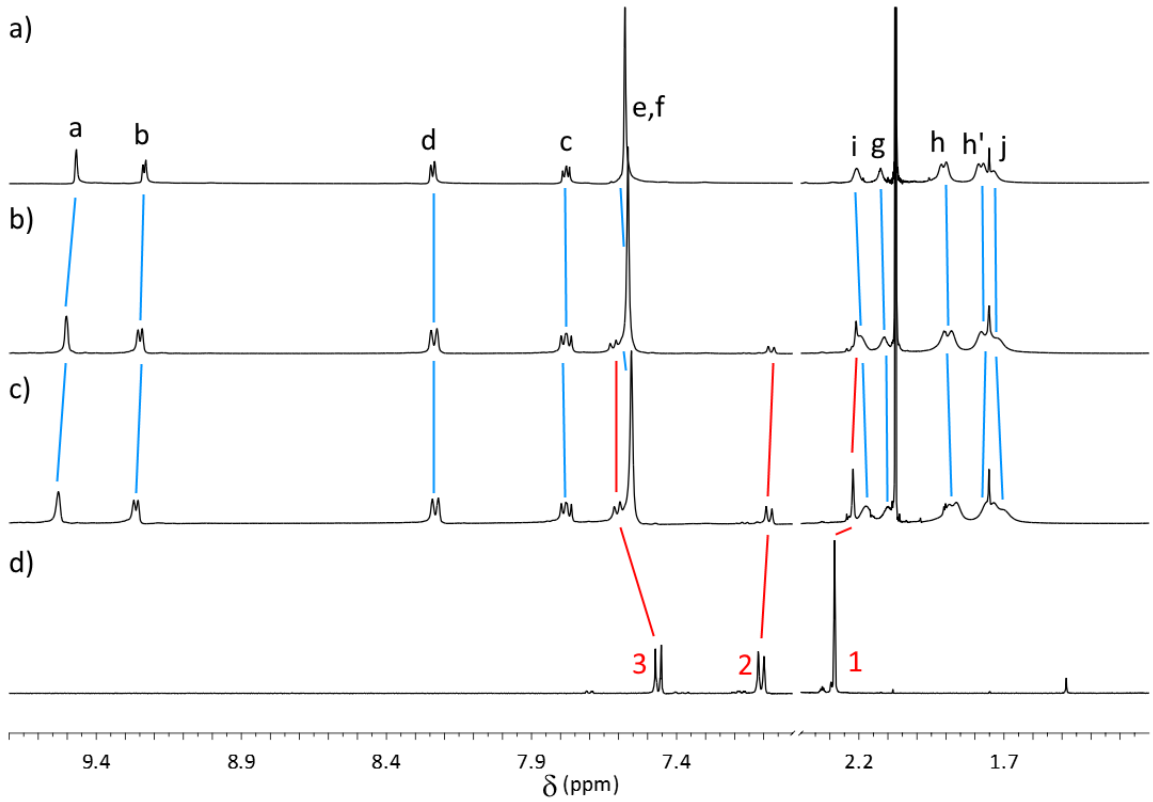

Figure 2.7 Partial stacked ^{1}H NMR spectra (600 MHz, [D_6]DMSO, 298 K, [**C**] = 2.5 mM) of a) **C**$(BF_4)_4$, b) **C**$(BF_4)_4$ + 1 eq. **Para-Ts**, c) **C**$(BF_4)_4$ + 2 eq. **Para-Ts**, and d) **Para-Ts**.

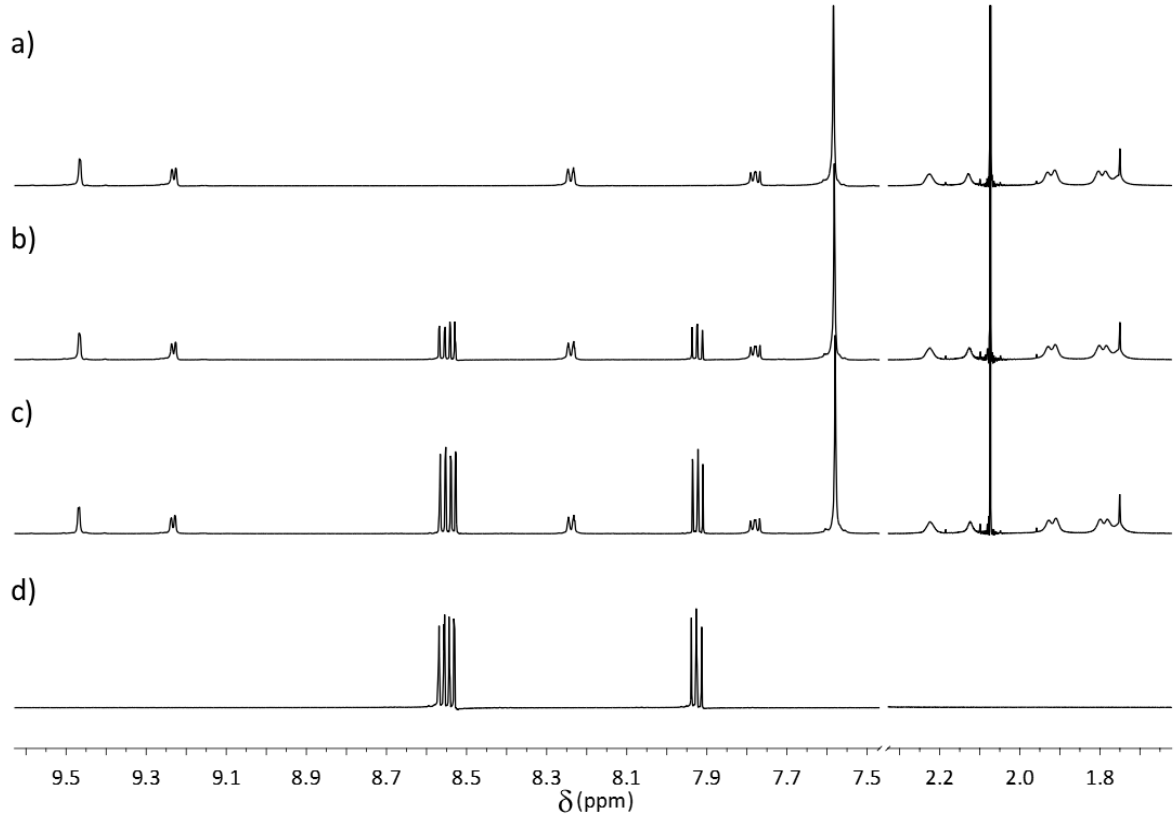

Figure 2.8 Partial stacked ^{1}H NMR spectra (600 MHz, [D_6]DMSO, 298 K, [**C**] = 1.25 mM) of a) **C**$(BF_4)_4$, b) **C**$(BF_4)_4$ + 4 eq. **Nap-H**, c) **C**$(BF_4)_4$ + 8 eq. **Nap-H**, and d) **Nap-H**.

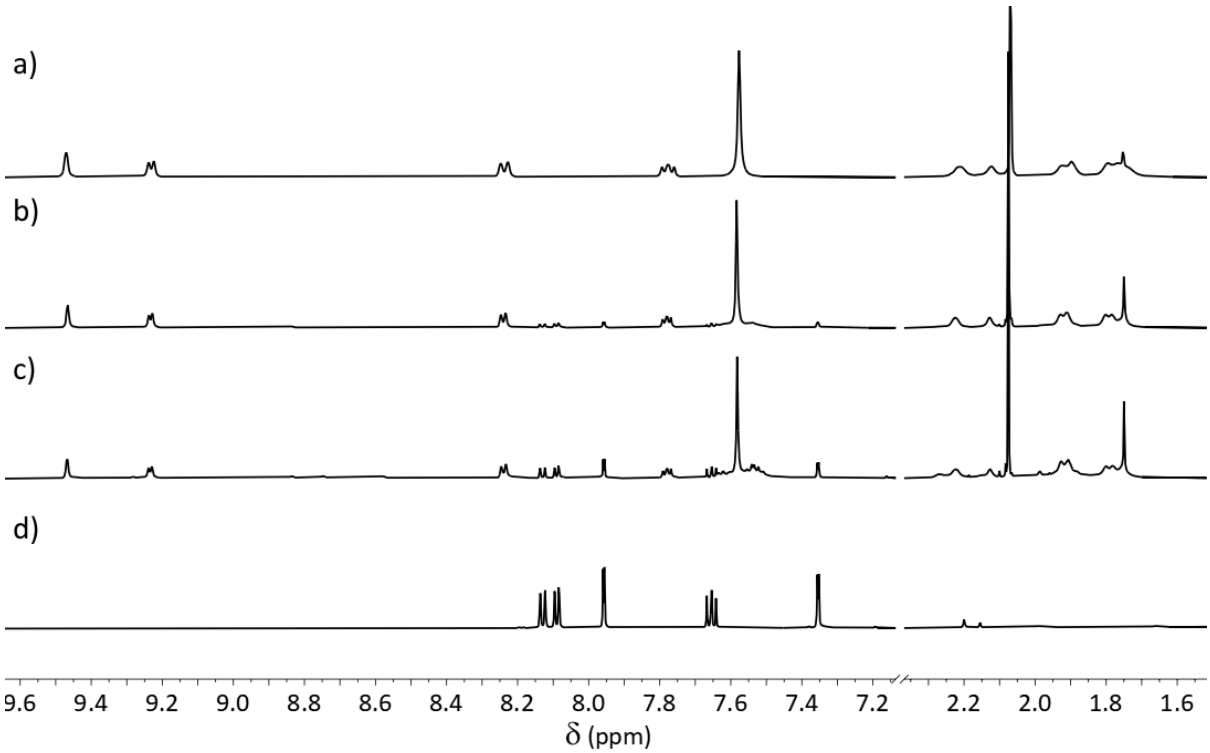

Figure 2.9 Partial stacked ^{1}H NMR spectra (600 MHz, [D_6]DMSO, 298 K, [**C**] = 1.25 mM) of a) **C**(BF_4)$_4$, b) **C**(BF_4)$_4$ + 4 eq. **Nap-NH$_2$**, c) **C**(BF_4)$_4$ + 8 eq. **Nap-NH$_2$**, and d) **Nap-NH$_2$**.

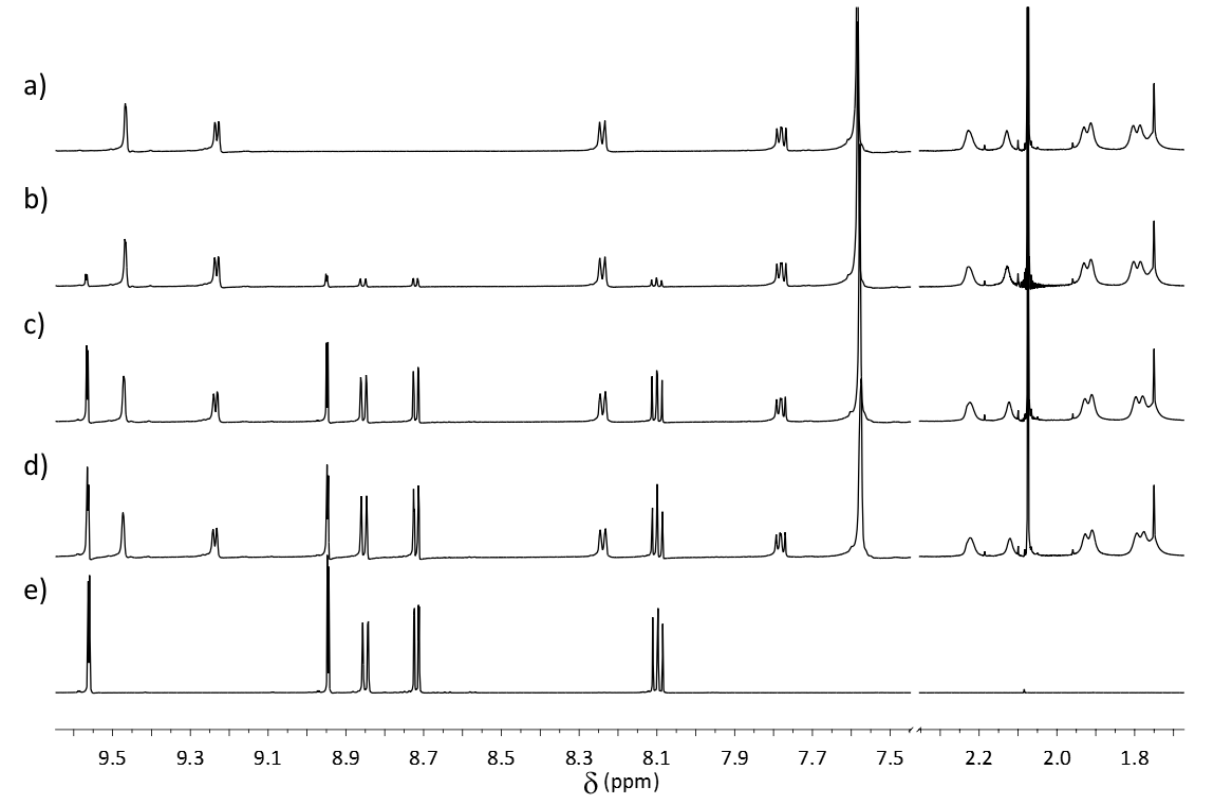

Figure 2.10 Partial stacked ^{1}H NMR spectra (600 MHz, [D_6]DMSO, 298 K, [**C**] = 1.25 mM) of a) **C**(BF_4)$_4$, b) **C**(BF_4)$_4$ + 1 eq. **Nap-NO$_2$**, c) **C**(BF_4)$_4$ + 4 eq. **Nap-NO$_2$**, d) **C**(BF_4)$_4$ + 8 eq. **Nap-NO$_2$**, and e) **Nap-NO$_2$**.

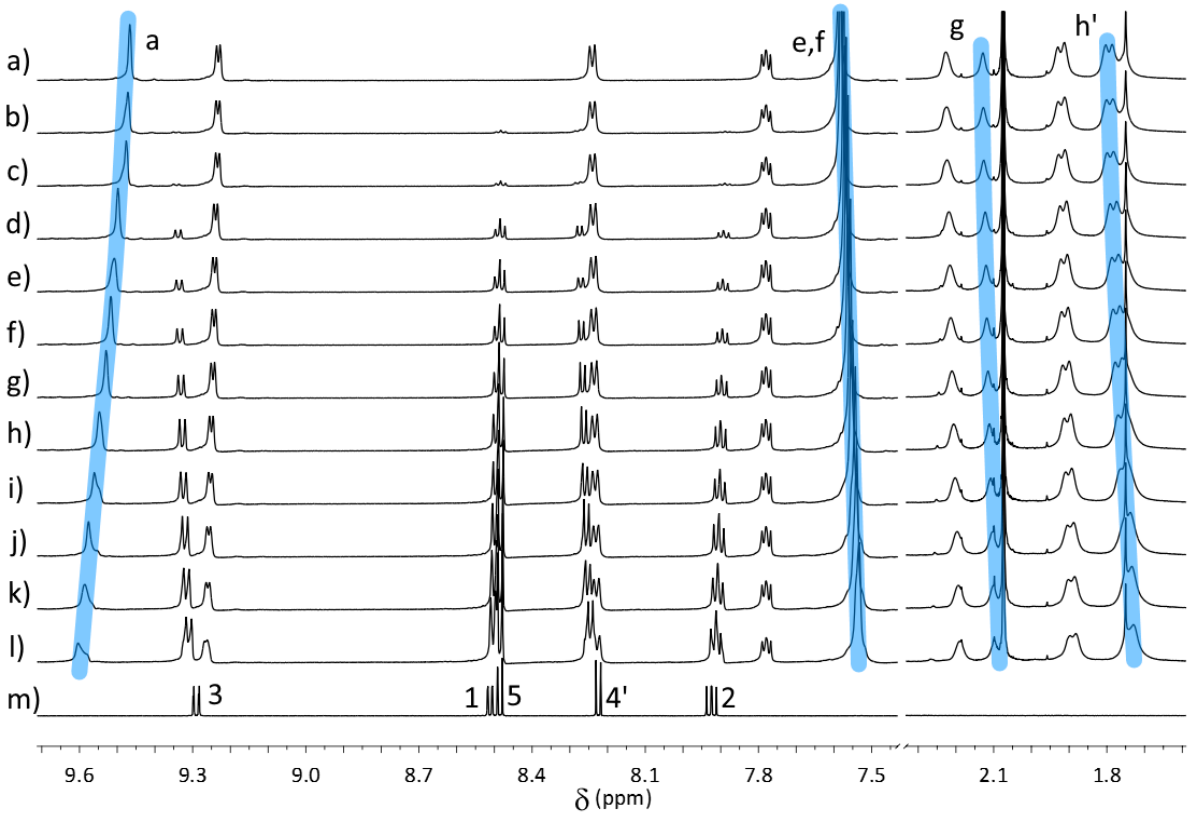

Figure 2.11 Partial stacked ^{1}H NMR spectra (600 MHz, [D_6]DMSO, 298 K, [**C**] = 1.25 mM) of a) **C**$(BF_4)_4$, b) **C**$(BF_4)_4$ + 0.3 eq. **Nap-SO$_3$**, c) **C**$(BF_4)_4$ + 0.6 eq. **Nap-SO$_3$**, d) **C**$(BF_4)_4$ + 1.2 eq. **Nap-SO$_3$**, e) **C**$(BF_4)_4$ + 1.6 eq. **Nap-SO$_3$**, f) **C**$(BF_4)_4$ + 2.0 eq. **Nap-SO$_3$**, g) **C**$(BF_4)_4$ + 3.0 eq. **Nap-SO$_3$**, h) **C**$(BF_4)_4$ + 4.0 eq. **Nap-SO$_3$**, i) **C**$(BF_4)_4$ + 5.0 eq. **Nap-SO$_3$**, j) **C**$(BF_4)_4$ + 6.5 eq. **Nap-SO$_3$**, k) **C**$(BF_4)_4$ + 8.0 eq. **Nap-SO$_3$**, l) **C**$(BF_4)_4$ + 10.0 eq. **Nap-SO$_3$**, and m) **Nap-SO$_3$**.

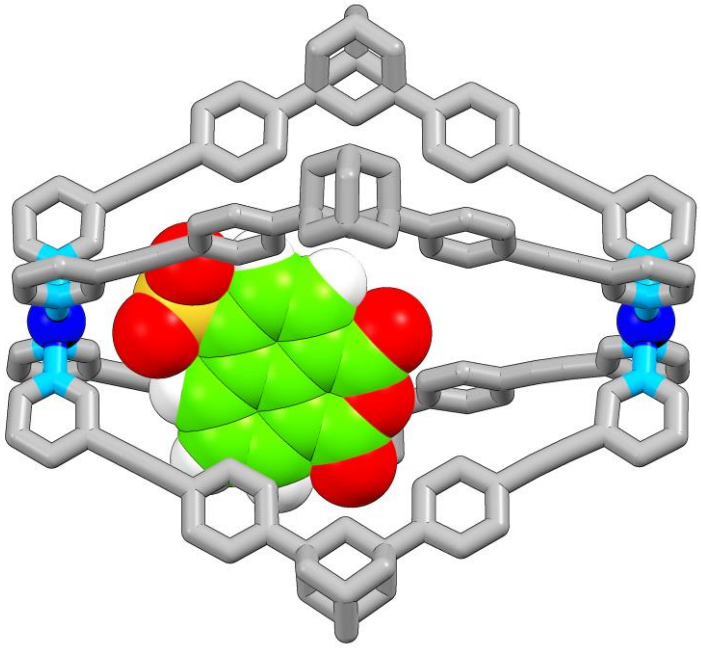

Figure 2.12 Depiction of the MMFF[6] of the 1:1 adduct of **C** and **nap-SO$_3$**: host in tube depiction, guest in spacefilling depiction. Colours: carbon grey for the cage and green for the guests, nitrogen light blue, oxygen red, palladium dark blue, sulphur orange. Model available as an xyz file.

2.3.3. Naphthalimide sulfonates

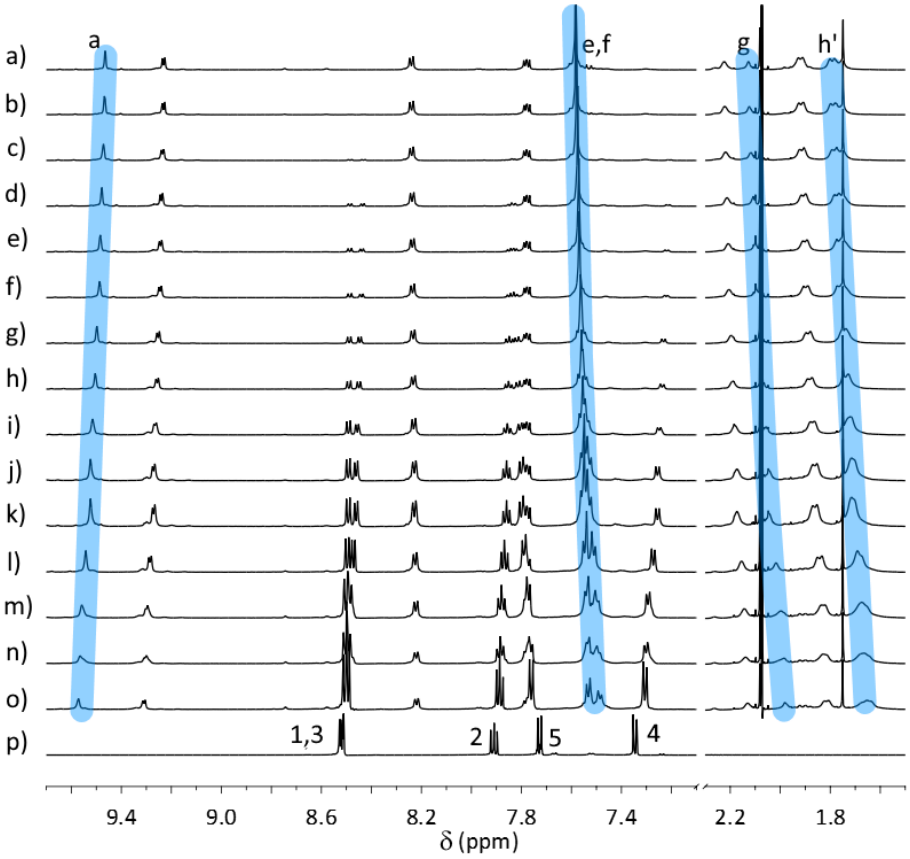

Figure 2.13 Partial stacked ^{1}H NMR spectra (600 MHz, [D_6]DMSO, 298 K, [**C**] = 1.25 mM) of a) **C**$(BF_4)_4$, b) **C**$(BF_4)_4$ + 0.1 eq. **Para-H**, c) **C**$(BF_4)_4$ + 0.2 eq. **Para-H**, d) **C**$(BF_4)_4$ + 0.4 eq. **Para-H**, e) **C**$(BF_4)_4$ + 0.6 eq. **Para-H**, f) **C**$(BF_4)_4$ + 0.9 eq. **Para-H**, g) **C**$(BF_4)_4$ + 1.3 eq. **Para-H**, h) **C**$(BF_4)_4$ + 1.6 eq. **Para-H**, i) **C**$(BF_4)_4$ + 2.3 eq. **Para-H**, j) **C**$(BF_4)_4$ + 3.1 eq. **Para-H**, k) **C**$(BF_4)_4$ + 4.0 eq. **Para-H**, l) **C**$(BF_4)_4$ + 5.5 eq. **Para-H**, m) **C**$(BF_4)_4$ + 7.5 eq. **Para-H**, n) **C**$(BF_4)_4$ + 8.8 eq. **Para-H**, o) **C**$(BF_4)_4$ + 11.0 eq. **Para-H**, and p) **Para-H**.

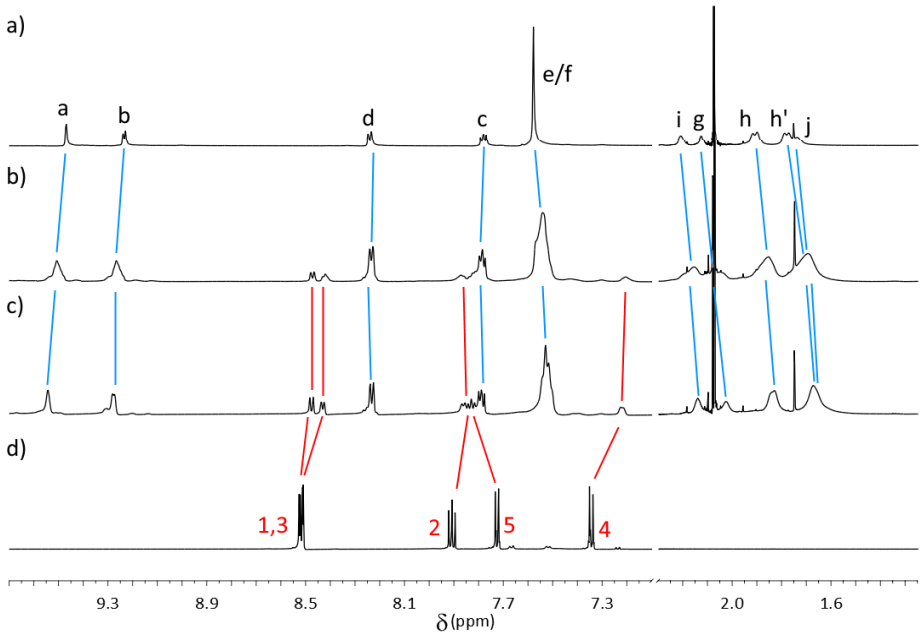

Figure 2.14 Partial stacked ^{1}H NMR spectra (600 MHz, [D_6]DMSO, 298 K, [**C**] = 2.5 mM) of a) **C**$(BF_4)_4$, b) **C**$(BF_4)_4$ + 1 eq. **Para-H**, c) **C**$(BF_4)_4$ + 2 eq. **Para-H**, and d) **Para-H**.

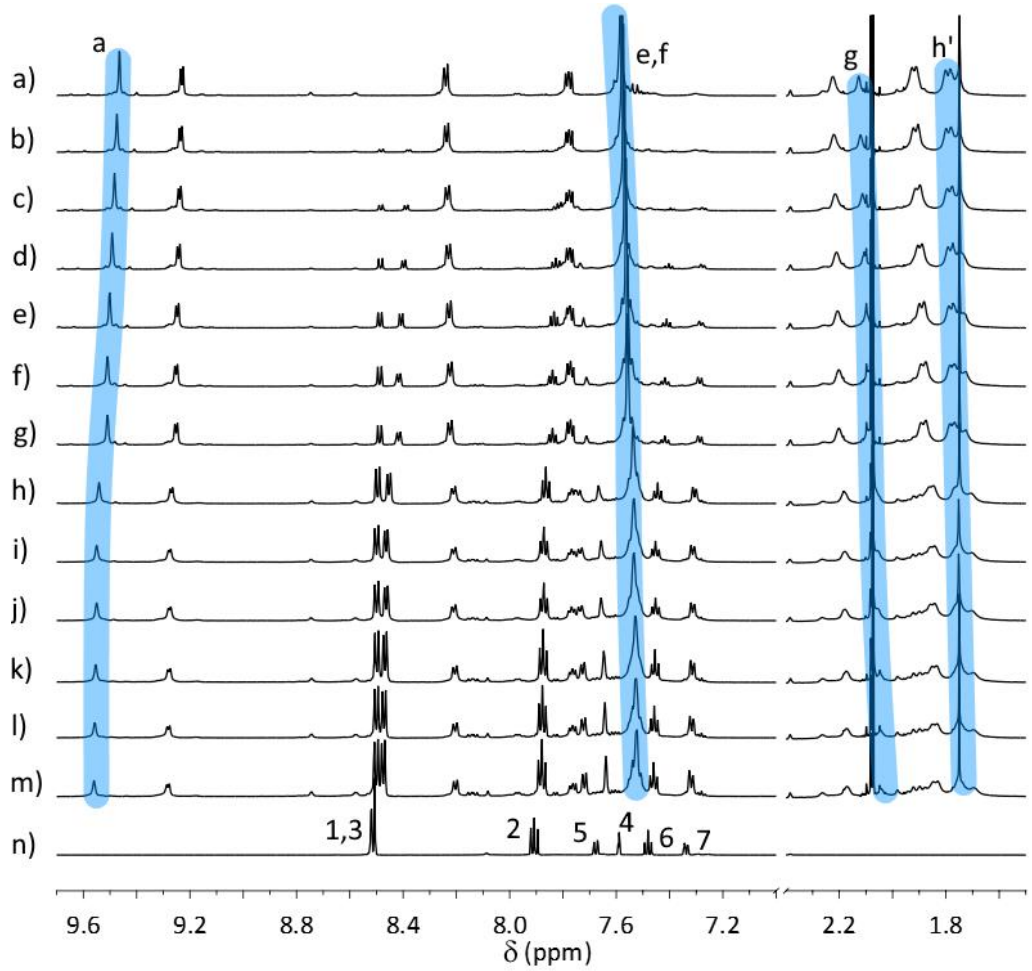

Figure 2.15 Partial stacked ^{1}H NMR spectra (600 MHz, [D_6]DMSO, 298 K, [**C**] = 1.25 mM) of a) **C**$(BF_4)_4$, b) **C**$(BF_4)_4$ + 0.3 eq. **Meta-H**, c) **C**$(BF_4)_4$ + 0.6 eq. **Meta-H**, d) **C**$(BF_4)_4$ + 1.0 eq. **Meta-H**, e) **C**$(BF_4)_4$ + 1.5 eq. **Meta-H**, f) **C**$(BF_4)_4$ + 1.8 eq. **Meta-H**, g) **C**$(BF_4)_4$ + 2.6 eq. **Meta-H**, h) **C**$(BF_4)_4$ + 3.6 eq. **Meta-H**, i) **C**$(BF_4)_4$ + 5.0 eq. **Meta-H**, j) **C**$(BF_4)_4$ + 6.8 eq. **Meta-H**, k) **C**$(BF_4)_4$ + 8.6 eq. **Meta-H**, l) **C**$(BF_4)_4$ + 10.0 eq. **Meta-H**, m) **C**$(BF_4)_4$ + 11.0 eq. **Meta -H**, n) **Meta-H**.

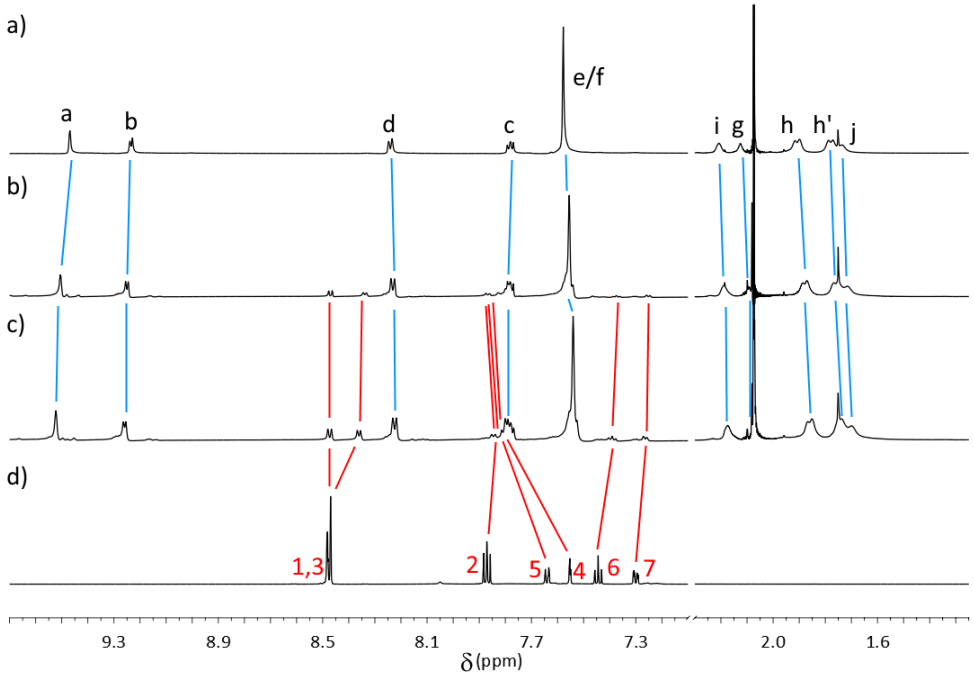

Figure 2.16 Partial stacked ^{1}H NMR spectra (600 MHz, [D_6]DMSO, 298 K, [**C**] = 2.5 mM) of a) **C**$(BF_4)_4$, b) **C**$(BF_4)_4$ + 1 eq. **Meta-H**, c) **C**$(BF_4)_4$ + 2 eq. **Meta-H**, and d) **Meta-H**.

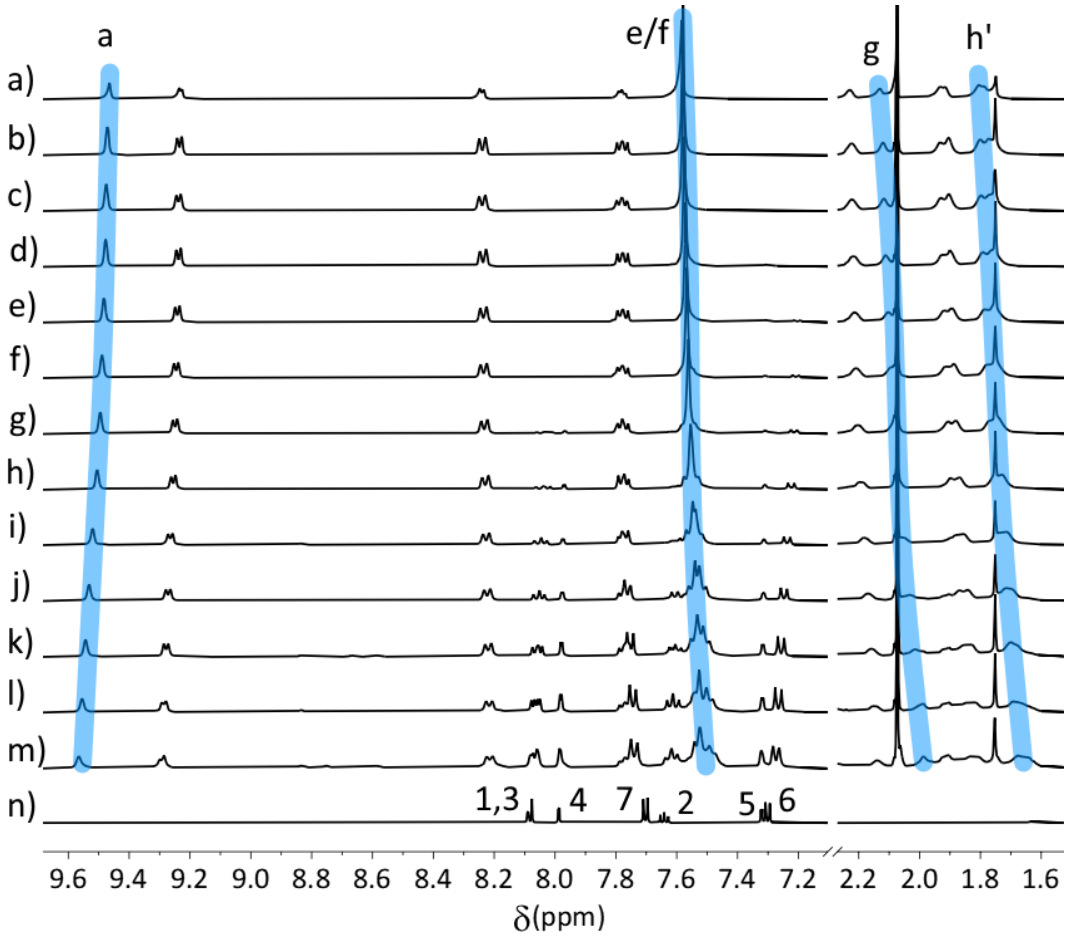

Figure 2.17 Partial stacked ^{1}H NMR spectra (600 MHz, [D_6]DMSO, 298 K, [**C**] = 1.25 mM) of a) **C**$(BF_4)_4$, b) **C**$(BF_4)_4$ + 0.13 eq. **Para-NH$_2$**, c) **C**$(BF_4)_4$ + 0.26 eq. **Para-NH$_2$**, d) **C**$(BF_4)_4$ + 0.40 eq. **Para-NH$_2$**, e) **C**$(BF_4)_4$ + 0.53 eq. **Para-NH$_2$**, f) **C**$(BF_4)_4$ + 0.70 eq. **Para-NH$_2$**, g) **C**$(BF_4)_4$ + 1.0 eq. **Para-NH$_2$**, h) **C**$(BF_4)_4$ + 1.8 eq. **Para-NH$_2$**, i) **C**$(BF_4)_4$ + 2.4 eq. **Para-NH$_2$**, j) **C**$(BF_4)_4$ + 3.4 eq. **Para-NH$_2$**, k) **C**$(BF_4)_4$ + 4.8 eq. **Para-NH$_2$**, l) **C**$(BF_4)_4$ + 6.6 eq. **Para-NH$_2$**, m) **C**$(BF_4)_4$ + 8.6 eq. **Para-NH$_2$**, n) **Para-NH$_2$**.

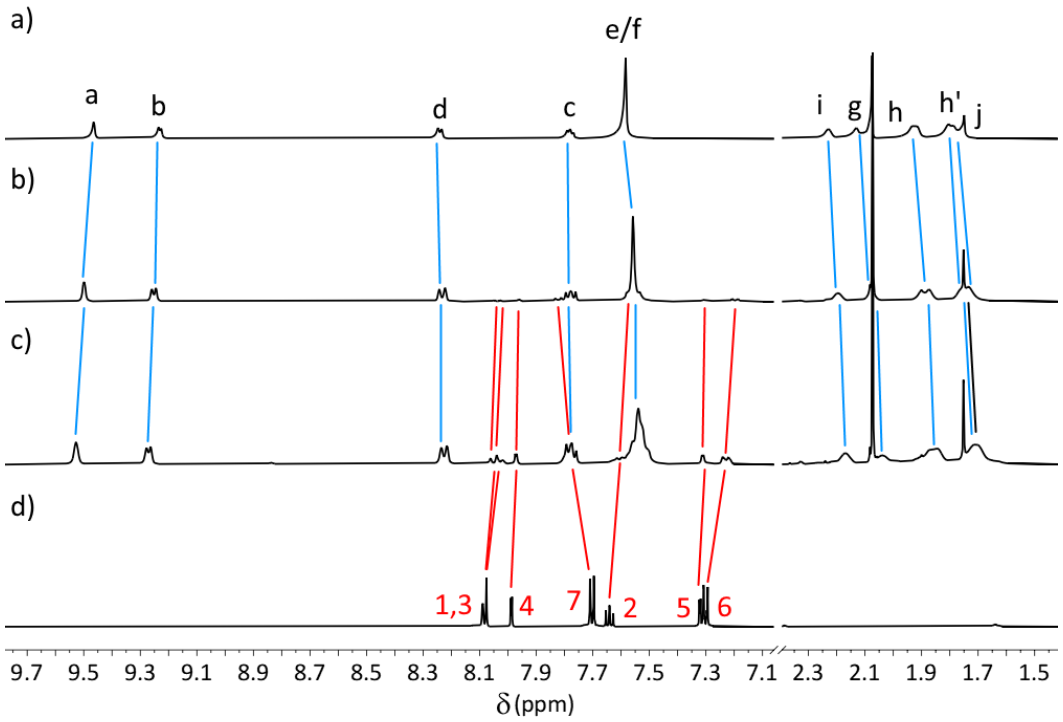

Figure 2.18 Partial stacked ^{1}H NMR spectra (600 MHz, [D_6]DMSO, 298 K, [**C**] = 2.5 mM) of a) **C**$(BF_4)_4$, b) **C**$(BF_4)_4$ + 1 eq. **Para-NH$_2$**, c) **C**$(BF_4)_4$ + 2 eq. **Para-NH$_2$**, and d) **Para-NH$_2$**.

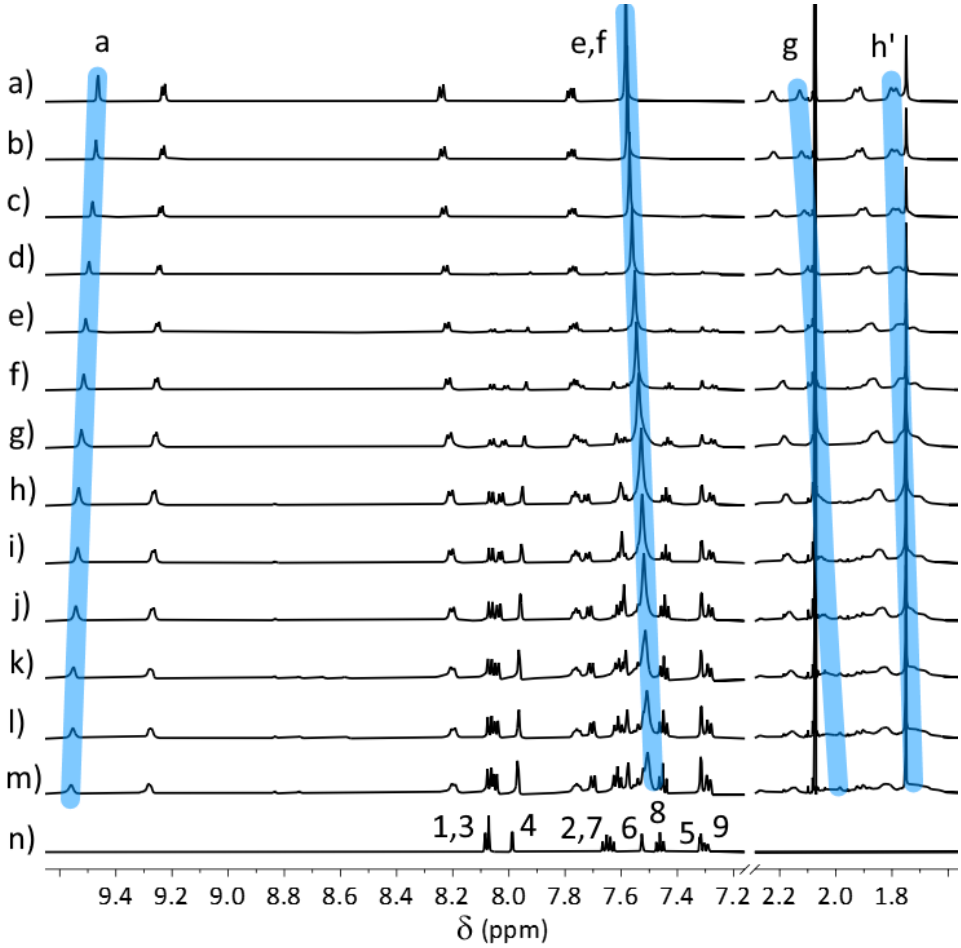

Figure 2.19 Partial stacked ^{1}H NMR spectra (600 MHz, [D$_6$]DMSO, 298 K, [**C**] = 1.25 mM) of a) **C**(BF$_4$)$_4$, b) **C**(BF$_4$)$_4$ + 0.20 eq. **Meta-NH$_2$**, c) **C**(BF$_4$)$_4$ + 0.50 eq. **Meta-NH$_2$**, d) **C**(BF$_4$)$_4$ + 0.90 eq. **Meta-NH$_2$**, e) **C**(BF$_4$)$_4$ + 1.40 eq. **Meta-NH$_2$**, f) **C**(BF$_4$)$_4$ + 1.70 eq. **Meta-NH$_2$**, g) **C**(BF$_4$)$_4$ + 2.40 eq. **Meta-NH$_2$**, h) **C**(BF$_4$)$_4$ + 3.00 eq. **Meta-NH$_2$**, i) **C**(BF$_4$)$_4$ + 3.50 eq. **Meta-NH$_2$**, j) **C**(BF$_4$)$_4$ + 4.30 eq. **Meta-NH$_2$**, k) **C**(BF$_4$)$_4$ + 5.0 eq. **Meta-NH$_2$**, l) **C**(BF$_4$)$_4$ + 6.5 eq. **Meta-NH$_2$**, m) **C**(BF$_4$)$_4$ + 8.0 eq. **Meta-NH$_2$**, n) **Meta-NH$_2$**.

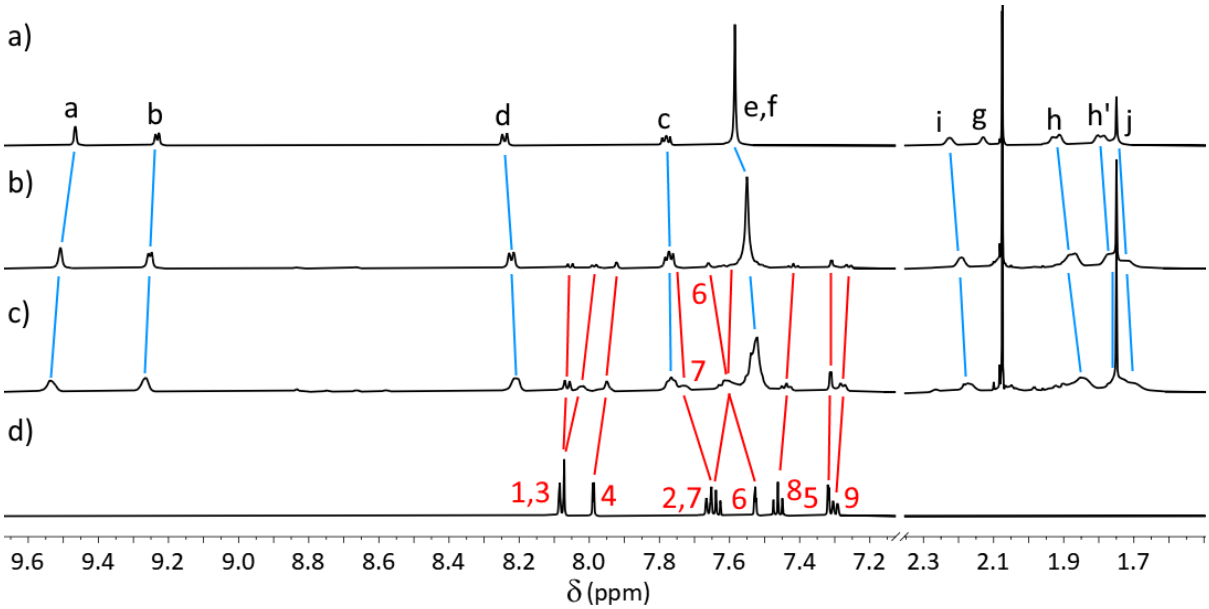

Figure 2.20 Partial stacked ^{1}H NMR spectra (600 MHz, [D$_6$]DMSO, 298 K, [**C**] = 2.5 mM) of a) **C**(BF$_4$)$_4$, b) **C**(BF$_4$)$_4$ + 1 eq. **Meta-NH$_2$**, c) **C**(BF$_4$)$_4$ + 2 eq. **Meta-NH$_2$**, and d) **Meta-NH$_2$**.

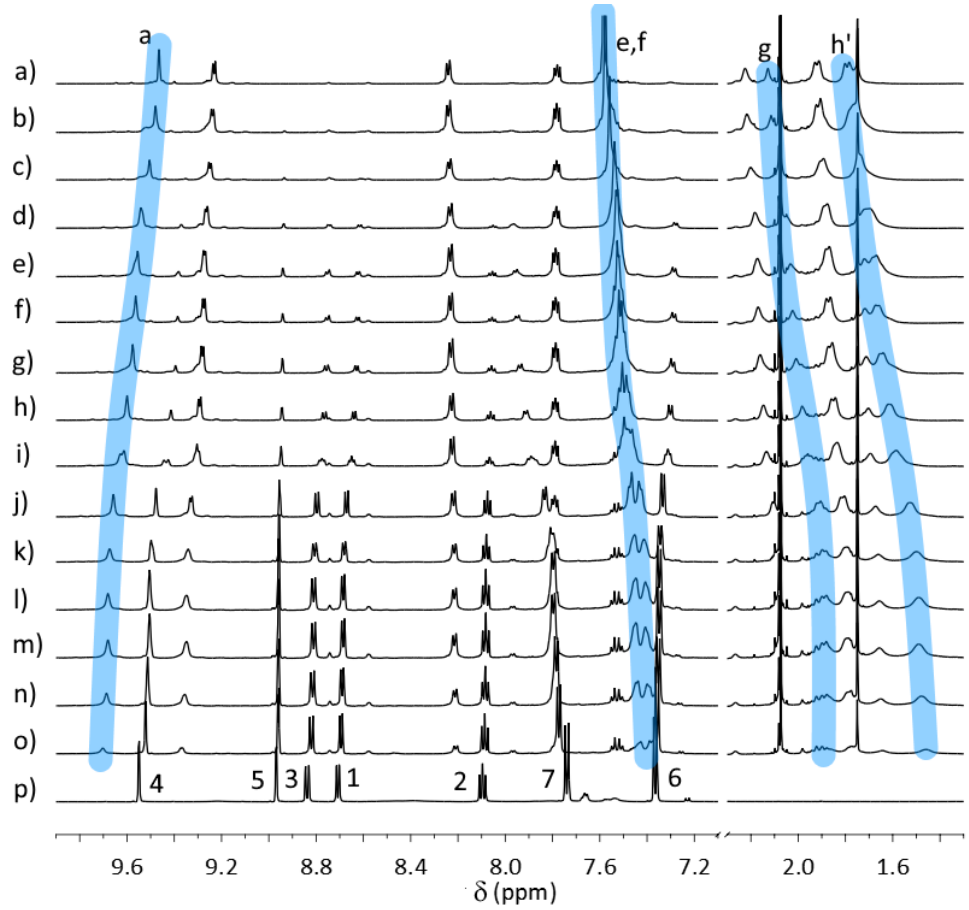

Figure 2.21 Partial stacked ^{1}H NMR spectra (600 MHz, [D_6]DMSO, 298 K, [**C**] = 1.25 mM) of a) **C**$(BF_4)_4$, b) **C**$(BF_4)_4$ + 0.25 eq. **Para-NO$_2$**, c) **C**$(BF_4)_4$ + 0.5 eq. **Para-NO$_2$**, d) **C**$(BF_4)_4$ + 0.75 eq. **Para-NO$_2$**, e) **C**$(BF_4)_4$ + 1.0 eq. **Para NO$_2$**, f) **C**$(BF_4)_4$ + 1.2 eq. **Para-NO$_2$**, g) **C**$(BF_4)_4$ + 1.4 eq. **Para-NO$_2$**, h) **C**$(BF_4)_4$ + 1.6 eq. **Para-NO$_2$**, i) **C**$(BF_4)_4$ + 2.2 eq. **Para-NO$_2$**, j) **C**$(BF_4)_4$ + 3.0 eq. **Para-NO$_2$**, k) **C**$(BF_4)_4$ + 4.0 eq. **Para-NO$_2$**, l) **C**$(BF_4)_4$ + 5.8 eq. **Para-NO$_2$**, m) **C**$(BF_4)_4$ + 7.8 eq. **Para-NO$_2$**, n) **C**$(BF_4)_4$ + 9.5 eq. **Para-NO$_2$**, o) **C**$(BF_4)_4$ + 11.0 eq. **Para-NO$_2$**, and p) **Para-NO$_2$**.

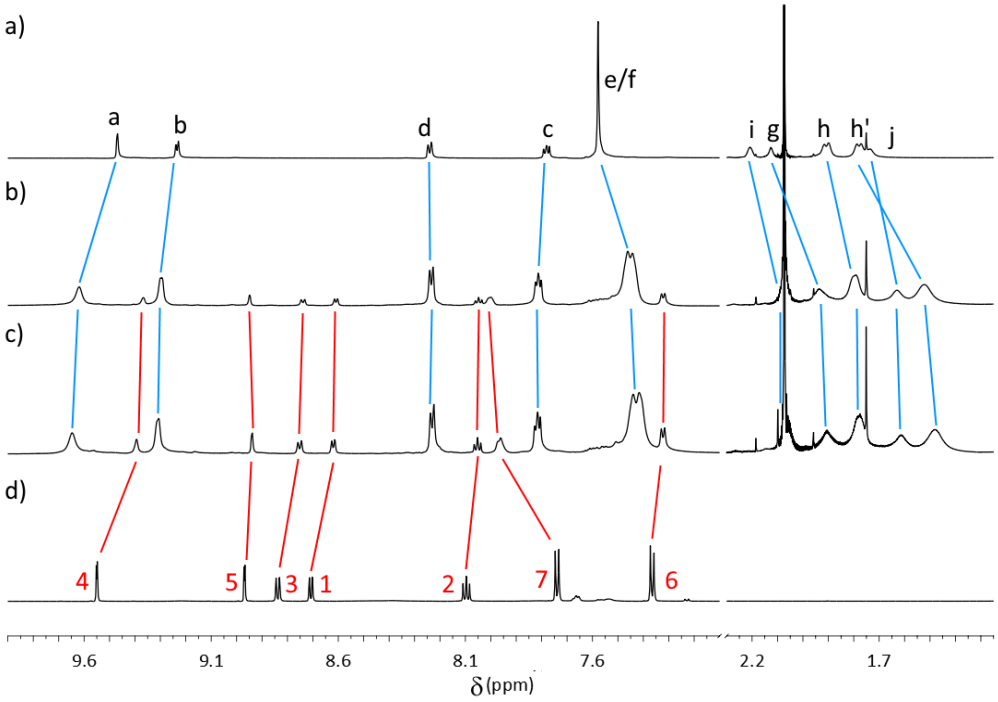

Figure 2.22 Partial stacked ^{1}H NMR spectra (600 MHz, [D_6]DMSO, 298 K, [**C**] = 2.5 mM) of a) **C**$(BF_4)_4$, b) **C**$(BF_4)_4$ + 1 eq. **Para-NO$_2$**, c) **C**$(BF_4)_4$ + 2 eq. **Para-NO$_2$**, and d) **Para-NO$_2$**.

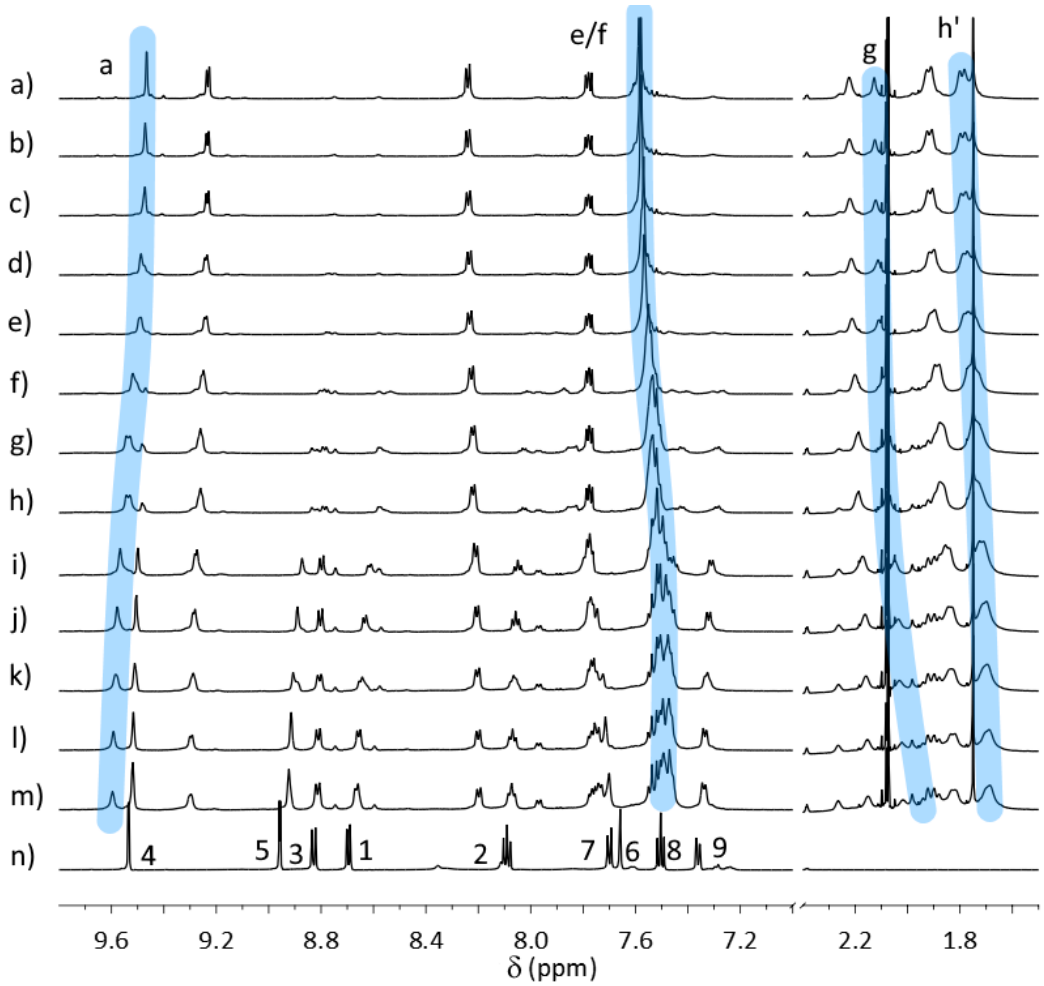

Figure 2.23 Partial stacked ^{1}H NMR spectra (600 MHz, [D_6]DMSO, 298 K, [**C**] = 1.25 mM) of a) **C**$(BF_4)_4$, b) **C**$(BF_4)_4$ + 0.1 eq. **Meta-NO$_2$**, c) **C**$(BF_4)_4$ + 0.2 eq. **Meta-NO$_2$**, d) **C**$(BF_4)_4$ + 0.3 eq. **Meta-NO$_2$**, e) **C**$(BF_4)_4$ + 0.5 eq. **Meta-NO$_2$**, f) **C**$(BF_4)_4$ + 0.8 eq. **Meta-NO$_2$**, g) **C**$(BF_4)_4$ + 1.5 eq. **Meta-NO$_2$**, h) **C**$(BF_4)_4$ + 2.2 eq. **Meta-NO$_2$**, i) **C**$(BF_4)_4$ + 4.0 eq. **Meta-NO$_2$**, j) **C**$(BF_4)_4$ + 5.6 eq. **Meta-NO$_2$**, k) **C**$(BF_4)_4$ + 7.5 eq. **Meta-NO$_2$**, l) **C**$(BF_4)_4$ + 9.5 eq. **Meta-NO$_2$**, m) **C**$(BF_4)_4$ + 11.0 eq. **Meta -NO$_2$**, n) **Meta-NO$_2$**.

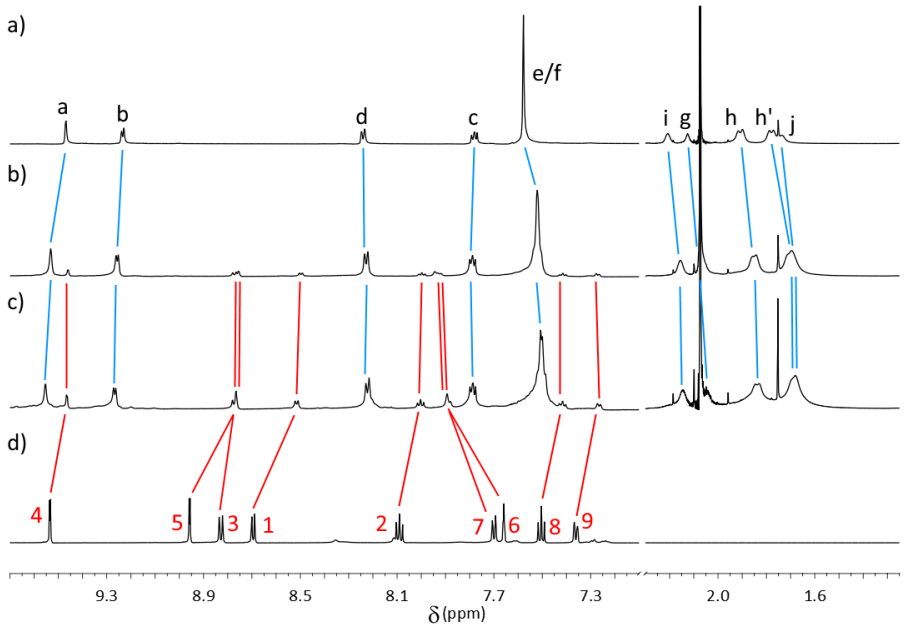

Figure 2.24 Partial stacked ^{1}H NMR spectra (600 MHz, [D_6]DMSO, 298 K, [**C**] = 2.5 mM) of a) **C**$(BF_4)_4$, b) **C**$(BF_4)_4$ + 1 eq. **Meta-NO$_2$**, c) **C**$(BF_4)_4$ + 2 eq. **Meta-NO$_2$**, and d) **Meta-NO$_2$**.

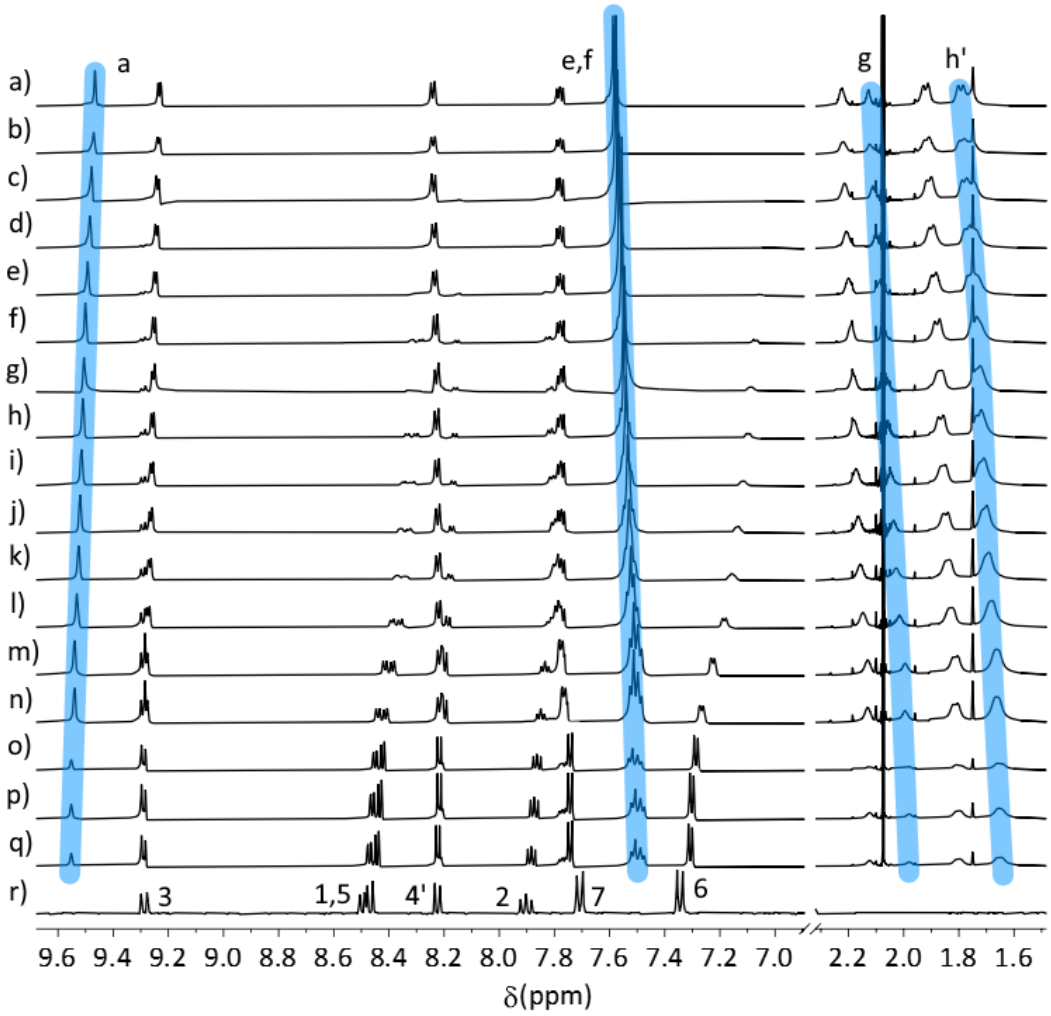

Figure 2.25 Partial stacked ^{1}H NMR spectra (600 MHz, [D_6]DMSO, 298 K, [**C**] = 1.25 mM) of a) **C**$(BF_4)_4$, b) **C**$(BF_4)_4$ + 0.15 eq. **Para-SO$_3$**, c) **C**$(BF_4)_4$ + 0.32 eq. **Para-SO$_3$**, d) **C**$(BF_4)_4$ + 0.50 eq. **Para-SO$_3$**, e) **C**$(BF_4)_4$ + 0.62 eq. **Para-SO$_3$**, f) **C**$(BF_4)_4$ + 0.79 eq. **Para-SO$_3$**, g) **C**$(BF_4)_4$ + 0.90 eq. **Para-SO$_3$**, h) **C**$(BF_4)_4$ + 1.00 eq. **Para-SO$_3$**, i) **C**$(BF_4)_4$ + 1.25 eq. **Para-SO$_3$**, j) **C**$(BF_4)_4$ + 1.54 eq. **Para-SO$_3$**, k) **C**$(BF_4)_4$ + 1.75 eq. **Para-SO$_3$**, l) **C**$(BF_4)_4$ + 2.10 eq. **Para-SO$_3$**, m) **C**$(BF_4)_4$ + 2.80 eq. **Para-SO$_3$**, n) **C**$(BF_4)_4$ + 3.20 eq. **Para-SO$_3$**, o) **C**$(BF_4)_4$ + 6.00 eq. **Para-SO$_3$**, p) **C**$(BF_4)_4$ + 8.00 eq. **Para-SO$_3$**, q) **C**$(BF_4)_4$ + 11.00 eq. **Para-SO$_3$**, and r) **Para-SO$_3$**.

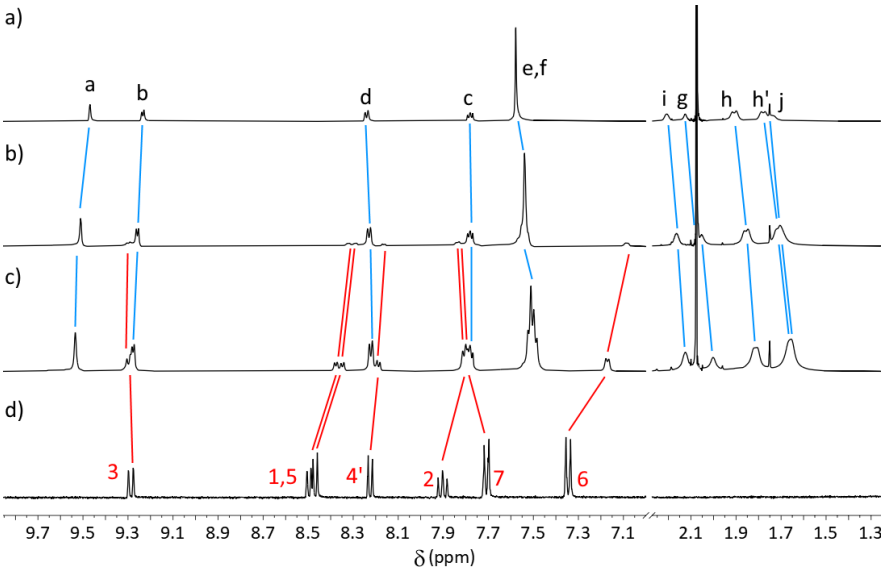

Figure 2.26 Partial stacked ^{1}H NMR spectra (600 MHz, [D_6]DMSO, 298 K, [**C**] = 1.25 mM) of a) **C**$(BF_4)_4$, b) **C**$(BF_4)_4$ + 1 eq. **Para-SO$_3$**, c) **C**$(BF_4)_4$ + 2 eq. **Para-SO$_3$**, and d) **Para-SO$_3$**.

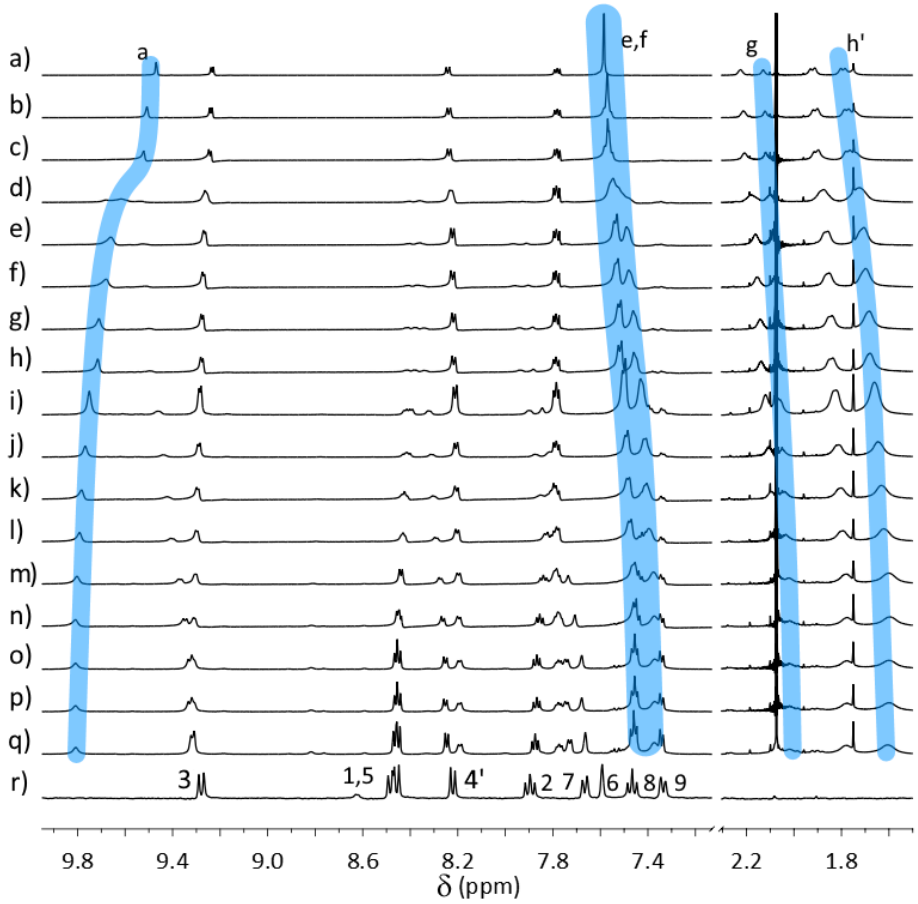

Figure 2.27 Partial stacked ^{1}H NMR spectra (600 MHz, [D_6]DMSO, 298 K, [**C**] = 1.25 mM) of a) **C**$(BF_4)_4$, b) **C**$(BF_4)_4$ + 0.16 eq. **Meta-SO$_3$**, c) **C**$(BF_4)_4$ + 0.33 eq. **Meta-SO$_3$**, d) **C**$(BF_4)_4$ + 0.50 eq. **Meta-SO$_3$**, e) **C**$(BF_4)_4$ + 0.75 eq. **Meta-SO$_3$**, f) **C**$(BF_4)_4$ + 0.85 eq. **Meta-SO$_3$**, g) **C**$(BF_4)_4$ + 0.90 eq. **Meta-SO$_3$**, h) **C**$(BF_4)_4$ + 1.00 eq. **Meta-SO$_3$**, i) **C**$(BF_4)_4$ + 1.30 eq. **Meta-SO$_3$**, j) **C**$(BF_4)_4$ + 1.66 eq. **Meta-SO$_3$**, k) **C**$(BF_4)_4$ + 2.00 eq. **Meta-SO$_3$**, l) **C**$(BF_4)_4$ + 2.50 eq. **Meta-SO$_3$**, m) **C**$(BF_4)_4$ + 3.00 eq. **Meta-SO$_3$**, n) **C**$(BF_4)_4$ + 4.00 eq. **Meta-SO$_3$**, o) **C**$(BF_4)_4$ + 6.00 eq. **Meta-SO$_3$**, p) **C**$(BF_4)_4$ + 8.00 eq. **Meta-SO$_3$**, q) **C**$(BF_4)_4$ + 11.00 eq. **Meta-SO$_3$**, and r) **Meta-SO$_3$**.

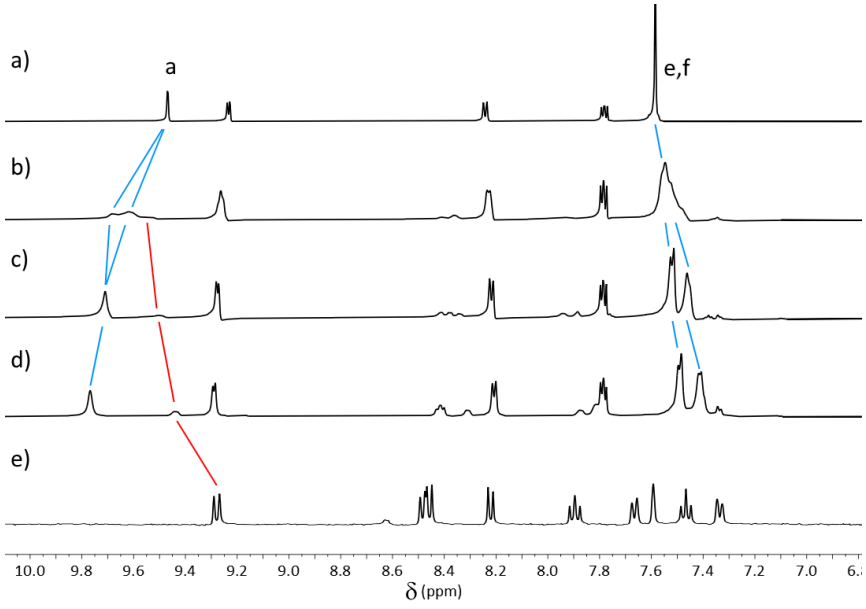

Figure 2.28 Partial stacked ^{1}H NMR spectra (600 MHz, [D_6]DMSO, 298 K, [**C**] = 1.25 mM) of a) **C**$(BF_4)_4$, b) **C**$(BF_4)_4$ + 0.5 eq. **meta-SO$_3$**, c) **C**$(BF_4)_4$ + 1.0 eq. **meta-SO$_3$**, d) **C**$(BF_4)_4$ + 2.0 eq. **meta-SO$_3$**, and e) **meta-SO$_3$**, showing broadening and splitting of the H_a proton at 0.5 eq. guest.

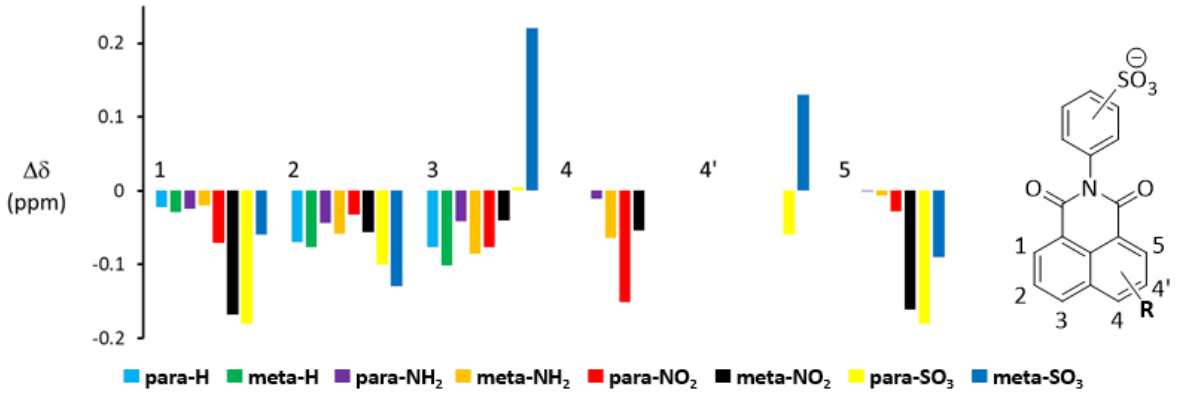

Figure 2.29 Magnitude and direction of change of ^{1}H NMR chemical shits (600 MHz, [D_6]DMSO, 298 K) of resonances from the naphthalimide moiety of the guests when combined 1:1 with **C**$(BF_4)_4$ at 1.25 mM.

2.3.4. Binding isotherms for guests

Binding isotherms from ^{1}H NMR spectroscopic titrations, show a mean value for the H_e and H_f resonances, due to crowding and lack of clarity in several cases. Where it was difficult to pick peaks for a resonance due to spectral crowding/overlapping peaks, the isotherm is not shown beyond this point. Shifts shown in absolute terms, with a sign beside each isotherm indicating whether the shift was downfield (+) or upfield (-).

Using the mole ratio method,[7] the binding isotherms for the $-NH_2$, -H, and $-NO_2$ substituted guests (as well as model guests **para-Ts** and **nap-SO$_3$**, *vide supra*) as well as for **para-SO$_3$** indicate 1:2 host/guest stoichiometry. The isotherms for **meta-SO$_3$** indicated 1:1 binding stoichiometry. Generally, the H_a proton of the cage was most reliable in determining host-guest stoichiometry.

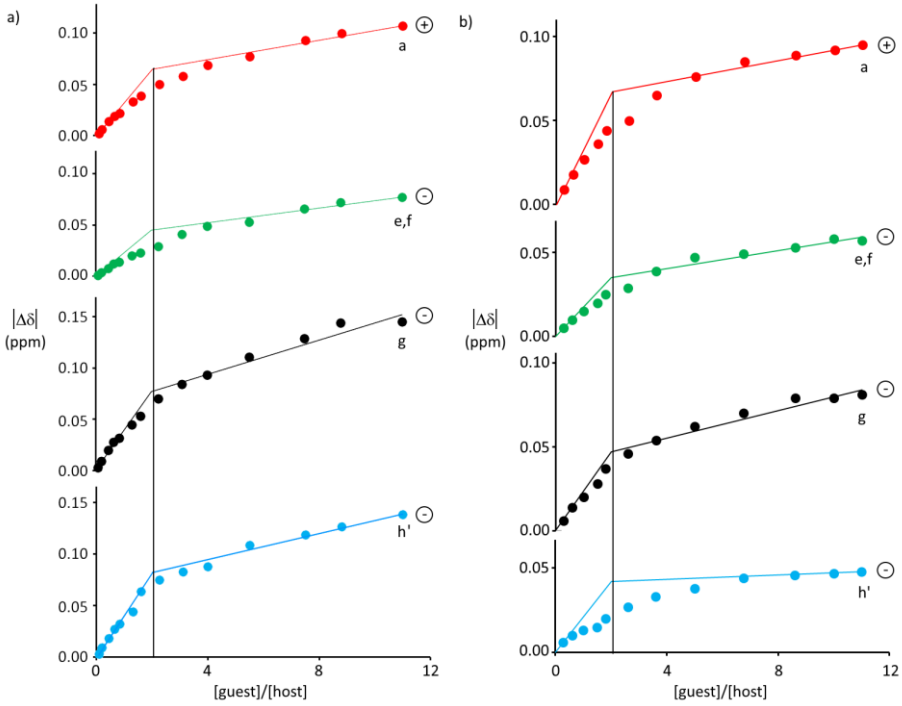

Figure 2.30 Changes in chemical shift of **C**$(BF_4)_4$ (600 MHz, [D_6]DMSO, 298 K, 1.25 mM) for key proton resonances (in absolute terms, actual direction of shift denoted in each case by **+** for downfield, **-** for upfield) upon introduction of a) **para-H** and b) **meta-H**.

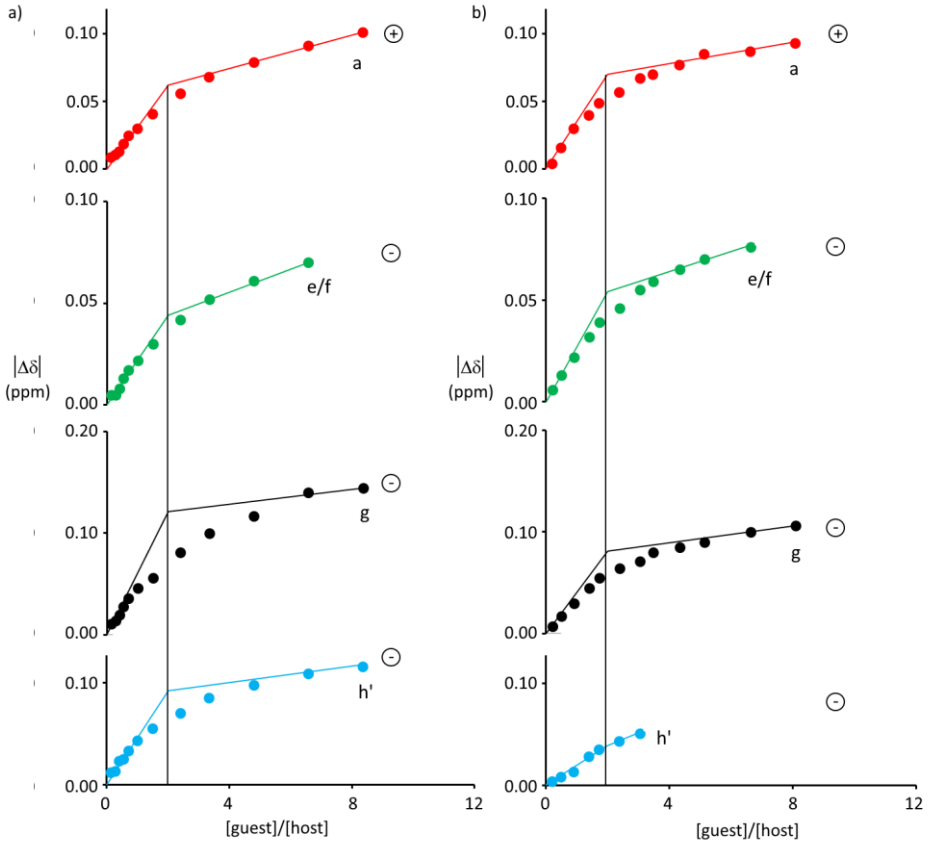

Figure 2.31 Changes in chemical shift of **C**$(BF_4)_4$ (600 MHz, [D_6]DMSO, 298 K, 1.25 mM) for key proton resonances (in absolute terms, actual direction of shift denoted in each case by **+** for downfield, **-** for upfield) upon introduction of a) **para-NH_2** and b) **meta-NH_2**. The extent of chemical shift for protons e/f and h' was unclear at higher equivalencies for these guests due to overlapping peaks.

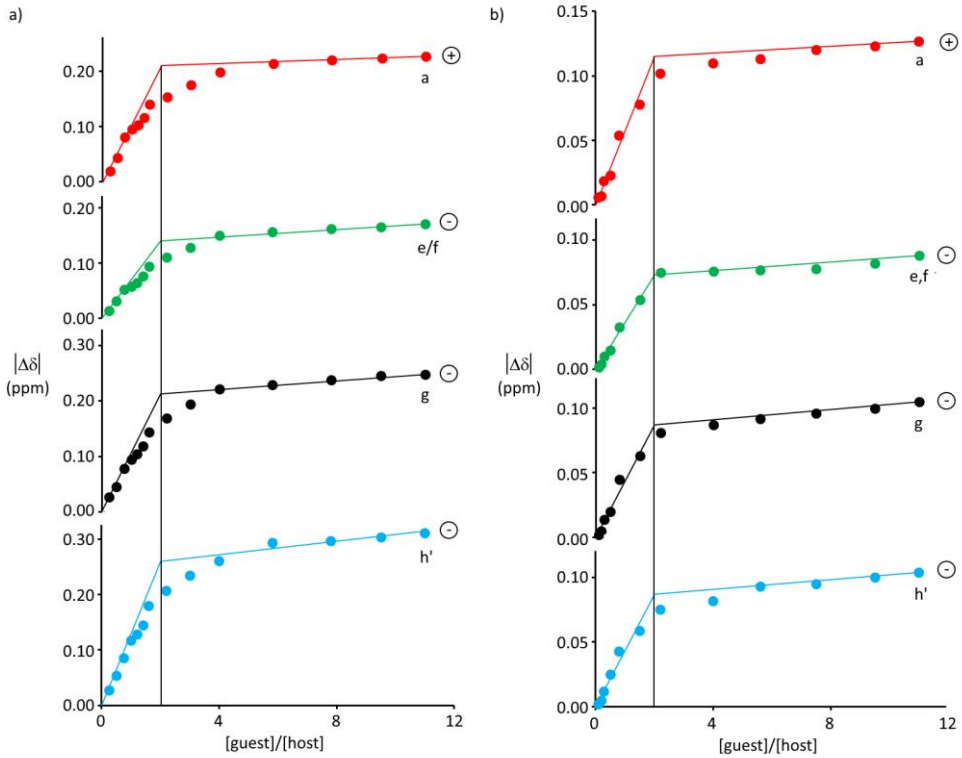

Figure 2.32 Changes in chemical shift of **C**$(BF_4)_4$ (600 MHz, [D_6]DMSO, 298 K, 1.25 mM) for key proton resonances (in absolute terms, actual direction of shift denoted in each case by **+** for downfield, **-** for upfield) upon introduction of a) **para-NO_2** and b) **meta-NO_2**.

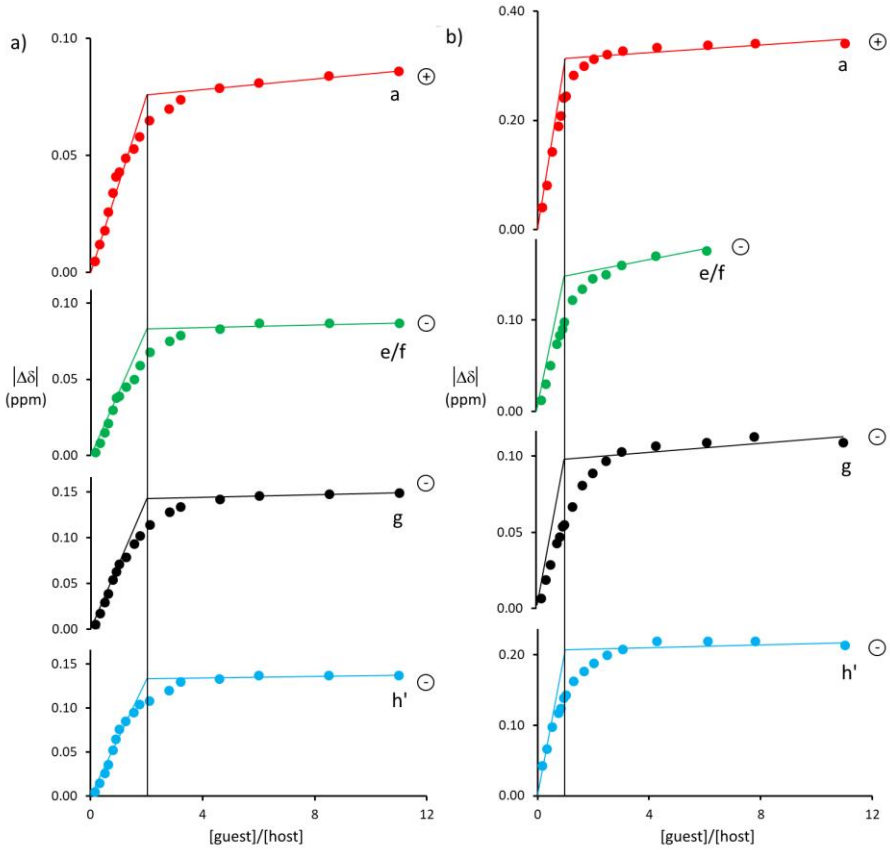

Figure 2.33 Changes in chemical shift of **C**$(BF_4)_4$ (600 MHz, [D_6]DMSO, 298 K, 1.25 mM) for key proton resonances (in absolute terms, actual direction of shift denoted in each case by **+** for downfield, **-** for upfield) upon introduction of a) **para-SO_3** and b) **meta-SO_3**. The extent of chemical shift for protons e/f was unclear at higher equivalencies for **meta-SO_3** due to overlapping peaks.

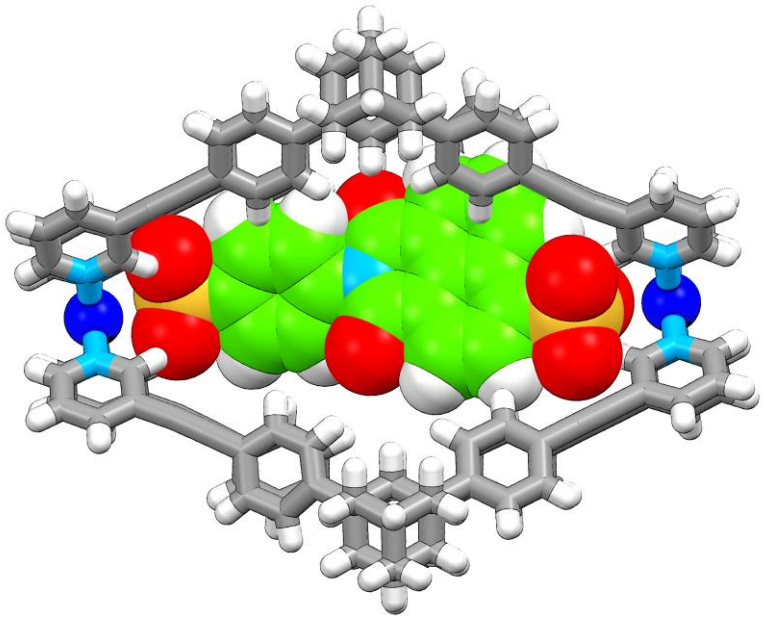

Figure 2.34 Depiction of the MMFF[6] of the 1:1 adduct of **C** and **para-SO_3**, showing that the fit is too tight: host in tube depiction, guest in spacefilling depiction. Colours: carbon grey for the cage and green for the guests, nitrogen light blue, oxygen red, palladium dark blue, sulphur orange. Model available as an xyz file.

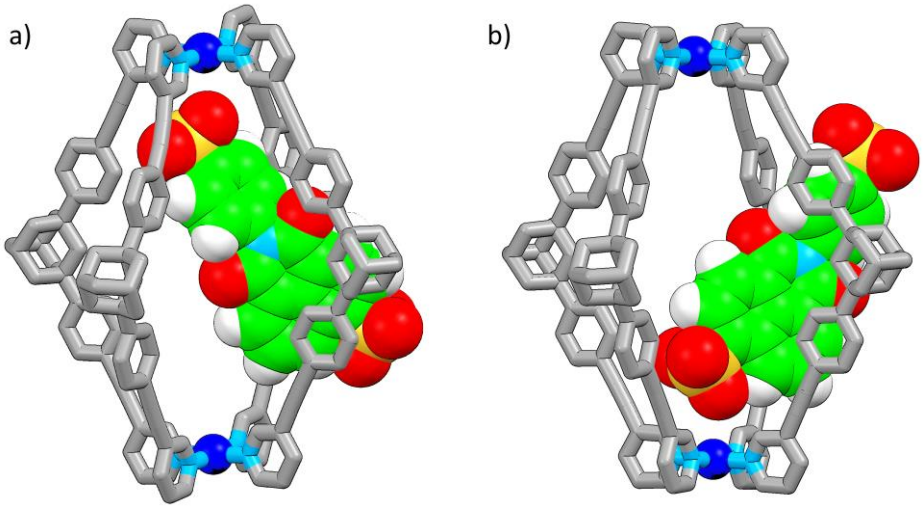

Figure 2.35 MMFF models[6] of [**para-SO_3⊂C**]$^{2+}$, hydrogen bonding through either a) the phenylsulfonate, or b) the naphthalimide sulfonate. Hydrogen bonding through the phenylsulfonate gives better overlap between the adamantane core and the naphthalimide. Host in tube depiction, guest in spacefilling depiction. Colours: carbon grey for the cage and green for the guests, nitrogen light blue, oxygen red, palladium dark blue, sulphur orange.

2.4. Calculation of binding constants

Binding constants were calculated[8] using 1:2 host/guest stoichiometry for all guests except for **meta-SO_3**, which was calculated for a 1:1 adduct. This decision was made based upon the binding equivalencies shown via the mole ratio method, with corroboration from crystallography of host/guest adducts. Note also that binding constants for **meta-SO_3** calculated for 1:2 stoichiometry are nonsensical and/or of high error.

Constants were calculated from the chemical shift of proton H_a, rather than all proton resonances (i.e., $H_{e/f,\ g,h'}$). This decision was made for several reasons: 1) consistency with **para-Ts** for which this was the only host resonance to shift, and with **nap-SO_3** for which other shifts were small, 2) in several other cases, shifts from the *bis*(phenyl)adamantane core were small in magnitude (~0.05 ppm over the titration, or less) and thus more prone to uncertainty, 3) the H_a proton resonance was in all cases the least crowded by other peaks, with the least ambiguity regards peak picking and/or isotherm truncation, and 4) this environment was, in our judgement, the least prone to additional contact from guests (namely due to attraction between their naphthalimide area and the *bis*(phenyl)adamanthane core) at high guest-to-host equivalencies.

In deciding between different 1:2 binding models, full binding was discounted on the basis of failed fits and high errors (some larger than the constant), and additive binding discounted for high errors (some larger than the constant). Between non-cooperative and statistical models, statistical 1:2 binding gave higher errors (in many cases over 30%). We therefore find it most likely that the guests bound in a 1:2 fashion in the cage do so in a manner best described as non-cooperative. A repeat was carried out for the two guests with highest binding affinity, with excellent to fair agreement.

Table 2.1 Binding constants established from ^{1}H NMR spectroscopic titrations for guests with **C**$(BF_4)_4$ in this study. Constants with errors higher than 30% shown in red. For non-cooperative and statistical models, K_{12} is unstated as it is by definition one quarter of K_{11}.

	1:2 Binding						1:1 Binding
	Full		Non-cooperative	Statistical	Additive		
	K_{11} (M^{-1})	K_{12} (M^{-1})	K_{11} (M^{-1})	K_{11} (M^{-1})	K_{11} (M^{-1})	K_{12} (M^{-1})	K (M^{-1})
para-Ts	69 ± 2	-1 ± 0.2	76 ± 2	324 ± 7	350 ± 30	110 ± 10	-
nap-SO_3	52 ± 2	-93 ± 4	176 ± 7	229 ± 8	157 ± 9	17 ± 5	-
para-NH_2	700 ± 200	26 ± 6	420 ± 50	800 ± 90	520 ± 90	40 ± 20	-
meta-NH_2	Fit failed		360 ± 30	1400 ± 200	290 ± 30	-9 ± 3	-
para-H	1100 ± 200	-24 ± 3	800 ± 200	1500 ± 500	1100 ± 400	50 ± 20	-
meta-H	380 ± 30	-58 ± 4	670 ± 80	1500 ± 300	1400 ± 400	140 ± 30	-
para-NO_2	Error > constant		1800 ± 300	6000 ± 2000	Error > constant		-
meta-NO_2	Fit failed		1400 ± 400	4000 ± 3000	Error > constant		-
para-SO_3	Fit failed		3700 ± 500	10000 ± 3000	Error > constant		-
meta-SO_3	Error > constant		16000 ± 8000	Error > constant	Error > constant		6100 ± 900

2.5. Plotted fits for guest-binding isotherms

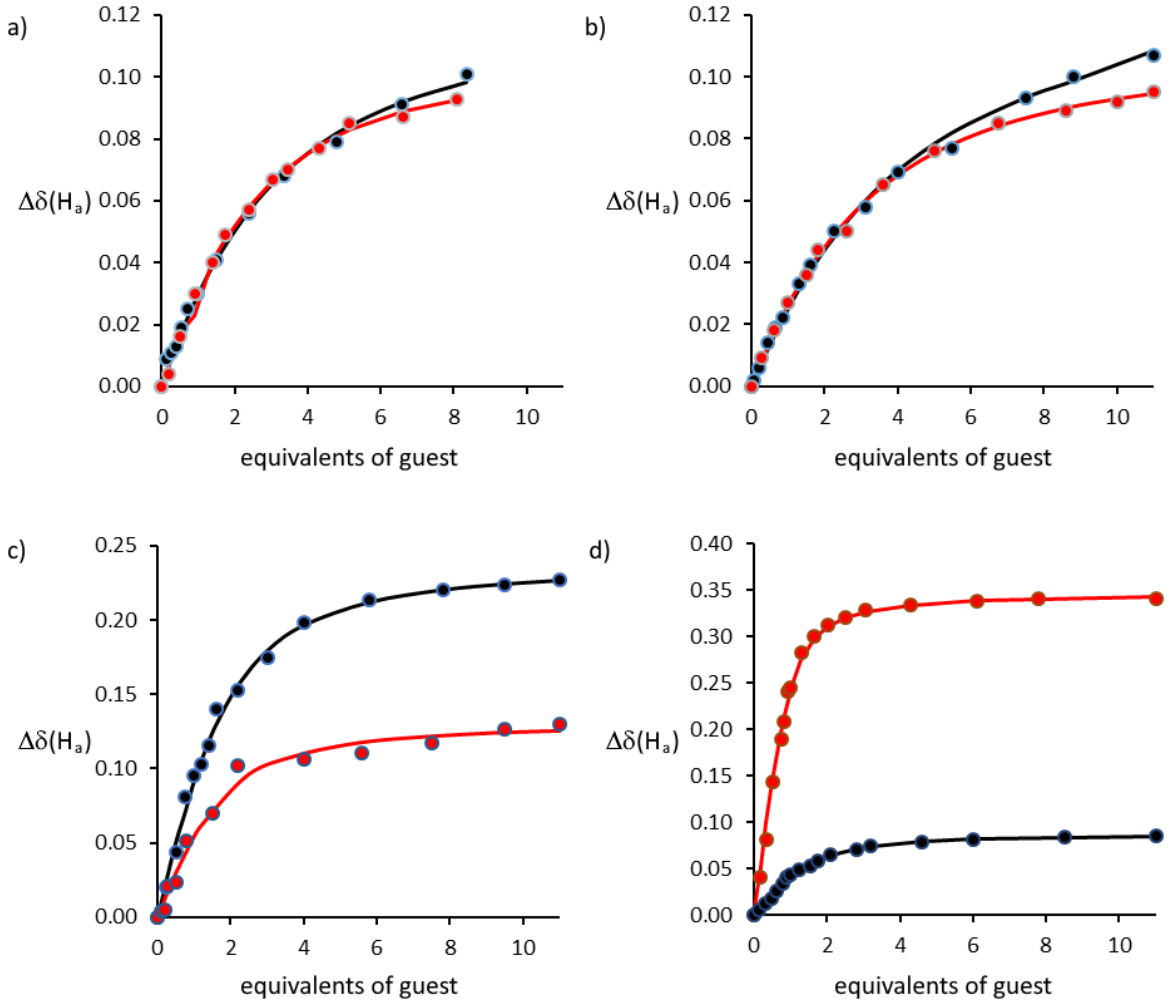

Figure 2.36 Calculated curves for binding constants from ^{1}H NMR titrations (600 MHz, [D$_6$]DMSO, 298 K), black traces (calculated) and points (observed) for *para* substituted guests, red traces (calculated) and points (observed) for *meta* substituted guests, R = a) –NH$_2$, b) –H, c) –NO$_2$, and d) –SO$_3$.

2.5.1. Job method

The Job method was carried out on two guests with the cage: **para-SO$_3$** and **meta-SO$_3$**. This was carried out *via* ^{1}H NMR spectroscopy (500 MHz, [D$_6$]DMSO, 298 K). Total concentration was held constant at 2.5 mM, and the mole fraction of the cage (and guest) varied. Cross-checking using integration of the peaks in ^{1}H NMR spectra indicated the correct equivalencies for each spectrum were present. The H$_a$ proton was used for the analysis. [H$_m$G$_n$] was calculated as follows:

$$[H_mG_n] = [H_0]\frac{\Delta\delta\,(H_a)}{\delta H_mG_n - \delta(H_a)}$$

where [H$_0$] = the initial concentration of cage, $\Delta\delta$(H$_a$) = the change in chemical shift of H$_a$ between mole fraction = 1 and the given mole fraction, δH$_m$G$_n$ = the chemical shift of H$_a$ when the cage is fully occupied (extrapolated from the spectra at high [G$_0$]:[H$_0$]), and δ(H$_a$) is the chemical shift of H$_a$ for a given mole fraction.

3. Computational work

All DFT calculations were performed using the ORCA program version 4.0.[9] All structures were fully optimized using the BP86[10] functional with a def2-SVP basis set.[11] The resolution of identity approximation[12] was also used in the BP86 calculations, with a def2-SVP/J auxiliary basis set.[13] SCF iterations were considered converged when the energy change was less than 1×10^{-8} a.u. The geometry was considered optimized when the following tolerances were met: Gradient = 5×10^{-6} a.u., RMS gradient = 1×10^{-4} a.u., maximum gradient = 3×10^{-4} a.u., RMS displacement = 2×10^{-3} a.u., maximum displacement = 4×10^{-3} a.u.. To reduce numerical error in the DFT integration, more grid points were used for both the angular and radial grids via the keyword "Grid4" for the SCF iterations and for the final energy evaluation. A CPCM indefinite field solvent field was applied. The following constraints were applied for the calculations: for the cage, all the cage atoms were constrained to their coordinates from the cationic portion of the X-ray structure of **C**$(BF_4)_4$ and the **para-NO₂** guest and DMSO allowed to optimise.

Stated as:

$$[(\textbf{para-NO}_2)(\text{DMSO})\subset\textbf{C}]^{3+} \rightleftharpoons [(\textbf{para-NO}_2)\subset\textbf{C}]^{3+} + \text{DMSO}$$

And taking ΔE of products minus reactants gave an energy difference favouring [(**para-NO₂**)(DMSO)⊂**C**]$^{3+}$ of -12.9 kJ mol^{-}.

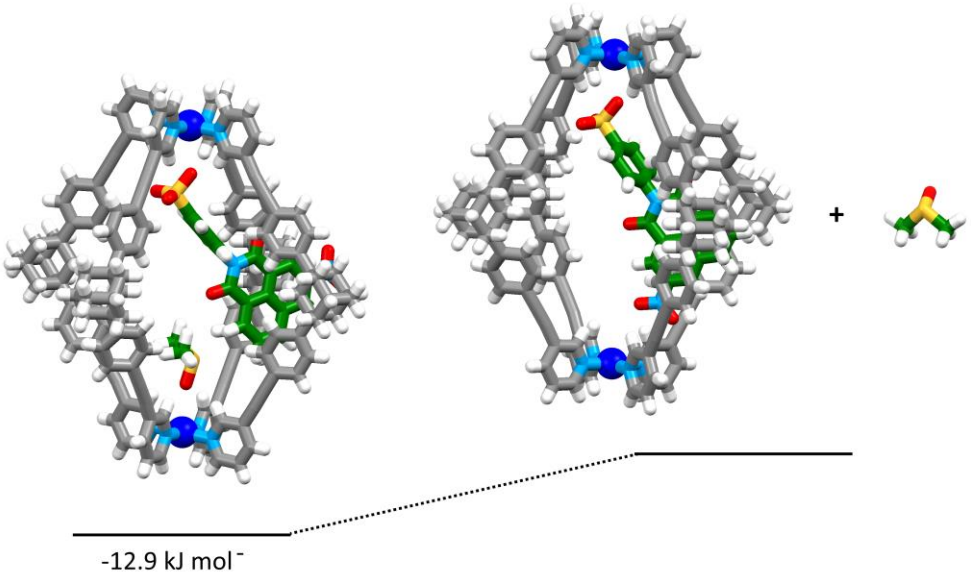

Figure 3.1 Depiction of the DFT structures of [(**para-NO₂**)(DMSO)⊂**C**]$^{3+}$, [(**para-NO₂**)⊂**C**]$^{3+}$, and DMSO. Files are available in xyz format.

4. References

[1] T. Fukaminato, T. Sasaki, T. Kawai, N. Tamai, M. Irie, *J. Am. Chem. Soc.* **2004**, *126*, 14843-14849.

[2] A. B. Carter, R. J. Laverick, D. J. Wales, S. O. Akponasa, A. J. Scott, T. D. Keene, J. A. Kitchen, *Crystal Growth & Design* **2017**, *17*, 5129-5144.

[3] in *CrysAlisPro*, Agilent Technologies, Yarnton, England, **2012**.

[4] G. M. Sheldrick, *Acta Crystallogr., Sect. A: Found. Crystallogr.* **2008**, *64*, 112-122.

[5] O. V. Dolomanov, L. J. Bourhis, R. J. Gildea, J. A. K. Howard, H. Puschmann, *J. Appl. Crystallogr.* **2009**, *42*, 339-341.

[6] in *Spartan '16*, Wavefunction, Inc., Irvine, CA, **2016**.

[7] a) A. S. Meyer, G. H. Ayres, *Journal of the American Chemical Society* **1957**, *79*, 49-53; b) D. Brynn Hibbert, P. Thordarson, *Chem Commun (Camb)* **2016**, *52*, 12792-12805.

[8] a) P. Thordarson, *Chemical Society Reviews* **2011**, *40*, 1305-1323; b) www.supramolecular.org

[9] F. Neese, *WIREs Comput. Mol. Sci.* **2012**, *2*, 73-78.

[10] a) A. D. Becke, *Phys. Rev. A: Gen. Phys.* **1988**, *38*, 3098-3100; b) Perdew, *Phys. Rev. B: Condens. Matter* **1986**, *33*, 8822-8824; c) Perdew, Yue, *Phys. Rev. B: Condens. Matter* **1986**, *33*, 8800-8802.

[11] A. Schaefer, H. Horn, R. Ahlrichs, *J. Chem. Phys.* **1992**, *97*, 2571-2577.

[12] F. Neese, *J. Comput. Chem.* **2003**, *24*, 1740-1747.

[13] a) K. Eichkorn, O. Treutler, H. Oehm, M. Haeser, R. Ahlrichs, *Chem. Phys. Lett.* **1995**, *240*, 283-290; b) K. Eichkorn, O. Treutler, H. Oehm, M. Haeser, R. Ahlrichs, *Chem. Phys. Lett.* **1995**, *242*, 652-660; c) K. Eichkorn, F. Weigend, O. Treutler, R. Ahlrichs, *Theor. Chem. Acc.* **1997**, *97*, 119-124.